



COMMONWEALTH OF KENTUCKY
DEPARTMENT OF HIGHWAYS
FRANKFORT

MITCHELL W. TINDER
COMMISSIONER OF HIGHWAYS

May 25, 1967

ADDRESS REPLY TO
DEPARTMENT OF HIGHWAYS
DIVISION OF RESEARCH
533 SOUTH LIMESTONE STREET
LEXINGTON, KENTUCKY 40508
Telephone 606-254-4475

H-2-20

MEMORANDUM

TO: W. B. Drake
Assistant State Highway Engineer
Chairman, Research Committee

SUBJECT: Research Report, Interim; "Flow Behavior
of Asphalt Cements;" KYHPR-64-20
HPR-1(2), Part II

A few years ago the term "rheology" (flow) was familiar to only a few scholars and researchers; the term embraces the whole science of material mechanics -- elasticity, viscosity, creep, and relaxation. In a simpler sense, however, paving asphalts (bitumens) are glues or cements which hold aggregate particles together; if the glue were ideally elastic (Hookean), it could be represented as being analogous to a simple spring; but, inasmuch as bitumens are semi-solids and exhibit properties of both solids and liquids -- that is, elasticity and viscosity --, tractive or cohesive resistance necessarily becomes an extremely complex combination of mechanical moduli, temperature and time. A rheological model is, therefore, conceptually, a complete mechanistic analog of the behavior of a real material. Rheological coefficients are ultimately applicable to the design of paving mixtures and pavement structures. Although the ultimate objective has not yet been achieved, the true nature and quality of bituminous cements is best described in these terms -- for example, there is considerable interest nationally in developing specifications in which asphalt cements will be designated according to ranges of viscosity. The report submitted herewith relates interim progress toward these objectives.

Mr. Mossbarger resigned from the Department June 30, 1966; Dr. Deacon rejoined our research staff last August and has continued the study to its present stage. The report, of course, reflects their joint authorship and individual dedication. The investigative work continued while the report was in

1
2
3
4
5
6
7
8
9
10
11
12
13
14
15
16
17
18
19
20
21
22
23
24
25
26
27
28
29
30
31
32
33
34
35
36
37
38
39
40
41
42
43
44
45
46
47
48
49
50
51
52
53
54
55
56
57
58
59
60
61
62
63
64
65
66
67
68
69
70
71
72
73
74
75
76
77
78
79
80
81
82
83
84
85
86
87
88
89
90
91
92
93
94
95
96
97
98
99
100

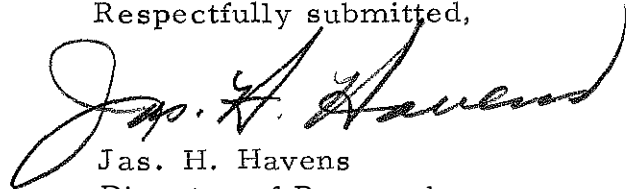
May 25, 1967

preparation. Additional measurements at low temperatures are either in progress or are planned.

Special attention is invited to the rational treatment of viscosity coefficients and to the evident necessity of discreet obedience to discrete definitions and measurement techniques. The curve-fitting technique employed in the viscoelastic analysis is thought to be somewhat original and may be useful in analyses of other types of data. The time-temperature superpositioning technique summarily portrays the viscoelastic character of a material throughout a given range of temperature.

The report does not require any Departmental action at this time; it is being issued as reference information and is somewhat pertinent to matter of viscosity-grading of asphalt cements, as mentioned previously.

Respectfully submitted,



Jas. H. Havens
Director of Research
Secretary, Research Committee

JHH:em

Attachment

cc: Member, Research Committee

A. O. Neiser

R. O. Beauchamp

T. J. Hopgood

R. A. Johnson

H. G. Mays

1
2
3
4
5
6
7
8
9
10
11
12
13
14
15
16
17
18
19
20
21
22
23
24
25
26
27
28
29
30
31
32
33
34
35
36
37
38
39
40
41
42
43
44
45
46
47
48
49
50
51
52
53
54
55
56
57
58
59
60
61
62
63
64
65
66
67
68
69
70
71
72
73
74
75
76
77
78
79
80
81
82
83
84
85
86
87
88
89
90
91
92
93
94
95
96
97
98
99
100

Research Report

FLOW BEHAVIOR OF ASPHALT CEMENTS
KYHPR-64-20: HPR-1(2)

by
W. A. Mossbarger, Jr., Former Research Engineer
and
J. A. Deacon, Research Engineer

Division of Research
DEPARTMENT OF HIGHWAYS
Commonwealth of Kentucky

In cooperation with the
U.S. Department of Transportation
Federal Highway Administration
Bureau of Public Roads

The opinions, findings, and conclusions
in this report are not necessarily those of
the Department of Highways or the Bureau of
Public Roads.

May, 1967

PREFACE

The Kentucky Department of Highways in cooperation with the Bureau of Public Roads is conducting a continuing investigation of the fundamental mechanical properties of flexible pavement materials. The ultimate objective of this investigation is to gain sufficient knowledge of the fundamental mechanical behavior of these materials to support the establishment of a responsive flexible pavement design procedure.

A preliminary report (1), issued in 1964, contained the results of the preparatory phase of this investigation. This report summarized from a theoretical point of view efforts that had been made to quantify the mechanical response of viscoelastic materials to known conditions of loading. In addition, it described the development of a rotating coaxial cylinder viscometer which was designed to measure the creep response in shear of solid or semi-solid bituminous materials. The usefulness of this viscometer was verified by testing a rubberized asphalt cement at several temperature and torque levels. It was found that rubber, when added to the asphalt cement in significant quantities, tended to increase, at the higher temperatures, the steady-state viscosity, the stiffness, the retardation time of the viscoelastic response, and the complexity of flow.

The current report summarizes results of a second phase of the continuing investigation in which the preparatory efforts have been expanded to encompass the creep testing of 13 asphalt

cements in a second rotating coaxial cylinder viscometer. The 13 asphalt cements were selected to represent a variety of crude sources, penetration grades, and manufacturing processes. Design and construction of the viscometer, which were accomplished as a portion of this phase, reflect the basic features of the earlier viscometer modified on the basis of the recommendations contained in the first report (1).

In analyzing the data reported herein, efforts were made to apply existing theories for simple ideal materials such as the Newtonian liquid and the Bingham plastic whenever these theories produced results in reasonable accord with the actual data. In many instances, however, it was necessary to combine these simple theories with somewhat more complex concepts of linear viscoelasticity in order to adequately characterize the deformation properties of the materials.

TABLE OF CONTENTS

	Page
PREFACE.....	iii
LIST OF TABLES.....	vii
LIST OF FIGURES.....	ix
INTRODUCTION.....	1
THEORETICAL CONSIDERATIONS.....	7
Steady-State Liquids	
Viscoelastic Materials	
Other Materials	
APPARATUS, MATERIALS, AND PROCEDURE.....	25
Apparatus	
Materials	
Test Procedure	
PRESENTATION OF RESULTS.....	37
Tests at 104 ^o F	
Tests at 77 ^o F	
Tests at 39.2 ^o F	
ANALYSIS OF RESULTS.....	61
Apparent Viscosity	
Temperature Susceptibility	
Viscosity-Penetration Relationship	
Time-Temperature Superposition	
CONCLUSIONS.....	85
REFERENCES.....	89
APPENDIX A -- TEST PROCEDURE.....	95
APPENDIX B - CURVE-FITTING TECHNIQUE.....	99

TABLE OF CONTENTS (Cont'd.)

	Page
APPENDIX C - COMPUTER PROGRAM FOR VISCOELASTIC ANALYSIS.....	107
APPENDIX D - VISCOELASTIC ANALYSIS OF DATA.....	123

LIST OF TABLES

Table		Page
1	Effective Dimensions of Cup, Bob, and Specimen.....	31
2	Crude Sources, Penetration Grades, and Manufacturing Processes for Asphalt Cements.....	32
3	Results of Standard Tests on Asphalts.....	34
4	Test Program.....	35
5	Material Parameters Evaluated at 104°F.....	41
6	Classification of Asphalts by Plastic Viscosity at 104°F.....	42
7	Material Parameters Evaluated at 77°F.....	44
8	Classification of Asphalts by Plastic Viscosity at 77°F.....	45
9	Elastic and Steady-State Material Parameters Evaluated at 39.2°F.....	46
10	Classification of Asphalts by Plastic Viscosity at 39.2°F.....	49
11	Viscoelastic Material Parameters Evaluated at 39.2°F.....	58
12	Comparison Between Viscosities Obtained with Rotating Coaxial Cylinder Viscometer and Sliding Plate Viscometer.....	69
13	Fundamental Differences Between Viscometers and Test Procedures.....	72
14	Temperature Susceptibility.....	74
15	Material Parameters Evaluated at 0°F (Asphalt 53).....	78
16	Shift Factors.....	82

1
2
3
4
5
6
7
8
9
10
11
12
13
14
15
16
17
18
19
20
21
22
23
24
25
26
27
28
29
30
31
32
33
34
35
36
37
38
39
40
41
42
43
44
45
46
47
48
49
50
51
52
53
54
55
56
57
58
59
60
61
62
63
64
65
66
67
68
69
70
71
72
73
74
75
76
77
78
79
80
81
82
83
84
85
86
87
88
89
90
91
92
93
94
95
96
97
98
99
100

LIST OF FIGURES

Figure		Page
1	General Mechanical Model Applicable to Rubberized Asphalt Cements (<u>1</u>).....	6
2	Cross Section Through Rotating Coaxial Cylinder Viscometer.....	7
3	Flow Behavior of Newtonian Liquid in Rotating Coaxial Cylinder Viscometer.....	12
4	Flow Behavior of Bingham Plastic in Rotating Coaxial Cylinder Viscometer.....	15
5	Flow Curves for Various Steady-State Liquids...	18
6	Flow Behavior of Various Steady-State Liquids in Rotating Coaxial Cylinder Viscometer.....	18
7	Generalized Voigt Body.....	20
8	Creep Curve for a Material Exhibiting Instantaneous Elastic Deformation, Retarded Deformation, and Steady-State Flow..	22
9	Viscometer and Related Equipment Assembled for Testing.....	26
10	Rotating Coaxial Cylinder Viscometer without Weights (Large Cup and Bob).....	26
11	Rotating Coaxial Cylinder Viscometer with Weights (Small Cup and Bob).....	28
12	Large Cup-and-Bob Assembly.....	28
13	Pouring Mold Used with Large Cup-and-Bob Assembly.....	29
14	Small Cup-and-Bob Assembly.....	29
15	Creep Curves for Asphalt 72 at Three Temperatures.....	38
16	Steady-State Angular Velocity vs. CT Product for 104 ^o F Tests.....	40

LIST OF FIGURES (Cont'd.)

Figure		Page
17	Steady-State Angular Velocity vs. CT Product for 77°F Tests.....	43
18	Steady-State Angular Velocity vs. CT Product for 39.2°F Tests.....	48
19	Experimental Creep Functions for Asphalt 72 at 39.2°F.....	50
20	Average Creep Functions for All Asphalts at 39.2°F.....	52
21	Viscoelastic Analysis for Asphalt 72 at 39.2°F.....	54
22	Comparison Between Observed and Computed Creep Functions for Asphalt 72.....	57
23	Comparison Between Observed and Computed Creep Functions for Asphalt 3.....	57
24	Evaluation of Angular Velocity by Secant Method	62
25	Comparison of Viscosities of Asphalt 3 at 39.2°F.....	63
26	Evaluation of Angular Velocity in Region of Steady-State Flow.....	64
27	Theoretical Comparison of Steady-State, Apparent Viscosity, η_a , and Plastic Viscosity, η_p	66
28	Comparison Between Viscosities Obtained with Rotating Coaxial Cylinder Viscometer and Sliding Plate Viscometer (Asphalt C-10 at 45°F).....	68
29	Comparison Between Limiting Viscosity and Plastic Viscosity.....	71
30	Largest and Smallest Temperature Susceptibilities.....	75
31	Relationship Between Plastic Viscosity and Penetration (100 g., 5 sec.) at 77°F.....	77

LIST OF FIGURES (Cont'd.)

Figure		Page
32	Relationship Between Plastic Viscosity and Penetration (200 g., 60 sec.) at 39.2°F.....	77
33	Average Creep Functions for Asphalt 53.....	80
34	Relationship Between Shift Factor and Temperature.....	81
35	Master Creep Function for Asphalt 53 (Reference Temperature of 50°F).....	83
C-1	Source Program for Viscoelastic Analysis.....	115
C-2	Source Program for Matinv Subprogram.....	120
D-1	Viscoelastic Analysis for Asphalt 3 at 39.2°F.....	124
D-2	Viscoelastic Analysis for Asphalt 13 at 39.2°F.....	126
D-3	Viscoelastic Analysis for Asphalt 45 at 39.2°F.....	128
D-4	Viscoelastic Analysis for Asphalt 53 at 39.2°F.....	130
D-5	Viscoelastic Analysis for Asphalt 67 at 39.2°F.....	132
D-6	Viscoelastic Analysis for Asphalt 71 at 39.2°F.....	134
D-7	Viscoelastic Analysis for Asphalt 72 at 39.2°F.....	136
D-8	Viscoelastic Analysis for Asphalt 91 at 39.2°F.....	139
D-9	Viscoelastic Analysis for Asphalt 116 at 39.2°F.....	140
D-10	Viscoelastic Analysis for Asphalt 127 at 39.2°F.....	142
D-11	Viscoelastic Analysis for Asphalt 200 at 39.2°F.....	144
D-12	Viscoelastic Analysis for Asphalt PR-103 at 39.2°F.....	147



INTRODUCTION

In the past, flexible pavement design procedures have been based largely upon empiricism; that is, empirical correlations between observed pavement performance and various traffic, pavement, and other parameters thought to be significant with respect to their effects on pavement performance. Recently, however, emphasis has shifted to analyses of stresses, strains, and deflections in the pavement structure (2,3). The basic intent is to limit the magnitudes of the critical stresses, strains, and deflections to levels below those thought to cause distress. Because of this emphasis on the mechanical behavior of the pavement structure and on the concept of critical levels of stresses and strains, this more fundamental approach is not unlike that commonly employed in conventional structural analyses.

There are at least five major determinations to be made before the theoretical approach can be translated into a design criterion. These include: (1) the development of a suitable technique for computing the mechanical response of a pavement structure to highway loads; (2) the adoption of standard methods of test for measuring the pertinent mechanical properties of the component layers; (3) the identification of those critical stresses, strains, and deflections which control the development of various forms of distress; (4) the establishment of tolerable levels of these critical stresses, strains, and deflections; and (5) a characterization of the loading and environmental variables. It is to the first two of these determinations that this continuing study is being directed.

The most suitable technique currently available for computing the mechanical response of a pavement structure to highway loads appears to be that which embodies the classical concepts of elastic analyses. Solutions are currently available for the computation of stresses, strains, and deflections in multi-layered elastic systems (4-6). These solutions have been found to approximate the behavior of pavements in service particularly for small stresses, short durations of loading, and limited strains or deformations (2, 7, and 8). However, the constituent materials which comprise a flexible pavement system are known to exhibit time-dependent mechanical behavior, the time-dependent character of which is not directly compatible with the doctrines of elastic theory.

This apparent incompatibility between the time-dependent mechanical behavior of the constituent materials in a pavement structure and the time-independent assumptions of elastic theory has turned the attention of several researchers to theories of mechanical behavior which encompass the time-dependent domain. Of particular significance is the theory of linear viscoelasticity which, despite being relatively new in its application to pavement materials, offers some promise in this regard. The major attention has focused on investigating convenient mathematical representations of viscoelastic behavior and on developing methods to measure this behavior. Suitable techniques for computing the mechanical response of a viscoelastic pavement structure to highway loads are generally unavailable though some preliminary work has been accomplished (9-14).

The general mechanical response of linear viscoelastic materials has been adequately reviewed (15-18). Ferry (19) has discussed suitable techniques for measuring viscoelastic behavior and has pointed out difficulties which often arise in instrumentation.

In 1944, Traxler et al. (20) investigated the flow characteristics of several asphalts from different sources and processed by various methods. They used a rotary viscometer and found that some asphalts do exhibit complex flow characteristics, the complexity being evaluated by the slope of a double logarithmic plot of stress against rate of strain. Van Der Poel (21, 22) studied the mechanical behavior of bitumens under both static and dynamic test conditions and presented the results in terms of static and dynamic stiffness moduli which were defined to be the ratio of stress to strain and the ratio of the amplitude of alternating stress to that of strain, respectively. His results indicated, as stated earlier by Saal (23), that the classification of bitumens, according to their rheological properties at normal temperatures, can generally be divided into three groups: (1) those that behave entirely or almost entirely as Newtonian liquids, (2) those which show elastic effects upon initial deformation and Newtonian flow thereafter, and (3) those which show almost complete resilience after comparatively slight deformation and for greater deformations cease to exhibit proportionality between stress and rate of strain. Brodnyan (24), Gaskins et al. (25), and Brodnyan et al. (26) investigated several different asphalts representing

a wide variety of industrial stocks and found that asphalt behavior is very similar to that of concentrated solutions of high polymers, that is, typical viscoelastic bodies. Corresponding studies by others (27-30) have indicated similar results.

Application of viscoelastic techniques to the study of bituminous mixes has also been attempted. Wood and Goetz (31) studied a sand-asphalt mixture subjected to static loading. They found that the mixture exhibited instantaneous elastic deformation, retarded elastic deformation, and flow. Upon removal of load, instantaneous elastic recovery was obtained. Pister and Monismith (32) reviewed the limitations imposed by elastic analyses of flexible pavements, and presented experimental data verifying the viscoelastic nature of bituminous mixes. They also illustrated the use of mechanical models to describe viscoelastic behavior and showed the formulation and solution of boundary value problems. In a later publication, Secor and Monismith (33) analyzed triaxial test data obtained on an asphalt concrete mixture and suggested a simplified mechanical model representing its viscoelastic response. The results of Baker and Papazian (34) indicated that elastic theory is satisfactory for small durations of time; however, they suggested that a more systematic and less empirical approach may be obtained by considering the behavior of flexible pavements to consist of both elastic and viscoelastic components. Papazian (35) presented a general review of linear viscoelastic theory and applied it to a study of asphalt concrete. He discussed the concept of complex material moduli, determined under dynamic test conditions, and illustrated methods for correlating dynamic with

static test results.

Recently, advances have been made in the application of viscoelastic concepts to the study of soils (36-41) which indicate that some soils exhibit viscoelastic properties.

As stated earlier, it is necessary to fully understand the mechanical behavior of the constituent materials in order to predict the mechanical response of the pavement structure. For this reason, attention has first been directed toward a study of the mechanical behavior of asphalt cements. This report summarizes the work that has been directed to this phase of the study. The foregoing literature review dictated, in large measure, the approach that was taken. The total mechanical behavior had to be analyzed: various common measurements of consistency such as apparent viscosity and penetration would not suffice since they are point measurements and greatly dependent upon the use of standardized test procedures and conditions. The rotating coaxial cylinder viscometer enabled the accumulation of data for a wide range of temperatures and stress levels and loading times which extended into the equilibrium or steady-state flow regime. This viscometer was also particularly suitable for an analysis of the total flow behavior based on a model of the type illustrated in Figure 1 or simplifications thereof.

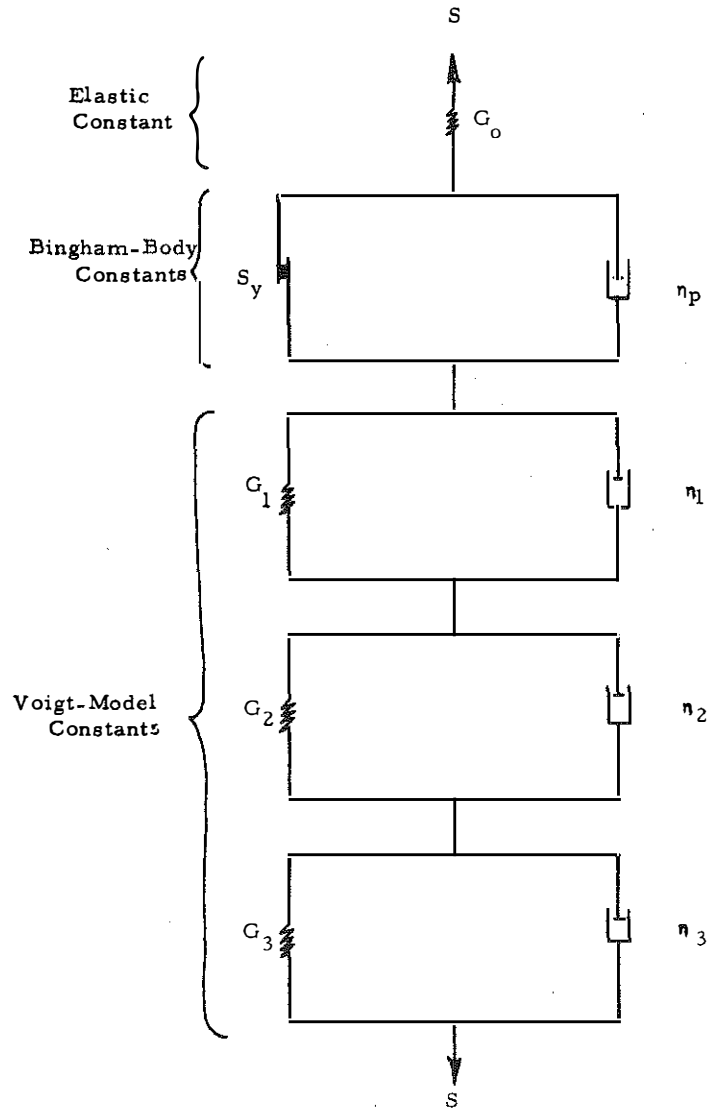


Figure 1. General Mechanical Model Applicable to Rubberized Asphalt Cements (1).

THEORETICAL CONSIDERATIONS

The creep behavior of certain ideal materials in the rotating coaxial cylinder viscometer can be readily determined. It is convenient first, however, to investigate the states of stress and strain in the viscometer when a constant torque is applied. A cross section through a rotating coaxial cylinder viscometer of the type employed in this study is depicted schematically in Figure 2. While testing, the cup is held stationary and a torque

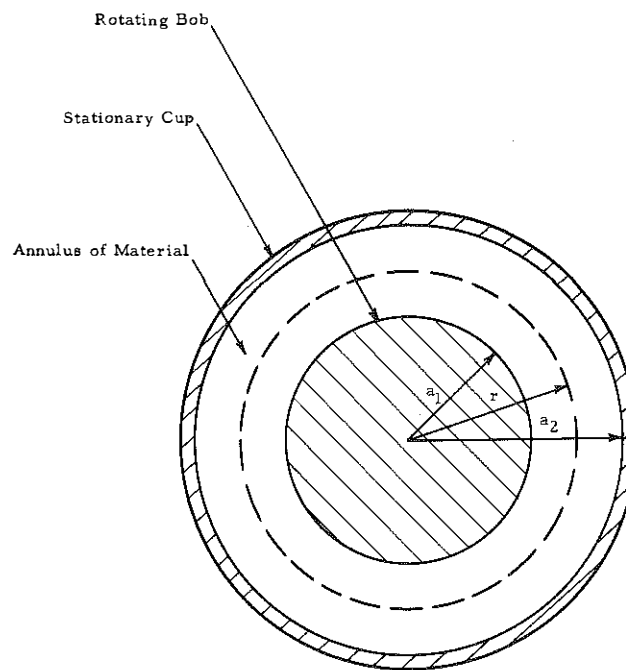


Figure 2. Cross Section through Rotating Coaxial Cylinder Viscometer.

is applied to the rotating bob. The resulting shear strain and rate of shear strain within the test material are given by the following equations (1, 42):

$$\gamma(r,t) = -r\partial\theta(r,t)/\partial r \quad (1)$$

and

$$\dot{\gamma}(r,t) = -r\partial\omega(r,t)/\partial r \quad (2)$$

where r = distance from axis of rotation to a point within the test material

t = elapsed time from beginning of test

$\gamma(r,t)$ = shear strain in test material at distance, r , and time, t

$\theta(r,t)$ = angle of rotation of a point in the test material at distance, r , and time, t , which is a function of both the angle of rotation of the bob relative to the cup and the response of the material to shear stress

$\dot{\gamma}(r,t) = \partial\gamma(r,t)/\partial t$ = rate of shear strain in test material at distance, r , and time, t

$\omega(r,t) = \partial\theta(r,t)/\partial t$ = angular velocity within test material at distance, r , and time, t .

The shear stress resulting from the application of a constant torque is described by the following equation:

$$S(r) = T/2\pi r^2 L \quad (3)$$

where $S(r)$ = shear stress at distance, r

T = constant torque applied to the bob

L = the length or height of the annulus of test material.

STEADY-STATE LIQUIDS

The behavior of certain ideal liquids is such that a steady-state flow condition is reached instantaneously after load application and the rate of strain is dependent only on the shearing stress. This behavior may be described in general by an equation

of the following form:

$$\dot{\gamma} = f\{S\} \quad (4)$$

where $f\{S\}$ = some time-independent function of stress.

When these materials are tested in a rotating coaxial cylinder viscometer, the rate of shear becomes:

$$\dot{\gamma}(r) = -rd\omega(r)/dr. \quad (5)$$

Combining Equations 4 and 5, the following equation is obtained:

$$f\{S(r)\} = -rd\omega(r)/dr. \quad (6)$$

Assuming no slippage occurs at the surfaces of the bob and cup, Equation 6 yields upon integration the following expression for angular velocity at a point:

$$\omega(r) = - \int_{a_2}^r f\{S(r)\} \frac{dr}{r} \quad (7)$$

where a_2 = radius of the stationary cup.

For the rotating coaxial cylinder viscometer, Equation 7 becomes:

$$\omega(r) = - \int_{a_2}^r f\left[\frac{T}{2\pi r^2 L}\right] \frac{dr}{r}. \quad (8)$$

Using the relationship, $dr/r = -dS/2S$, which was derived from Equation 3, a change in the variable of integration of Equation 8 yields:

$$\omega(r) = \frac{1}{2} \int_{S_2}^{S_r} \frac{f\{S\}}{S} dS \quad (9)$$

where S_r = shear stress at radius r

S_2 = shear stress at the inner wall of the cup.

The angular velocity of the bob relative to the cup can be obtained by selecting appropriate limits of integration in Equation 9 as follows:

$$\Omega = \omega(a_1) = \frac{1}{2} \int_{S_2}^{S_1} \frac{f\{S\}}{S} dS \quad (10)$$

where Ω = angular velocity of the bob relative to the cup
 S_1 = shear stress at surface of the bob.

Since the angular velocity, Ω , is constant for steady-state liquids, the angle of rotation of the bob relative to the cup is given by the following equation:

$$\theta = \Omega t \quad (11)$$

where θ = angle of rotation of bob relative to cup
 t = elapsed time.

Equations 10 and 11 yield the desired relationships for describing the behavior of ideal, steady-state liquids when subjected to a constant torque in a rotating coaxial cylinder viscometer. The first of these ideal liquids to be examined in detail is the Newtonian liquid.

Newtonian Liquid

The basic flow equation for a Newtonian liquid is:

$$\dot{\gamma} = f\{S\} = S/\eta \quad (12)$$

where η = coefficient of viscosity.

Substituting Equation 12 into Equation 10 one obtains upon integration

$$\Omega = CT/\eta \quad (13)$$

where $C = \frac{1}{4\pi L} (1/a_1^2 - 1/a_2^2)$.

The quantity, C, represents an instrument constant which is dependent upon the dimensions of the annulus of liquid. The angle of rotation as a function of time can be found by combining Equations 11 and 13 as follows:

$$\theta = C\tau t/\eta. \quad (14)$$

The rate of shear is found by substituting Equations 3 and 13 into Equation 12 and is given by

$$\dot{\gamma}(r) = \left(\frac{2\Omega}{1/a_1^2 - 1/a_2^2} \right) 1/r^2. \quad (15)$$

The average rate of shear becomes:

$$\dot{\gamma}(av) = \left(\frac{2a_1a_2}{a_2^2 - a_1^2} \right) \Omega \quad (16)$$

where $\dot{\gamma}(av)$ = average rate of shear.

Figure 3 depicts the flow behavior of a Newtonian liquid in terms of the measurable parameters of the rotating coaxial cylinder viscometer. To evaluate the coefficient of viscosity for a Newtonian liquid, sufficient tests should be performed to enable the construction of curves similar to those shown on Figure 3. The coefficient of viscosity can be readily determined from the slope of the straight line of Figure 3b.

Bingham Plastic

The basic flow equation for a Bingham plastic is

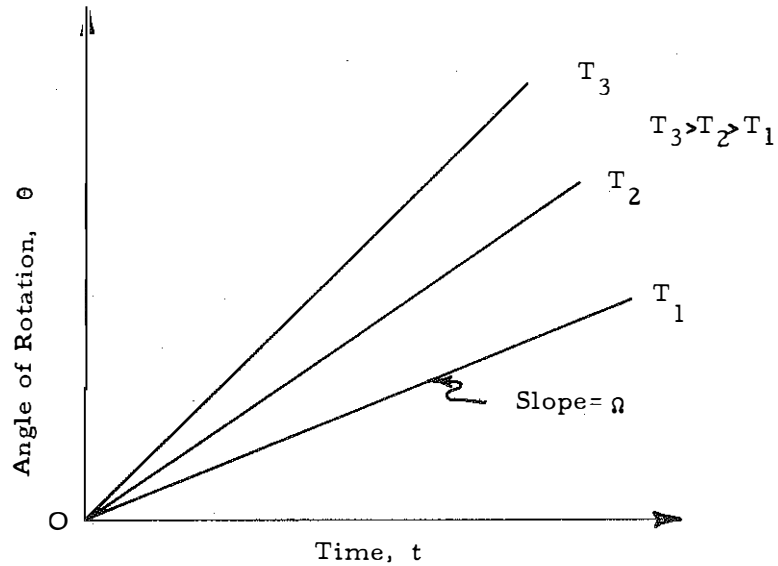
$$\dot{\gamma} = 0 \quad \text{for } S \leq S_y \quad (17a)$$

and

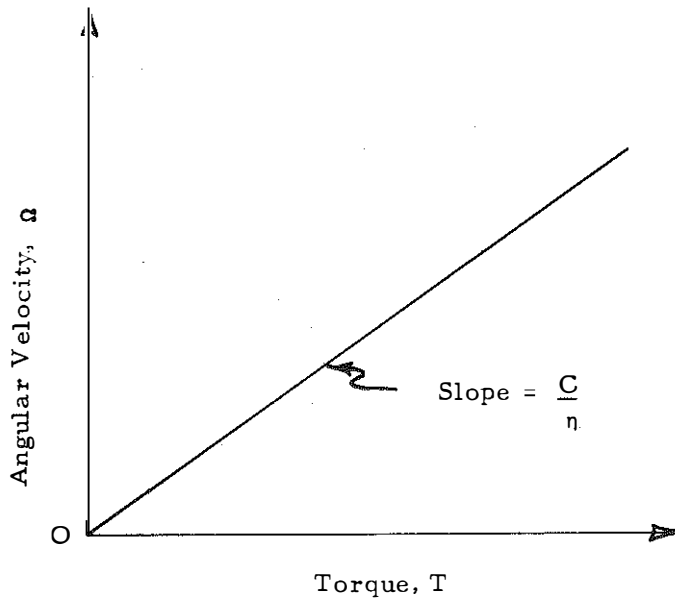
$$\dot{\gamma} = \frac{S - S_y}{\eta_p} \quad \text{for } S > S_y \quad (17b)$$

where S_y = yield stress

η_p = coefficient of plastic viscosity.



a. Angle of Rotation as a Function of Time for Different Levels of Torque



b. Angular Velocity as a Function of Torque

Figure 3. Flow Behavior of Newtonian Liquid in Rotating Coaxial Cylinder Viscometer.

Flow occurs in these materials only when the applied shearing stress exceeds the yield stress. For this reason it is necessary to consider three distinct conditions of loading when

a Bingham plastic is sheared in a rotating coaxial cylinder viscometer.

The first condition occurs when the applied torque is so small that the maximum shear stress (at the surface of the bob) is less than the yield stress. For this condition no flow occurs and

$$\Omega = 0 \quad \text{for } S_1 \leq S_y \quad \text{or} \quad (18a)$$

$$T \leq 2\pi a_1^2 L S_y.$$

The second condition occurs when the yield stress is bracketed by a lower applied stress at the surface of the cup and a higher applied stress at the surface of the bob. Flow occurs only in that layer of material located between the surface of the bob and a critical radius, $r_c = (T/2\pi L S_y)^{1/2}$. The material located between this critical radius and the surface of the cup remains stationary. The angular velocity of the bob relative to the cup is then given by:

$$\Omega = \frac{1}{2} \int_{S_y}^{S_1} \frac{f\{S\}}{S} dS \quad (19)$$

which upon evaluation yields:

$$\Omega = \frac{1}{2\eta_p} \left[\frac{T}{2\pi a_1^2 L} - S_y - S_y \ln \left(\frac{T}{2\pi a_1^2 L S_y} \right) \right] \quad (18b)$$

$$\text{for } S_1 > S_y \geq S_2 \quad \text{or}$$

$$2\pi a_1^2 L S_y < T \leq 2\pi a_2^2 L S_y.$$

The third condition occurs when the applied stress at the surface of the cup exceeds the yield stress and flow occurs throughout the annulus of the material. The angular velocity becomes

$$\Omega = \frac{CT}{\eta_p} - \frac{S_y}{\eta_p} \ln \left(\frac{a_2}{a_1} \right) \quad \text{for } S_y < S_2 \text{ or} \quad (18c)$$
$$T > 2\pi a_2^2 L S_y.$$

The angle of rotation of the bob relative to the cup is simply the product of elapsed time and the appropriate angular velocity of Equation 18.

Figure 4 depicts the flow behavior of a Bingham plastic in terms of the measurable parameters of the rotating coaxial cylinder viscometer. To evaluate the constants, η_p and S_y , sufficient tests should be performed to enable the construction of curves similar to those shown on Figure 4. The coefficient of plastic viscosity can be readily determined from the slope of the inclined, straight-line portion of Figure 4b. The yield stress is best determined from the intercept at point B of Figure 4b. It can also be estimated from the torques corresponding to points A and C. These torques are related by the following equation:

$$T_A/T_C = (a_1/a_2)^2. \quad (20)$$

Other Steady-State Liquids

The preceding analysis demonstrates the procedures used for predicting the behavior of certain steady-state liquids, namely, the Newtonian liquid and the Bingham plastic, in a rotating

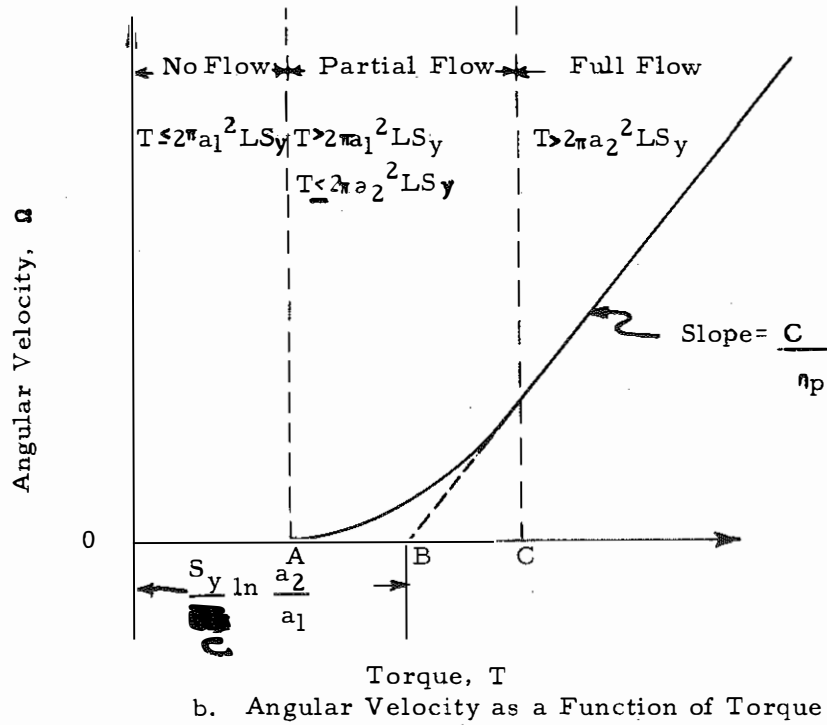
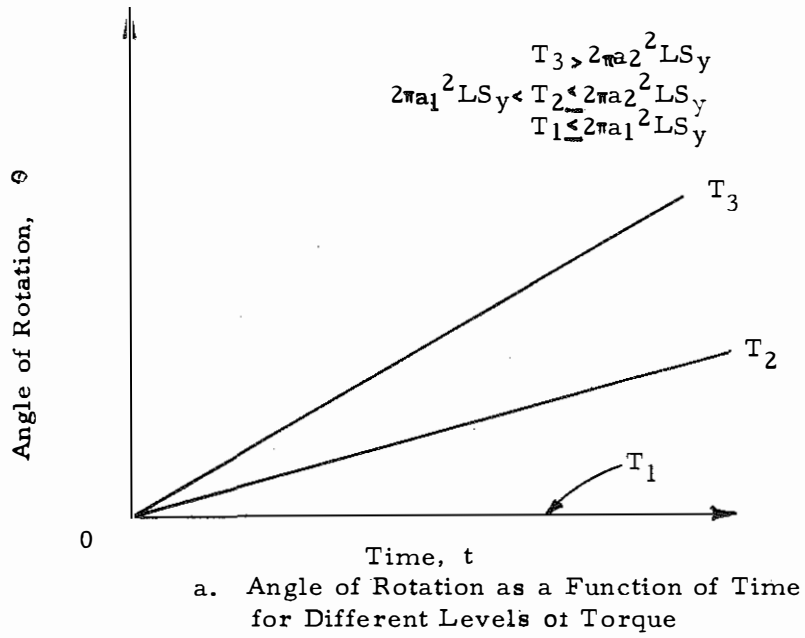


Figure 4. Flow Behavior of Bingham Plastic in Rotating Coaxial Cylinder Viscometer.

coaxial cylinder viscometer. While other steady-state liquids do not exhibit the same linear relationship between rate of shear strain and shear stress as do these materials, the procedures for deriving the equations which predict their behavior in this viscometer remain essentially the same and, hence, are not included herein. At the same time, it is useful to define the basic flow equations for several of these materials and to present the equations describing their behavior in the coaxial cylinder viscometer.

Pseudoplastic liquids obeying the power-law relationship (43) are described by the following basic flow equation:

$$\dot{\gamma} = (S/k)^{1/n} \quad (21)$$

where k = a material constant related to the consistency of the liquid

n = a material constant assuming values less than one.

The non-Newtonian properties of these liquids become more pronounced as n diverges from a value of one. Their behavior in the rotating coaxial cylinder viscometer is described by the following equation:

$$\Omega = \frac{n(2/k)^{1/n} (CT)^{1/n}}{(1/a_1^2 - 1/a_2^2)^{1/n}} \left[(1/a_1^2)^{1/n} - (1/a_2^2)^{1/n} \right] \quad (22)$$

The pseudoplastic liquids have no yield stress and the ratio of shear stress to rate of shear (the apparent viscosity) decreases with increasing shear rates.

Another of the steady-state liquids is the dilatent liquid which conforms to the same power-law flow equation as pseudoplastic.

liquids (Equation 21) with the exception that n exceeds the value of unity (43). Dilatent liquids exhibit no yield stress but, in contrast to pseudoplastics, their apparent viscosities increase with increasing rates of shear.

The final steady-state liquid to be considered is one conforming to the following basic flow equation:

$$\eta = (S/\eta_i) [1 + (S/G_i)] \quad (23)$$

where η_i = viscosity constant defined as the limiting value of S/η

G_i = constant with dimensions of stress (termed the internal shear modulus).

This equation has been employed by Ferry (42) to describe the behavior of polymeric systems at low rates of shear. The angular velocity for a creep test in the rotating coaxial cylinder viscometer is given by the following equation:

$$\Omega = (CT) \left[\frac{1}{\eta_i} + \frac{CT}{G_i} \left(\frac{a_1^2 + a_2^2}{a_2^2 - a_1^2} \right) \right] \quad (24)$$

The basic flow properties of the various steady-state liquids are graphically compared on Figure 5. Figure 6 depicts the type of behavior experienced when testing these materials in the rotating coaxial cylinder viscometer. It is recalled that, because of the steady-state nature of these liquids, their angles of rotation in the viscometer are linear functions of elapsed time.

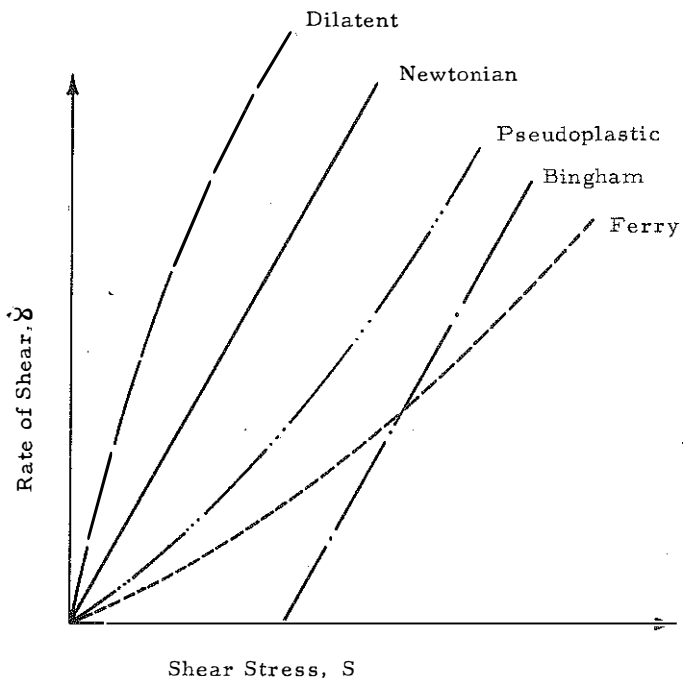


Figure 5. Flow Curves for Various Steady-State Liquids.

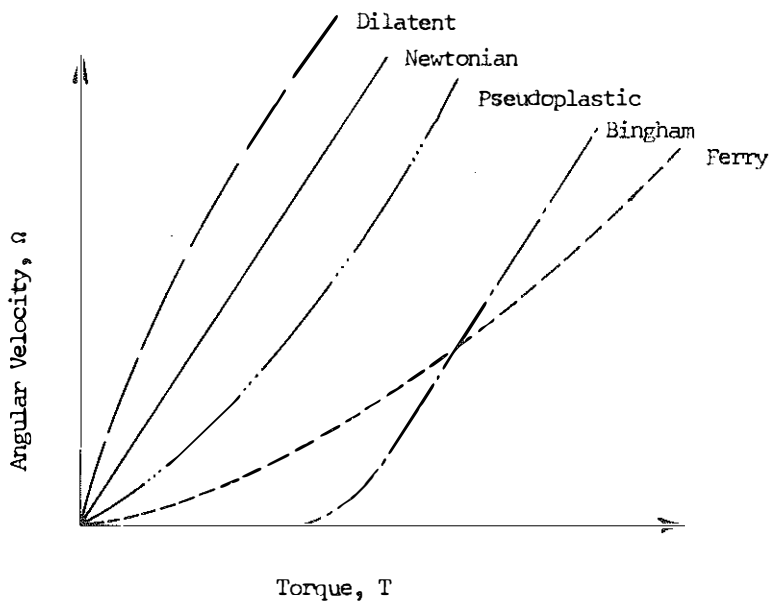


Figure 6. Flow Behavior of Various Steady-State Liquids in Rotating Coaxial Cylinder Viscometer.

VISCOELASTIC MATERIALS

When steady-state liquids are subjected to a constant torque in the rotating coaxial cylinder viscometer, a linear relationship is observed between the angle of rotation and time; that is, the angular velocity is independent of time. In contrast, a liquid for which the angular velocity is dependent on elapsed time may be called a non-steady-state liquid. Such liquids may exhibit either thixotropic or rheopectic behavior depending upon whether the shear strains cause a respective breakdown or formation of internal structure. However, neither of these two basic types of liquids possess properties of instantaneous and retarded elasticity and, upon load removal, elastic recovery.

To describe this somewhat more complex behavior, it is necessary to consider materials which simultaneously possess both elastic and viscous properties, that is, viscoelastic materials. Of particular interest is the special case where the ratio of stress to strain is a function only of elapsed time and not of the stress magnitude. Viscoelastic materials demonstrating this property are termed linear and are of primary importance since their mechanical behavior is mathematically tractable.

A linear viscoelastic material may be visualized in terms of the generalized Voigt body of Figure 7 (43). This mechanical model is composed of a series of elements, each of which consists of a spring and a dashpot which are connected in parallel. The relationship between strain and stress for a constant stress or creep test is as follows:

$$\gamma(t) = S_0 \sum_{k=1}^n J_k [1 - \exp(-t/\tau_k)] \quad (25)$$

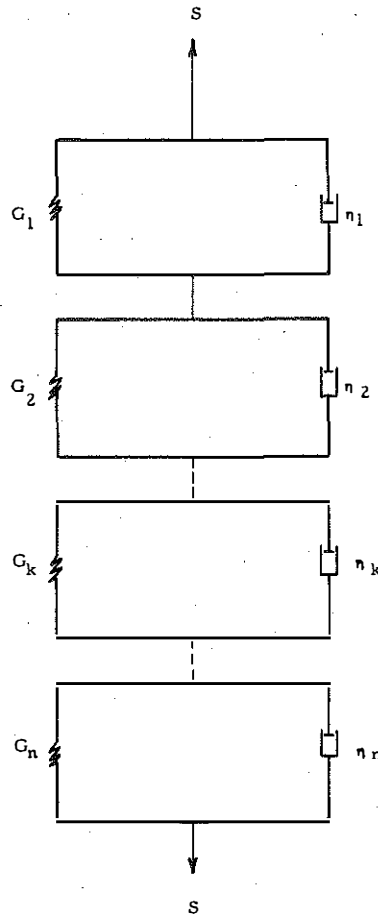


Figure 7. Generalized Voigt Body.

- where $\gamma(t)$ = shear strain at time, t
- S_0 = constant shear stress
- J_k = compliance ($1/G_k$)
- η_k = viscosity coefficient
- τ_k = retardation time (η_k/G_k)
- t = elapsed time
- G_k = shear modulus (rigidity modulus)
- n = number of elements.

The generalized Voigt body represents a linear viscoelastic material with a discrete spectrum of retardation times. As the number of elements in this model approaches infinity (that is, $n \rightarrow \infty$), the stress-strain relationship for a creep test may be more conveniently specified in terms of the following:

$$\gamma(t) = S_0 \int_0^{\infty} J(\tau) [1 - \exp(-t/\tau)] d\tau \quad (26)$$

where $J(\tau)$ = compliance distribution function
 τ = retardation time (continuous variable).

This concept of a distribution of retardation times simplifies the mathematical approach since the mechanical behavior of the material can be described in terms of the compliance distribution function, $J(\tau)$.

The relationship between angle of rotation and time for a linear viscoelastic material subjected to a constant torque in the coaxial cylinder viscometer can be derived using Equations 1, 3, and 25 and is given by the following expression:

$$\theta(t) = \sum_{k=1}^n CT J_k [1 - \exp(-t/\tau_k)]. \quad (27)$$

The corresponding angular velocity is

$$\Omega(t) = \frac{d\theta(t)}{dt} = \sum_{k=1}^n \frac{CTJ_k}{\tau_k} [\exp(-t/\tau_k)]. \quad (28)$$

The creep function, $\psi(t)$, for a linear viscoelastic material is defined as the ratio of strain to stress when the material is subjected to constant loading. Thus, from Equation 25, the creep function is

$$\psi(t) = \gamma(t)/S_0 = \sum_{k=1}^n J_k [1 - \exp(-t/\tau_k)] \quad (29)$$

where $\psi(t)$ = creep function.

But, from Equation 27,

$$\theta(t)/CT = \sum_{k=1}^n J_k [1 - \exp(-t/\tau_k)]. \quad (30)$$

On the basis of Equations 29 and 30, the creep function for a linear viscoelastic material may be evaluated using the coaxial cylinder viscometer in the following way:

$$\psi(t) = \theta(t)/CT. \quad (31)$$

OTHER MATERIALS

There are other engineering materials whose mechanical behavior may best be characterized by a series combination of an elastic element (spring), a viscous element (steady-state liquid), and a viscoelastic body (generalized Voigt body). When these more complex materials are subjected to a constant torque in the rotating coaxial cylinder viscometer, a creep curve similar to that illustrated in Figure 8 is observed. The total angle of rotation of the bob relative to the cup is depicted by curve 4.

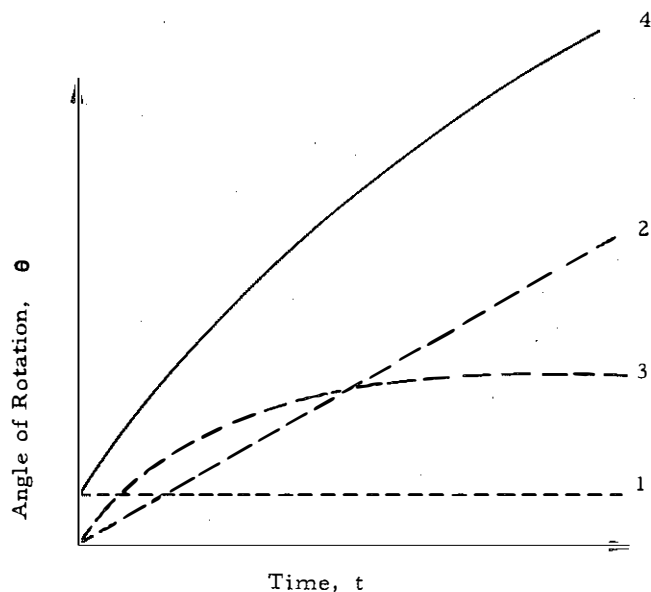


Figure 8. Creep Curve for a Material Exhibiting Instantaneous Elastic Deformation, Retarded Deformation, and Steady-State Flow.

Each ordinate on this curve may be considered to equal the sum of the corresponding ordinates on the remaining three curves.

The equation of curve 1, which represents an instantaneous elastic deformation, is

$$\theta_1 = CT/G_0 \quad (32)$$

where G_0 = elastic shear modulus.

Curve 2 represents the steady-state flow behavior of a steady-state liquid. Its equation is

$$\theta_2 = \Omega_0 t \quad (33)$$

where Ω_0 = the steady-state angular velocity given by Equation 13, 18, 22, or 24.

From Figure 8 and Equation 33, the steady-state portion of the angle of rotation is seen to linearly increase with time. Curve 3 represents the retarded elastic flow of the viscoelastic components. Equation 27, therefore, specifies the shape of this curve.

The total angle of rotation (curve 4) can be computed as follows:

$$\theta = \theta_1 + \theta_2 + \theta_3 \quad (34)$$

or

$$\theta = CT/G_0 + \Omega_0 t + \sum_{k=1}^n CT J_k [1 - \exp(-t/\tau_k)] \quad (35)$$

Equation 35 represents a general flow equation describing the response of a wide variety of engineering materials to creep loading in a rotating coaxial cylinder viscometer. The parameters of Equation 35 may be evaluated for a specific material by obtaining θ - t curves from a suitably designed creep test program. The procedures recommended for this type of evaluation are discussed in subsequent sections.

1
2
3
4
5
6
7
8
9
10
11
12
13
14
15
16
17
18
19
20
21
22
23
24
25
26
27
28
29
30
31
32
33
34
35
36
37
38
39
40
41
42
43
44
45
46
47
48
49
50
51
52
53
54
55
56
57
58
59
60
61
62
63
64
65
66
67
68
69
70
71
72
73
74
75
76
77
78
79
80
81
82
83
84
85
86
87
88
89
90
91
92
93
94
95
96
97
98
99
100

APPARATUS, MATERIALS, AND PROCEDURE

APPARATUS

The rotating coaxial cylinder viscometer is a modified version of one used in the preliminary phases of the study (1). Its function is to apply a creep stress in shear to an annular specimen of solid or semi-solid bitumen over a wide range of stresses and temperatures. Figure 9 shows the viscometer and related equipment assembled for testing.

As depicted in Figure 10, the viscometer consists of an inner cylinder (or bob) and an outer cylinder (or cup) which are mounted concentrically to form an annulus. This annulus is filled with the test material which is subjected to shear stresses by applying a torque to the bob. The bob is rigidly attached to an axle or spindle which is supported by a ball bearing at the upper plate of the apparatus. The torque is generated by the suspension of weights from the drive pulley at the upper end of the axle. To eliminate bending in the axle, equal weights are suspended over diagonally opposite idle pulleys.

The angle through which the bob rotates is measured by a rotary variable differential transformer, type R3B2S, manufactured by Schaevitz Engineering. This device produces a voltage having a magnitude which varies linearly with the angular position of its shaft for a range of $\pm 40^\circ$ from its null position. The voltage is monitored with a Sanborn, Model 321, carrier-amplifier recorder. An appropriate scale and vernier are also provided above the drive pulley for visual checking and calibration.

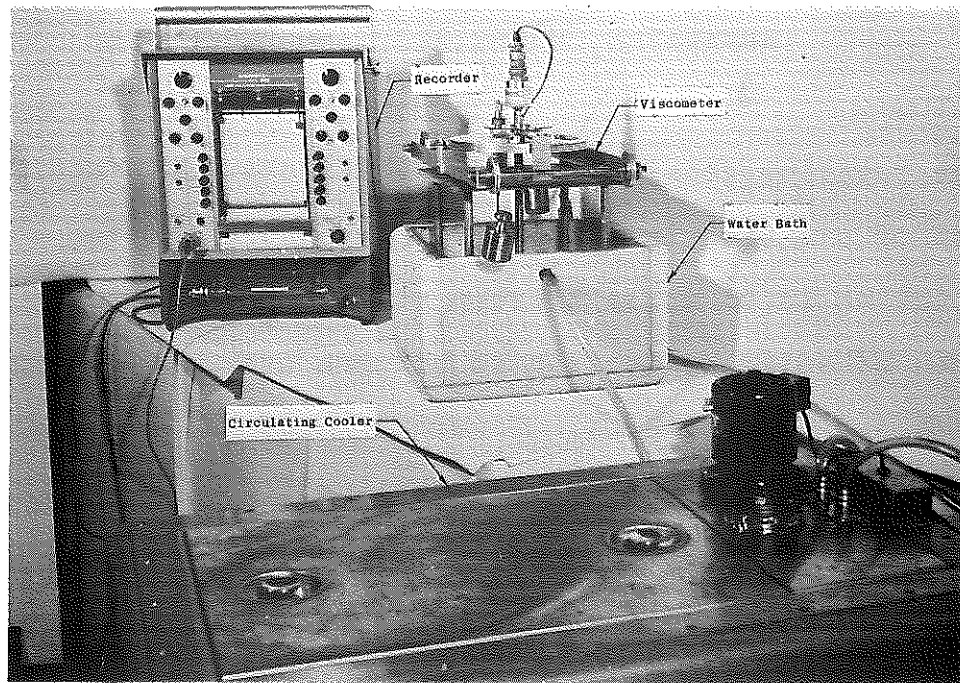


Figure 9. Viscometer and Related Equipment Assembled for Testing.

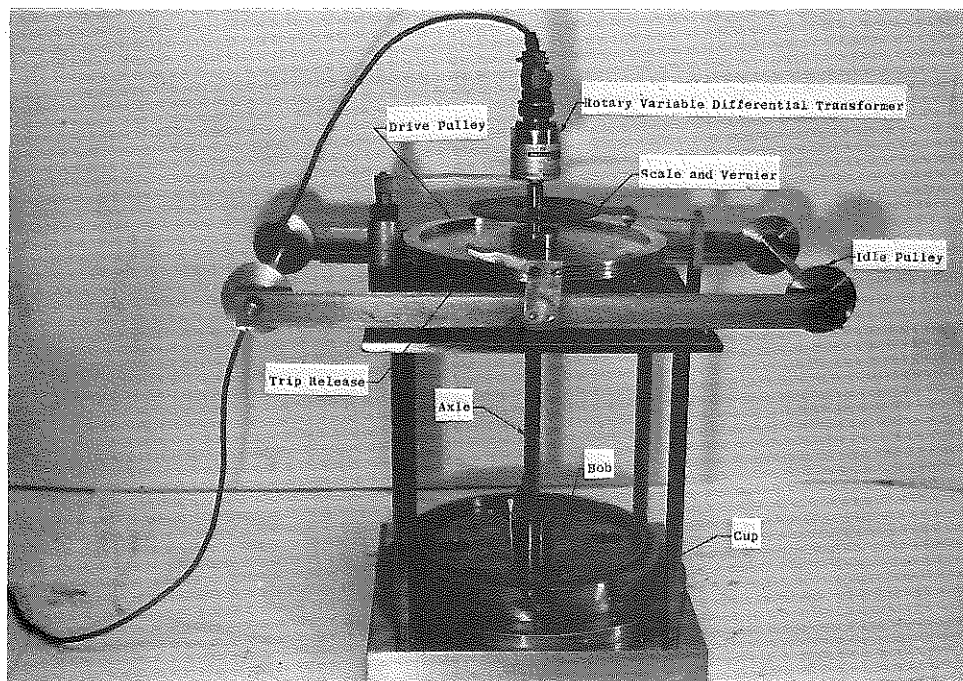


Figure 10. Rotating Coaxial Cylinder Viscometer without Weights (Large Cup and Bob).

In order to provide a wide range of shear rates, two different cup-and-bob assemblies are used. For testing the less viscous asphalts, the large cup and bob shown in Figure 10 may be used. The small cup and bob shown in Figure 11 are used for testing more viscous materials. For equal weights of the suspended loads, a lower shear rate is attained with the large cup-and-bob assembly.

Figure 12 shows the components of the large cup-and-bob assembly. The stainless steel bob contains a hardened steel, 60° conical bearing point which bears on a hardened steel cap screwed into the steel base plate. The cap contains a conical depression which receives the bearing point of the bob. This bearing arrangement is essentially free of friction and provides an excellent means for centering the bob.

During assembly the amalgamated brass ring is placed within the groove of the base plate. The stainless steel cup also fits within the groove and bears lightly against its outer edge. The bob extends into the groove of the base plate but bears only on the hardened steel bearing cap. Sufficient clearance is provided between the bob and the brass ring and between the bob and the base plate to insure freedom of rotation. When assembly is completed, mercury is poured into the annulus until its level is slightly above the lower edge of the bob. This prevents the test material from flowing beneath the bob and provides a completely fluid, floating bearing for the specimen which virtually eliminates end effects due to adhesion.

The pouring mold shown in Figure 13 is used to fill the annulus of the large cup-and-bob assembly with heated asphalt.

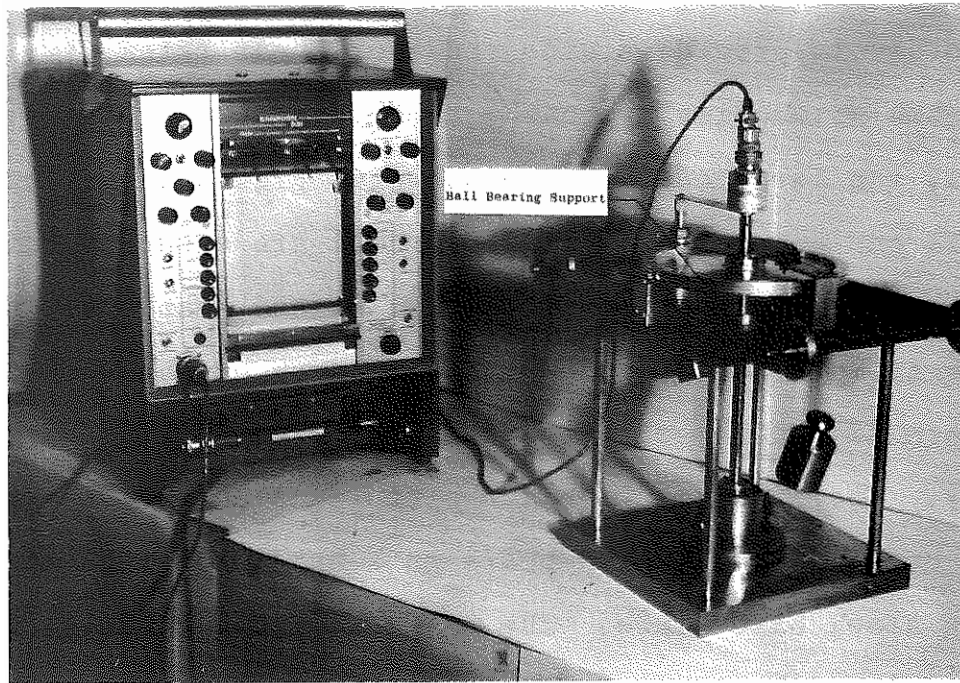


Figure 11. Rotating Coaxial Cylinder Viscometer with Weights (Small Cup and Bob).

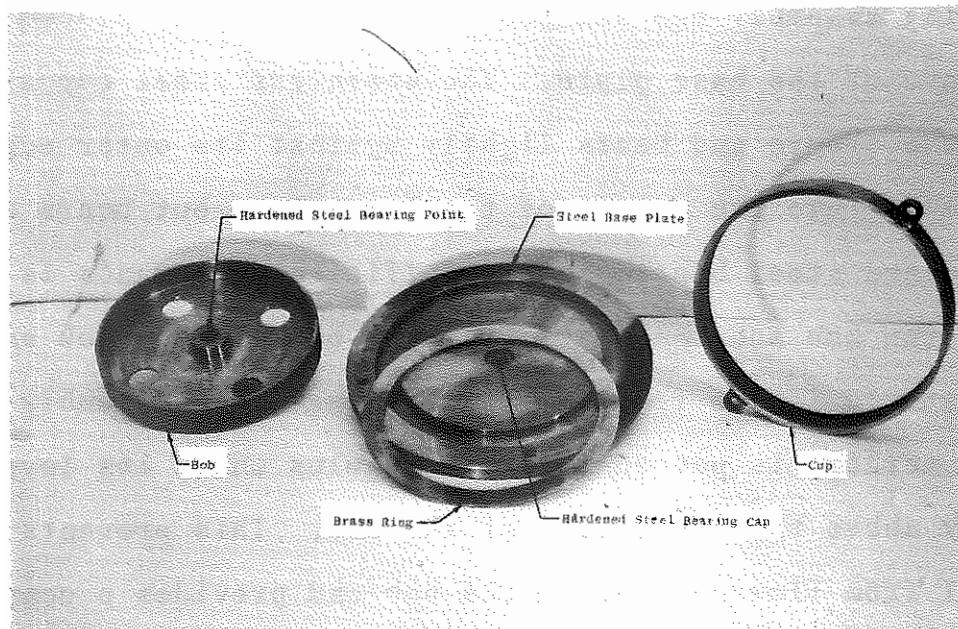


Figure 12. Large Cup-and-Bob Assembly.

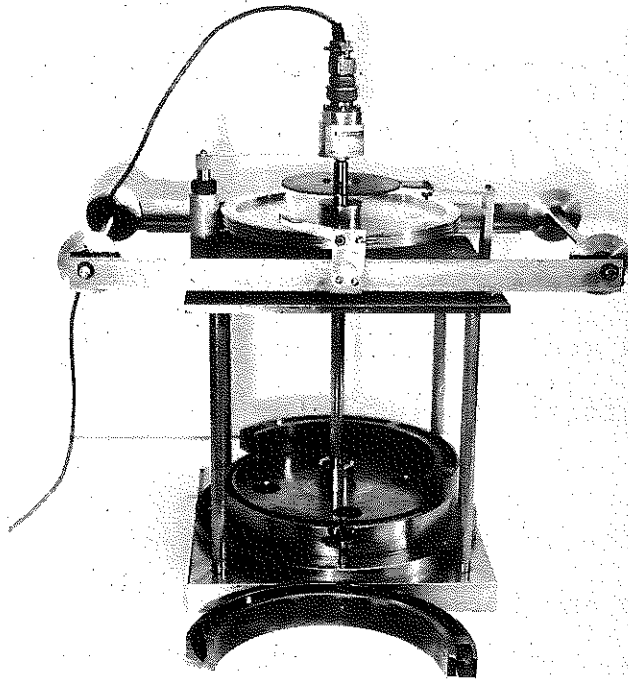


Figure 13. Pouring Mold Used with Large Cup-and-Bob Assembly.

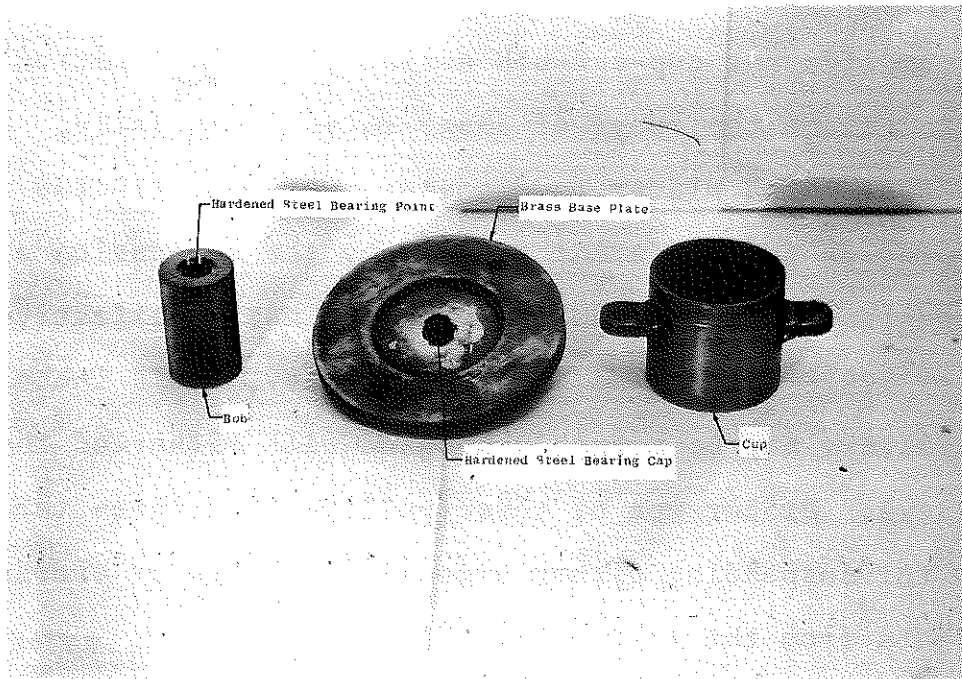


Figure 14. Small Cup-and-Bob Assembly.

This mold, which is constructed in two semi-circular sections, is supported by and temporarily mounted on the bob. Its narrow discharge opening ($3/32$ inch), which is centered over the annulus, permits the annulus to be progressively filled from the bottom to the top. This eliminates the necessity for heating the cup-and-bob assembly (which would be hazardous due to the presence of mercury) and prevents the inclusion of voids within the specimens.

Components of the small cup-and-bob assembly are shown in Figure 14. The cup and bob are made of stainless steel and the base plate of brass. The cup, bob, and base plate are assembled in much the same manner as for the larger assembly with the exception that no brass ring is used. A pouring mold is unnecessary due to the increased thickness of the annulus.

The two different cup-and-bob assemblies were constructed in order to extend the range of shear rates. Similarly, two drive pulleys, which differ in diameter, were constructed in order to provide two different torques by the suspension of a load of constant weight. The large pulley has an effective diameter of 7.875 inches and the small pulley, 3.875 inches. The idle pulleys may be properly aligned with either of the two drive pulleys. Proper use of these pulleys eliminates the necessity for suspending either excessively large or excessively small weights from the loading system.

Cups and bobs for both assemblies are provided with $1/64$ -inch-deep vertical grooves extending their full lengths. These grooves prevent the formation of slippage surfaces at the inter-

faces due to insufficient adhesion between the cup or bob and the specimen. The effective dimensions of the cups, bobs, and specimens are shown in Table 1.

TABLE 1
EFFECTIVE DIMENSIONS OF CUP, BOB, AND SPECIMEN

Item	Small Assembly	Large Assembly
Cup		
Diameter (in.)	2.005	7.741
Height (in.)	2.023	1.115
Bob		
Diameter (in.)	1.235	7.365
Specimen		
Thickness (in.)	0.385	0.188
Height (in.)	Variable, 2.023 Max.	Variable, 1.115 Max.

MATERIALS

The 13 asphalt cements used in this study were selected on the basis of the following factors: (1) crude source, (2) penetration grade, and (3) manufacturing process. Table 2 classifies the asphalts on the basis of these three factors. The asphalt numbers are identical to those used by the Bureau of Public Roads (44, 45) with the exception of asphalts PR-103 and PR-132 which were not evaluated by the Bureau. However, the asphalt samples were obtained from current production runs for which the refining processes and crude sources may have been slightly altered. Therefore, direct comparison between the results of this study and those of the earlier studies (44, 45) must be avoided.

TABLE 2
 CRUDE SOURCES, PENETRATION GRADES, AND
 MANUFACTURING PROCESSES FOR ASPHALT CEMENTS

Asphalt Number	Crude Source	Penetration Grade	Method of Manufacture ¹
3	Mexico	85-100	S
13	Venezuela	85-100	V,S
45	Arkansas	85-100	V,S
53	Midcontinent	85-100	V,O
67	Texas	85-100	V
71	Midcontinent	85-100	V,P,B
72	Oklahoma	85-100	V,P,O,F
91	California	85-100	V,S,B,O
116	Wyoming	85-100	V
127	Venezuela	60-70	V,S
200	Venezuela	120-150	V,S
PR-103	Unknown	141 ²	-3
PR-132	Unknown	24 ²	-3

¹V = vacuum distillation, S = steam distillation, O = blowing (oxidation), B = blending (different grade asphalts), P = propane fractionation, and F = fluxing (heavy oils).

²Test values.

³Petroleum pitch residue derived from cracking petroleum feed stocks for the production of ethylene.

Essentially six different crude sources based on geographical location were studied¹. To investigate the variation in mechanical properties as related to penetration grade, three different grades (PAC-3, PAC-5, and PAC-7) from the Venezuelan crude were studied. Attempts were made to obtain samples which represented straight-run distillation, straight-run distillation with air blowing, and cracking manufacturing processes. As seen in Table

¹These included Midcontinent, Gulf-Coastal, Rocky Mountain, Californian, Mexican, and Venezuelan crudes.

2, the asphalts are representative of the first two of these three processes. Asphalts manufactured by the cracking process were not available for testing. However, asphalts PR-103 and PR-132 were included in the test program since their properties are similar in nature to those of cracked asphalts despite their somewhat greater temperature susceptibilities.

The results of standard laboratory tests performed on the asphalt cements are presented in Table 3. The 85-100 penetration grade asphalts exhibited essentially similar properties with the exception of the low Saybolt Furol viscosities of asphalts 91 and 116. The thin film oven loss was somewhat high for asphalt 13 in comparison to the other 85-100 penetration asphalts but was properly ordered with respect to asphalts 127 and 200 which were obtained from the same crude source and refining process.

TEST PROCEDURE

Each asphalt was tested at temperatures of 39.2, 77, and 104°F. At each temperature, a minimum of three intensities of torque were applied. These intensities were chosen so as to provide significant angular displacements in a reasonable period of time. In order to avoid possible effects of strain history, a new specimen was used for each increment of torque. A single specimen was tested for each combination of temperature and torque.

Table 4 summarizes most of the testing reported as a portion of this study phase. Only the small cup-and-bob assembly was employed for these tests. The large drive pulley was used for

TABLE 3
RESULTS OF STANDARD TESTS ON ASPHALTS

Asphalt Number	Penetration			Ductility		Softening Point (°F)	Specific Gravity @77°F	Saybolt Furoil Viscosity @275°F (sec)	Thin Film Oven Test		
	Grade	100 gm 5 sec 77°F (.1 mm)	200 gm 60 sec 39.2°F (.1 mm)	Pen. ratio 39.2/77 (%)	5 cm/min 77°F (cm)				1 cm/min 39.2°F (cm)	% Loss	Pen. Res. Pen. Orig. (%)
3	85-100	87	43	49	150+	56	121	1.035	267	0.27	63
13	85-100	88	31	35	150+	84	125	1.032	253	0.73	37
45	85-100	92	29	32	150+	30	114	1.020	189	+0.09	62
53	85-100	86	33	38	150+	22	120	0.998	159	+0.28	67
67	85-100	90	41	46	150+	14	122	1.031	215	0.06	59
71	85-100	90	22	25	96	48	112	1.005	146	+0.02	64
72	85-100	95	37	39	150+	24	116	0.994	175	+0.54	58
91	85-100	96	25	26	150+	150+	111	1.013	84	0.09	69
116	85-100	88	28	32	150+	8	113	1.023	76	0.03	53
127	60-70	60	29	49	150+	16	119	1.033	348	0.65	50
200	120-150	122	40	33	150+	110	113	1.032	250	1.26	40
PR-103		141	50	35	-	110+	106	1.167	22	10.98	5
PR-132		24	2	8	-	-	134	1.163	43	7.54	0

TABLE 4
TEST PROGRAM

Asphalt Number	Temperature (°F)	Total Load (gms)	Approximate Shearing Stress			
			Maximum (d/cm ²)	Average (d/cm ²)	Minimum (d/cm ²)	
All Asphalts ¹	39.2	800	107,700	66,400	40,900	
		1,400	189,800	116,200	71,500	
		2,000	269,000	166,000	102,200	
	77	45	2,920	1,800	1,110	
		90	5,840	3,600	2,220	
		135	8,760	5,400	3,330	
		180	11,680	7,200	4,440	
	104	10	649	400	246	
		15	973	600	370	
		20	1,298	800	492	
		25	1,620	1,000	615	
	3 ²	39.2	800	107,700	66,400	40,900
			1,200	161,400	99,600	61,400
			1,600	215,000	133,000	81,800
			2,000	269,000	166,000	102,200
200 ²	39.2	400	53,800	33,200	20,400	
		600	80,600	49,800	30,700	
		800	107,700	66,400	40,900	
PR-132 ²	39.2	No Tests				
	77	180	11,680	7,200	4,440	
		360	23,300	14,400	8,900	
		540	35,000	21,600	13,300	
		720	46,700	28,800	17,800	

¹All asphalts were tested under these conditions with the exceptions noted below.

²The tabulated data indicate how the testing for specific asphalts differed from the general testing program.

tests at 39.2°F, and the small pulley was used at the remaining two temperatures. The maximum and minimum shearing stresses noted in Table 4 were located at the surfaces of the bob and cup, respectively, and were computed using Equation 3. The average shearing stress through the annulus of the specimens was computed as follows:

$$S_{av} = T/2\pi a_1 a_2 L. \quad (36)$$

The procedures for preparing the viscometer and specimens for testing and for conducting the creep tests are described in Appendix A. These procedures were prepared to guide laboratory personnel by standardization of the test methods.

After each set of tests was completed, arithmetic plots of θ vs. t and Ω_0^1 vs. CT were constructed. These plots were analyzed to ascertain the characteristics of observed flow behavior. The detailed procedures of data analysis are more fully described in subsequent sections.

Ω_0^1 is the steady-state angular velocity of the bob relative to the cup.

PRESENTATION OF RESULTS

Creep curves, which are plots of the angle of rotation of the bob relative to the cup and elapsed time, are the basic form of output from the viscometer. The graphs of such curves for asphalt 72 are shown in Figure 15. These graphs are similar in shape to those for all of the other asphalts and, therefore, may be considered typical creep curves. One graph has been constructed for each of the three test temperatures and an individual curve has been drawn for each value of the CT product -- that is, each level of shearing stress. The scales for each of these three graphs were chosen so as to best represent the extent of testing accomplished and, for this reason, are not identical. The curves do, however, retain their same relative shapes when identical scales are used.

It is readily apparent that the complexity of flow is influenced by the test temperature. For the duration of each test at temperatures of 104°F and 77°F, a linear relationship was observed between the angle of rotation and time. In each case, the experimental line may be assumed to pass through the origin. This behavior is indicative of steady-state flow. However, at 39°F a slight intercept with the angle-of-rotation axis was observed¹, a distinct curvature was noted for small times, and a linear condition was approached as the test progressed. This behavior is similar to that depicted by Figure 8 which

¹This is not readily apparent from Figure 15 because of the scale that was used for this presentation.

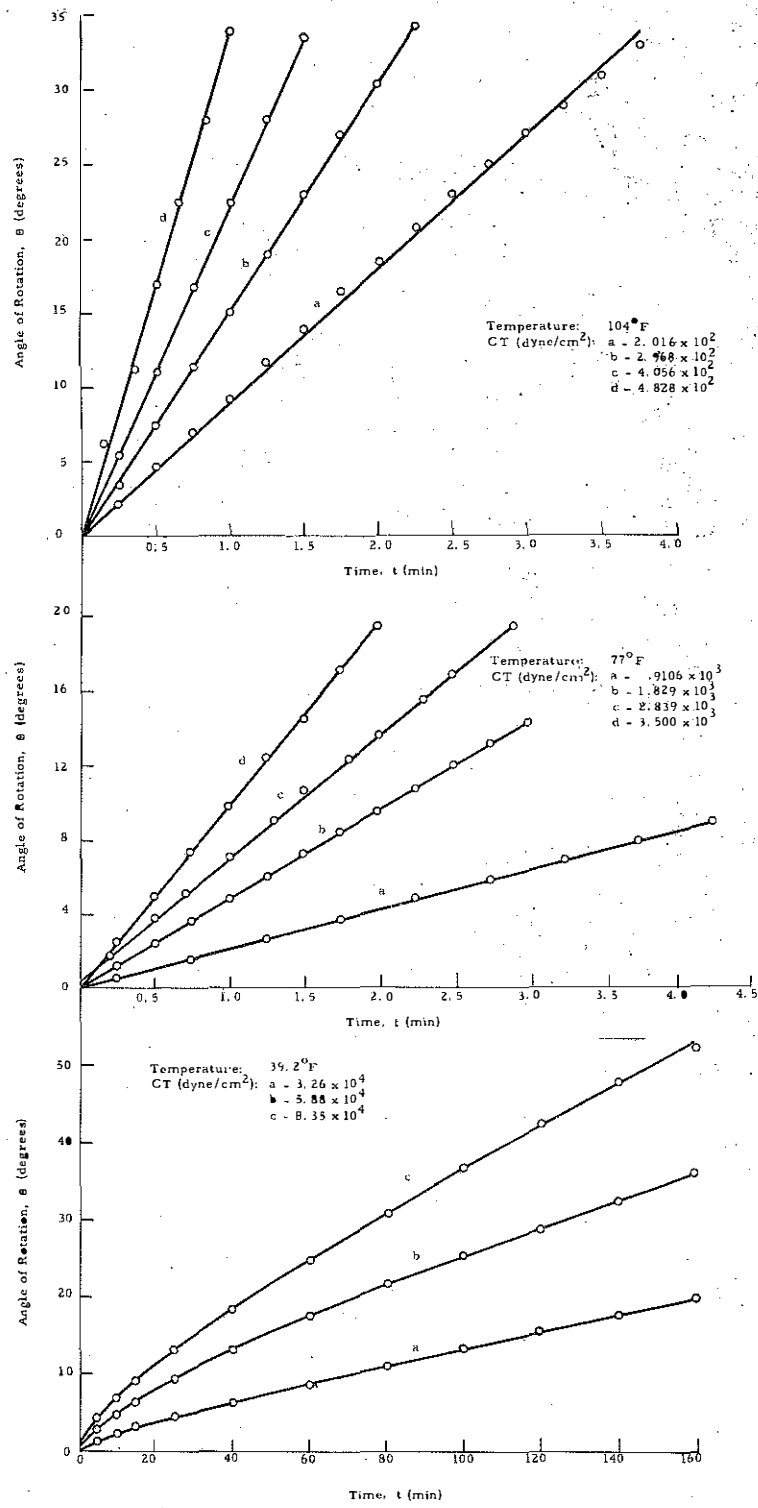


Figure 15. Creep Curves for Asphalt 72 at Three Temperatures.

represents a material exhibiting instantaneous elasticity, viscoelasticity, and steady-state flow.

TESTS AT 104°F

Angle of rotation vs. time plots were constructed for the tests at 104°F. The form of these plots revealed that all of the asphalts exhibited steady-state flow behavior at this temperature. The steady-state, angular velocity, Ω_0 , was then determined from the slope of the linear θ -t plot for each test condition. Figure 16 shows the relationship between the steady-state velocity and the CT product for each of the 13 asphalts. The curves of this figure show distinct linear relationships with extrapolated intercepts on the CT axis. Comparing this observed behavior with that summarized in Figure 6 for various ideal, steady-state liquids, it is concluded that each of the asphalts behave essentially as Bingham plastics at 104°F. The flow behavior of an ideal Bingham plastic in a rotating coaxial cylinder viscometer is more clearly depicted in Figure 4.

After the manner suggested in Figure 4, the yield stress, S_y , and the coefficient of plastic viscosity, η_p , were evaluated for each of the asphalts. The results of this evaluation are presented in Table 5. The yield stresses are quite small and range in value from 108 dynes/cm² to 216 dynes/cm². Since the minimum applied shearing stress of 246 dynes/cm² (from Table 4) exceeded all yield stresses, flow occurred throughout the annulus of the material and Equation 18c adequately describes the flow behavior.

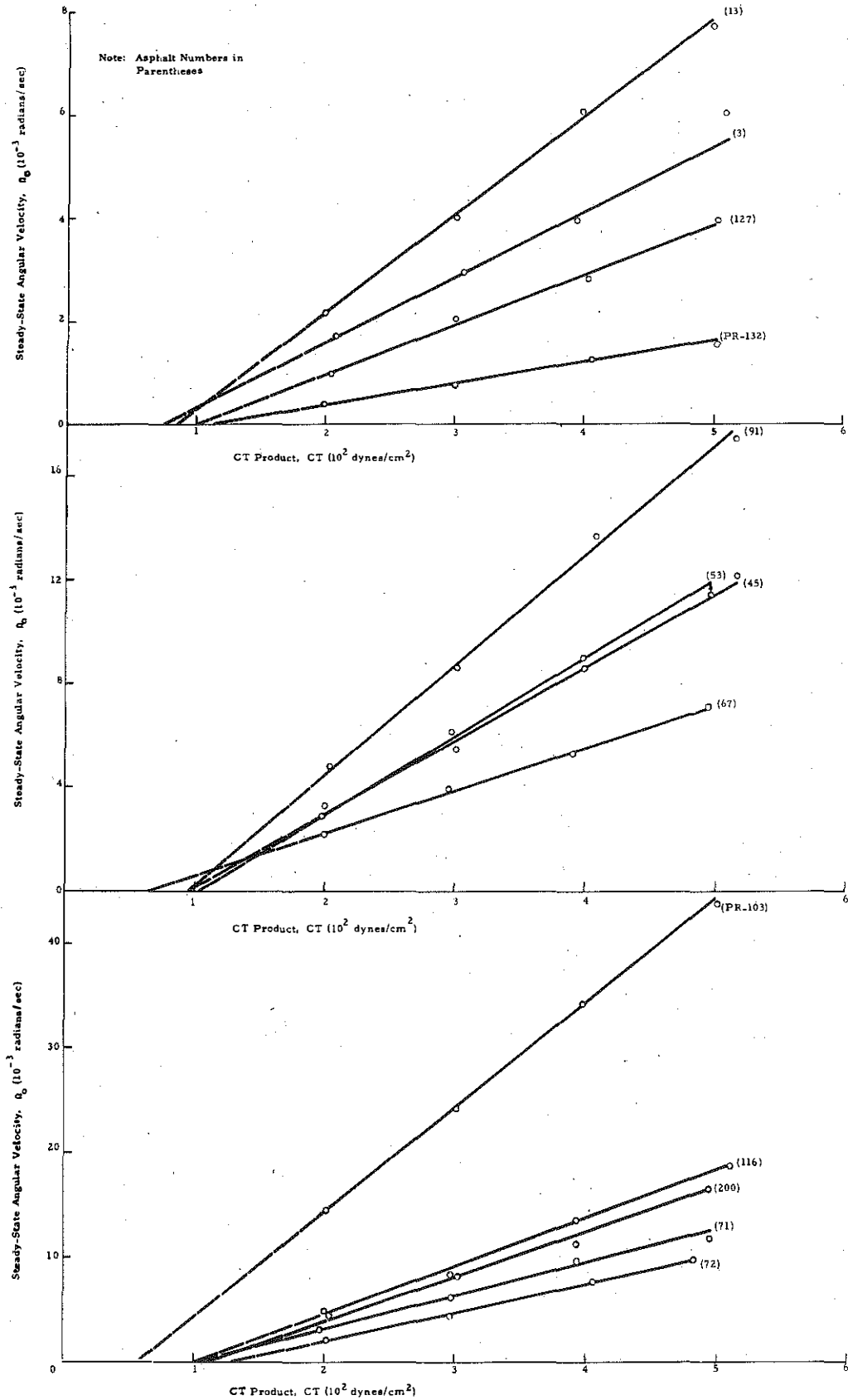


Figure 16. Steady-State Angular Velocity vs. CT Product for 104°F Tests.

TABLE 5

MATERIAL PARAMETERS EVALUATED AT 104°F

Asphalt Number	Yield Stress, S_y (10^2 dynes/cm 2) ^y	Coefficient of Plastic Viscosity, η_p (10^4 poises)
3	1.98	7.03
13	1.73	5.35
45	1.97	3.54
53	1.82	3.56
67	1.33	6.13
71	1.73	3.40
72	2.09	3.66
91	2.00	2.31
116	2.05	2.22
127	2.09	10.30
200	2.09	2.49
PR-103	1.08	1.02
PR-132	2.16	25.50

The coefficient of plastic viscosity exhibited considerably more variability among the asphalts than did the yield stress. The coefficient of plastic viscosity ranged from a minimum of 1.02×10^4 poises (asphalt PR-103) to a maximum of 25.50×10^4 poises (asphalt PR-132). No discernable relationship was found to exist between the yield stress and the coefficient of plastic viscosity.

The plastic viscosity measurements may be used to classify or group the asphalts on the basis of their consistency at 104°F. Such a classification is presented in Table 6. The viscosity intervals were selected so that their ranges were approximately identical on a logarithmic plot. It is interesting to note that two of the PAC-5 asphalts (91 and 116) were slightly less viscous at 104°F than the PAC-7 asphalt (200). It may be recalled that

TABLE 6

CLASSIFICATION OF ASPHALTS BY PLASTIC
VISCOSITY AT 104°F

Viscosity Interval (10 ⁴ poises)	Asphalt Numbers
1.0-1.6	PR-103
1.6-2.6	91,116,200
2.6-4.2	45,53,71,72
4.2-6.8	13,67
6.8-11.0	3,127
>11.0	PR-132

these two PAC-5 asphalts had relatively low Saybolt Furol viscosities and ring-and-ball softening points.

TESTS AT 77°F

The test results obtained at 77°F were analyzed in a manner similar to those at 104°F. Once again all of the asphalts exhibited steady-state flow throughout the test duration. Figure 17 shows the relationships between the steady-state, angular velocities and the CT product for all of the asphalts tested at this temperature.¹ As before, all of the asphalts (with the exception of asphalt 127) exhibited properties indicative of a Bingham plastic. Asphalt 127 had no discernable yield stress and was, therefore, assumed to exhibit pure Newtonian flow.

Table 7 summarizes the values of the material parameters evaluated at 77°F. The yield stresses are again quite low and

¹Asphalt PR-132, although tested at 77°F, was omitted from this figure because of its highly viscous properties when compared with the other asphalts. However, it also exhibited properties characteristic of a Bingham plastic.

Figure 17. Steady-State Angular Velocity vs. CT Product for 77°F Tests.

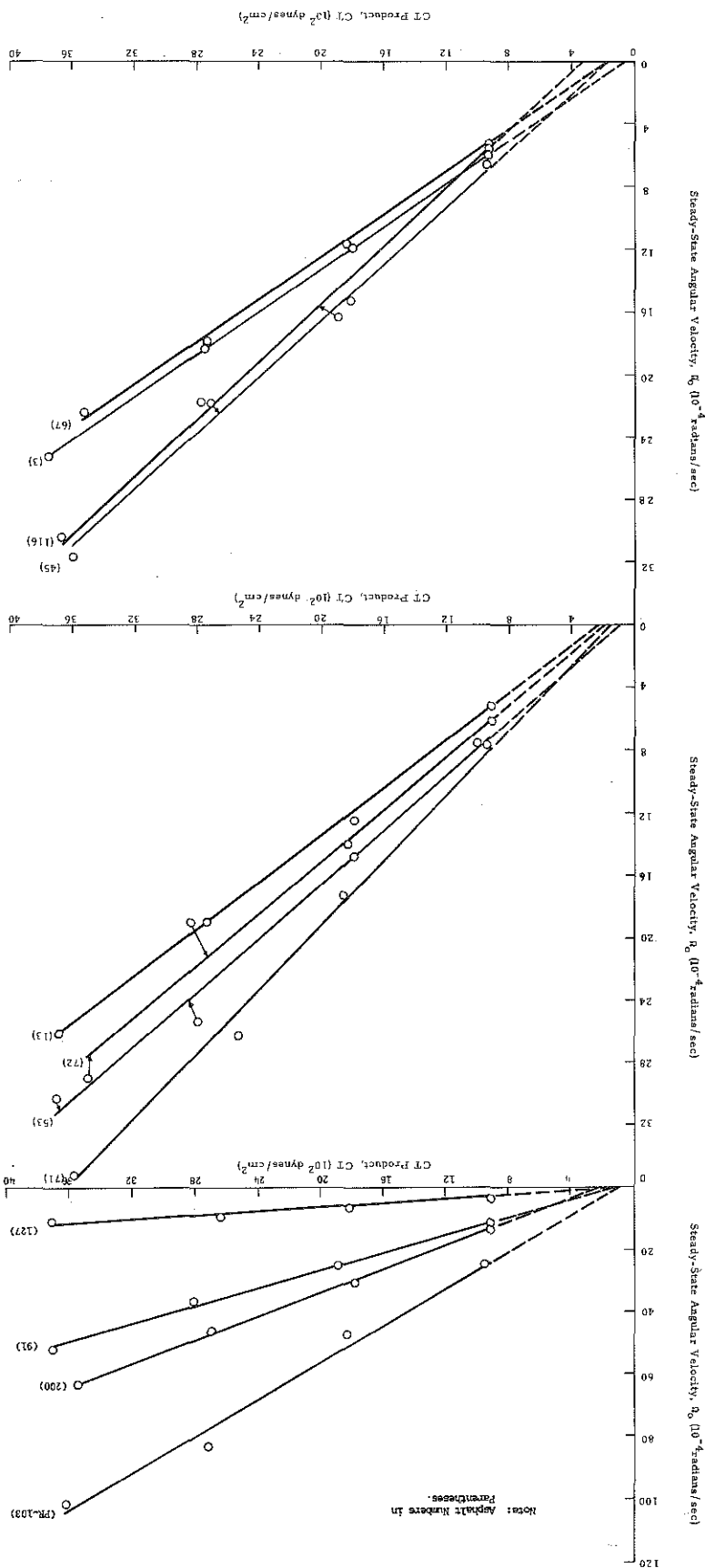


TABLE 7
MATERIAL PARAMETERS EVALUATED AT 77°F

Asphalt Number	Yield Stress, S_y (10^2 dynes/cm 2)	Coefficient of Plastic Viscosity, η_p (10^6 poises)
3	1.04	1.47
13	3.66	1.34
45	4.63	0.94
53	1.45	1.15
67	1.94	1.51
71	3.73	0.97
72	3.66	1.24
91	2.91	0.70
116	4.97	1.12
127	0	3.89
200	4.07	0.53
PR-103	8.56	0.34
PR-132	11.90	21.60

asphalts 3, 53, and 127 had smaller yield stresses at this temperature than they had at 104°F. This apparent inconsistency is attributed to a combination of experimental and graphical errors magnified in effect due to the small yield stress levels. Comparing the yield stresses of Table 7 with the minimum applied shearing stresses of Table 4, it is apparent that flow occurred throughout the annulus of each test specimen with the exception of asphalt PR-132. Asphalt PR-132 had a yield stress of 1,190 dynes/cm 2 which was slightly in excess of the minimum applied shearing stress of 1,110 dynes/cm 2 for one of the tests. Again no discernable relationship was found to exist between the yield stress and the coefficient of plastic viscosity.

The asphalts are grouped according to plastic viscosity at 77°F in Table 8. The asphalts maintained their same relative

TABLE 8
CLASSIFICATION OF ASPHALTS BY PLASTIC
VISCOSITY AT 77°F

Viscosity Interval (10^6 poises)	Asphalt Numbers
0.3-0.5	PR-103
0.5-0.8	91,200
0.8-1.4	13,45,53,71, 72,116
1.4-2.4	3,67
2.4-4.0	127
> 4.0	PR-132

grouping as at 104°F (Table 6) with the exception of asphalts 3, 13, and 116. Asphalts 3 and 13 became relatively less viscous due to their smaller temperature susceptibilities and asphalt 116 became relatively more viscous due to its greater temperature susceptibility.

TESTS AT 39.2°F

All of the test results at 39.2°F showed instantaneous elasticity and a combination of steady-state and viscoelastic flow. The creep curves were similar to those depicted in Figure 8 and Figure 15 (39.2°F). Each curve was analyzed by separating it into the three basic components (as shown in Figure 8); θ_1 which represents instantaneous elastic deformation, θ_2 which represents steady-state flow, and θ_3 which represents viscoelastic flow.

The instantaneous elastic deformation, θ_1 , is described by Equation 32. This equation may be used to evaluate the elastic

shear modulus, G_0 , providing θ_1 and CT are known. The angle, θ_1 , was determined by rapidly loading and unloading each sample a number of times and computing an average value for the instantaneous angle of rotation. This determination was made after each creep test was completed since θ_1 is time-independent and should not be influenced by previous stress history. The elastic shear modulus, G_0 , was determined from the slope of the linear plot of CT against θ_1 . Its value for each of the 12 asphalts tested at this temperature is summarized in Table 9.

TABLE 9
ELASTIC AND STEADY-STATE MATERIAL
PARAMETERS EVALUATED AT 39.2°F

Asphalt Number.	Elastic Modulus, G_0 (10^7 dynes/cm ²)	Yield Stress, S_y (10^4 dynes/cm ²)	Coefficient of Plastic Viscosity, η_p (10^8 poises)
3	2.67	1.12	3.32
13	3.20	1.46	5.51
45	3.04	0	8.66
53	2.70	0	9.85
67	2.26	2.75	5.11
71	1.89	1.86	9.52
72	2.08	1.10	9.63
91	1.95	0.37	4.61
116	2.04	2.05	19.40
127	1.83	0.90	14.80
200	1.56	0	2.47
PR-103	1.55	0	2.84
PR-132		Not Tested	

The steady-state flow deformation, θ_2 , is described by Equation 33. The steady-state, angular velocity of this equation was determined by computing the slope of the straight-line portion of each creep curve. A plot of these steady-state, angular velocities against CT product was made for each asphalt tested

at 39.2°F. The resulting graphs are presented in Figure 18. An analysis of these graphs indicates that the steady-state portion of flow is similar in some cases to that of Bingham plastics and in other cases to that of Newtonian materials. The distinction appears to be relatively insignificant, however, due to possible errors occasioned in extrapolation of the Ω_0 -CT curve to its intercept on the CT axis and the relatively small intercepts that were observed.

The yield stress, S_y , and the coefficient of plastic viscosity, η_p , were evaluated from the steady-state behavior of each asphalt using the curves of Figure 18. The results of this evaluation are also summarized in Table 9. The yield stresses are relatively small and are exceeded in every case by the minimum applied shearing stresses (compare with Table 4). Once again, this indicates that steady-state flow occurred throughout the annulus of the test material. The steady-state flow deformation, θ_2 , may then be computed using Equations 18c and 33.

The asphalts are grouped according to their plastic viscosity at 39.2°F in Table 10. Again there were slight readjustments from the groupings at 104°F (Table 6) and 77°F (Table 8) which were caused by different temperature susceptibilities of the various asphalts.

The viscoelastic flow deformation, θ_3 , is described by Equation 27. To evaluate the constants, J_k and τ_k , of Equation 27, the following procedure was employed. First, θ_3 was computed as follows:

$$\theta_3 = \theta - CT/G_0 - \Omega_0 t \quad (37)$$

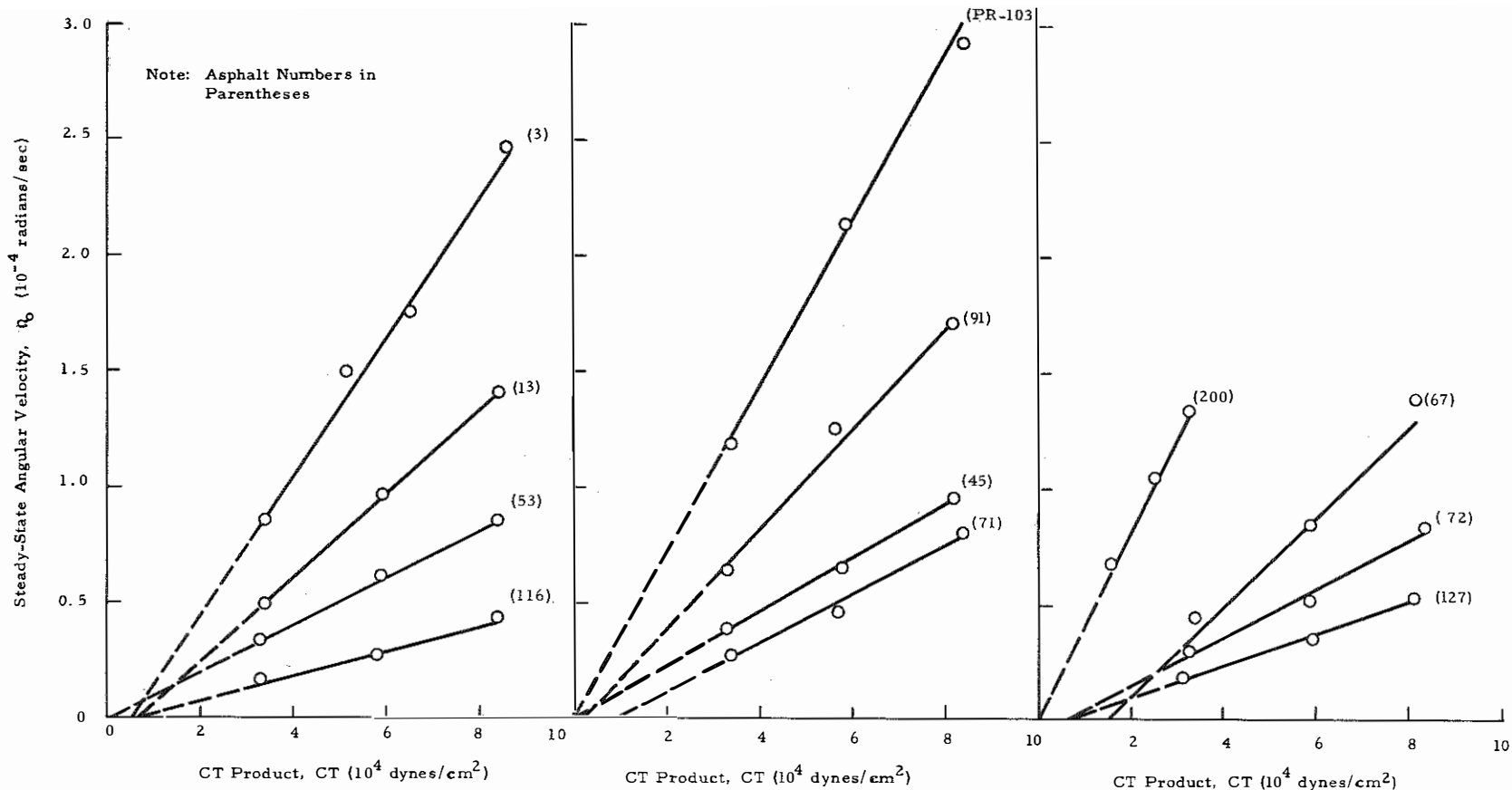


Figure 18. Steady-State Angular Velocity vs. CT Product for 39.2°F Tests.

TABLE 10

CLASSIFICATION OF ASPHALTS BY PLASTIC
VISCOSITY AT 39.2°F

Viscosity Interval (10^8 poises)	Asphalt Numbers
2.4-3.7	3, PR-103, 200
3.7-5.6	13, 67, 91
5.6-8.5	"
8.5-13.1	45, 53, 71, 72
13.1-20	116, 127

where θ_3 = viscoelastic flow deformation

θ = total observed angle of rotation

G_0 = experimentally evaluated elastic shear modulus

Ω_0 = experimentally evaluated steady-state angular velocity.

Equation 37 simply states that the viscoelastic flow deformation equals the total deformation less its components of steady-state flow and instantaneous elasticity. The quotient of θ_3 and the CT product is the creep function, ψ , for viscoelastic flow behavior and is ideally independent of shearing stress (see Equations 29 and 31). Thus,

$$\psi(t) = (\theta - CT/G_0 - \Omega_0 t)/CT. \quad (38)$$

The experimental creep function for each of the asphalts and each level of applied shearing stress was computed using the above procedures. Figure 19 shows the results for asphalt 72. The creep functions for the three different stress levels should theoretically coincide if the viscoelastic behavior were linear and there were no experimental errors. Figure 19 shows that the experimental creep functions for asphalt 72 are obviously not identical. The data for this asphalt are representative of those

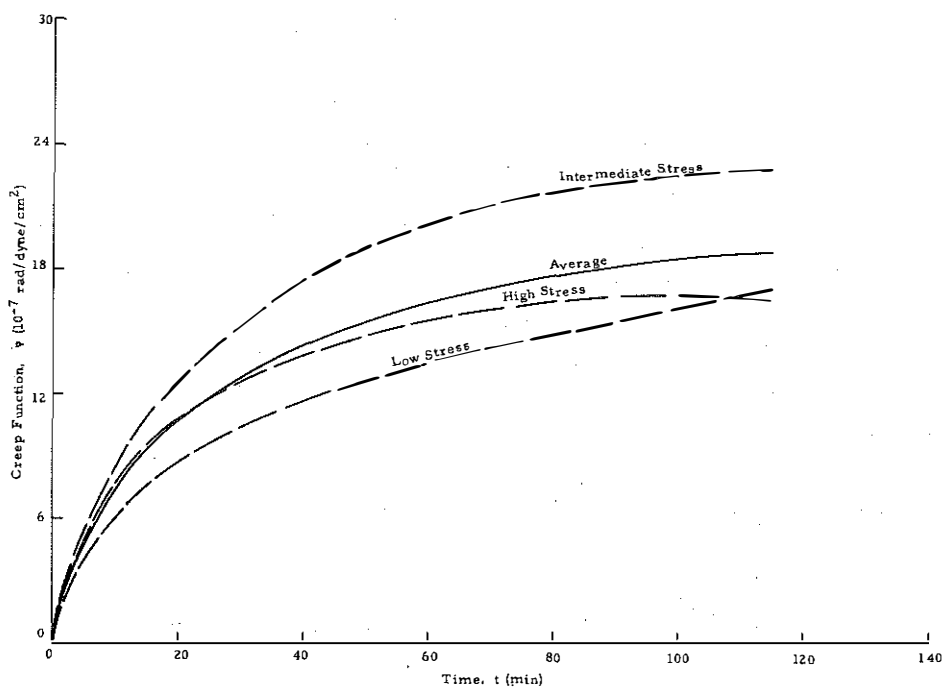


Figure 19. Experimental Creep Functions for Asphalt 72 at 39.2°F.

for the other asphalts. The results among the different asphalts were not predictable, however, in that the largest creep function generally occurred at the smallest stress level for six of the asphalts, at the intermediate level for four of the asphalts, and at the largest level for two of the asphalts.

Since there was apparently no consistent relationship between creep function and stress level, it was felt that the discrepancies among the creep functions could probably be attributed to experimental and graphical errors rather than to material behavior. This conclusion was substantiated by comparing the creep functions computed on the basis of the total angle of rotation, θ , with those computed on the basis of θ_3 . The absolute value of the

differences among the total-angle creep functions for the three stress levels averaged about 6 percent while for the θ_3 creep functions this average difference was about 25 percent. Since the discrepancies in the total-angle creep functions were acceptably small (average of 6 percent) and well within the limits of experimental error, the asphalts appear to behave linearly under the conditions of test employed herein. Therefore, the larger discrepancies observed in the θ_3 creep functions (average of 25 percent) are most probably due to experimental and graphical errors.

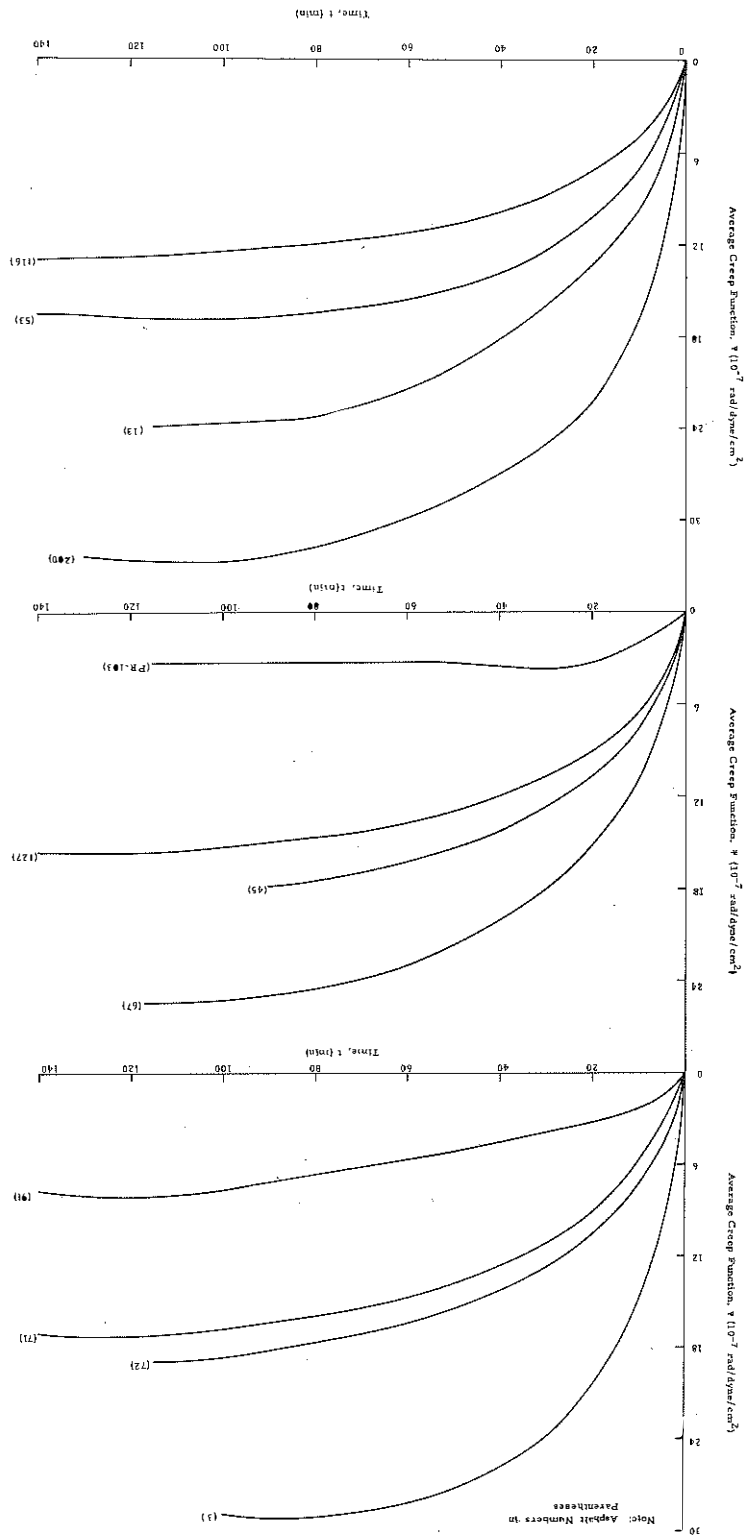
Despite these errors, it is felt that the creep functions do furnish a reliable indication of the general viscoelastic properties of the materials. Thus, an average creep function was calculated for each asphalt and this average was used in the evaluation of the viscoelastic parameters, G_k and τ_k . Figure 20 shows the average creep functions, computed on the basis of θ_3 , which were used in this analysis.

On the basis of Equation 29, the creep function for linear viscoelastic behavior is as follows:

$$\Psi(t) = \sum_{k=1}^n [1 - \exp(-t/\tau_k)]/G_k. \quad (39)$$

A curve-fitting technique, which is described in detail in Appendix B, was developed and used to evaluate the material parameters of Equation 39. The material parameters were selected so that a best fit by the least squares criterion was achieved between the theoretical relationship of Equation 39 and the observed, average creep functions for the various asphalts. The number of Voigt elements, n , was varied beginning

Figure 20. Average Creep Functions for All Asphalts at 39.2°F.



with one and increasing by increments of one until the computed values of the creep function were in satisfactory agreement with the observed values. The technique was programmed for the IBM 7040 computer: a discussion of this program is included as Appendix C.

A print-out of the results for asphalt 72 is included for illustration as Figure 21. The basic data for the analysis are given in the columns aligned beneath the heading "Data Sheet". The values of the observed, total angle of rotation and the θ_3 creep function computed for each value of the CT product are printed for selected values of elapsed time. The headings "THETA 1" and "CF 1" correspond to the observed, total angle of rotation and the computed creep function respectively for the smallest CT product noted in the heading; "THETA 2" and "CF 2" correspond to the intermediate CT product; and, finally, "THETA 3" and "CF 3" correspond to the largest CT product. Only three levels of the CT product are permitted. The average creep function for these three levels is shown in the last column of the "Data Sheet".

Information concerning the equation of best fit is given in the set of columns aligned beneath the heading, "Equation of Best Fit". One such set of columns is shown for each value of n , the number of Voigt elements in the model. For a two-element model, for example, "TAU1", "G1", and "VISC1" refer to the retardation time, shear modulus, and coefficient of viscosity, respectively, for the first element while "TAU2", "G2", and "VISC2" refer to the same values for the second element. The values shown for these parameters are those derived from the

Figure 21. Viscoelastic Analysis for Asphalt 72 at 59.2°F.

SAMPLE INFORMATION								TEST INFORMATION						CALCULATED INFORMATION					
SPECIAL TESTS				TEST OF USE FOR				TEST NUMBER		TEST DATE		TEST TIME		TEST LOCATION		TEST OPERATOR		TEST INSTRUMENT	
TEST NAME	TEST CODE	TEST RESULT	TEST UNIT	TEST NAME	TEST CODE	TEST RESULT	TEST UNIT	TEST NO.	TEST DATE	TEST TIME	TEST LOCATION	TEST OPERATOR	TEST INSTRUMENT	TEST NO.	TEST DATE	TEST TIME	TEST LOCATION	TEST OPERATOR	TEST INSTRUMENT
TEST 1	ASPHALT 72	59.2°F	ASPHALT 72	TEST 2	ASPHALT 72	59.2°F	ASPHALT 72	TEST 3	ASPHALT 72	59.2°F	ASPHALT 72	TEST 4	ASPHALT 72	59.2°F	ASPHALT 72	TEST 5	ASPHALT 72	59.2°F	ASPHALT 72
<p>Detailed table with columns for Modulus, Phase Angle, and other parameters. The table contains multiple rows of numerical data, including values for storage modulus, loss modulus, and phase angle across various frequencies.</p>																			

least squares criterion and, hence, represent the best values for the two-element model. The first three pairs of columns compare the observed total angles of rotation for the three stress levels with those calculated on the basis of the generalized model (Equation 35). The last two columns show a comparison between the observed average creep function and the creep function computed from Equation 39 using the tabulated values of G_k and τ_k . The standard deviations between the observed and calculated values are printed at the bottom of each pair of "observed" and "calculated" columns. As a matter of record, the output for all of the asphalts tested at 39.2°F is included as Appendix D.

The best correlation between the observed and computed creep functions was obtained for asphalt 72. Figure 22 depicts the data for this asphalt. The agreement between the observed creep function and that computed for the three-element model is considered quite acceptable and no significant improvement can be realized by increasing the number of elements. The worst correlation was obtained for asphalt 3, the data for which are shown in Figure 23. The two-element model is considered optimal in this instance since further increases in the number of elements do not significantly improve the correlation.

The viscoelastic material parameters for all of the asphalts are summarized in Table 11. The optimal number of Voigt elements was selected as that number beyond which significant increases in the degree of correlation between the observed and computed creep functions could not be achieved. This selection was made by

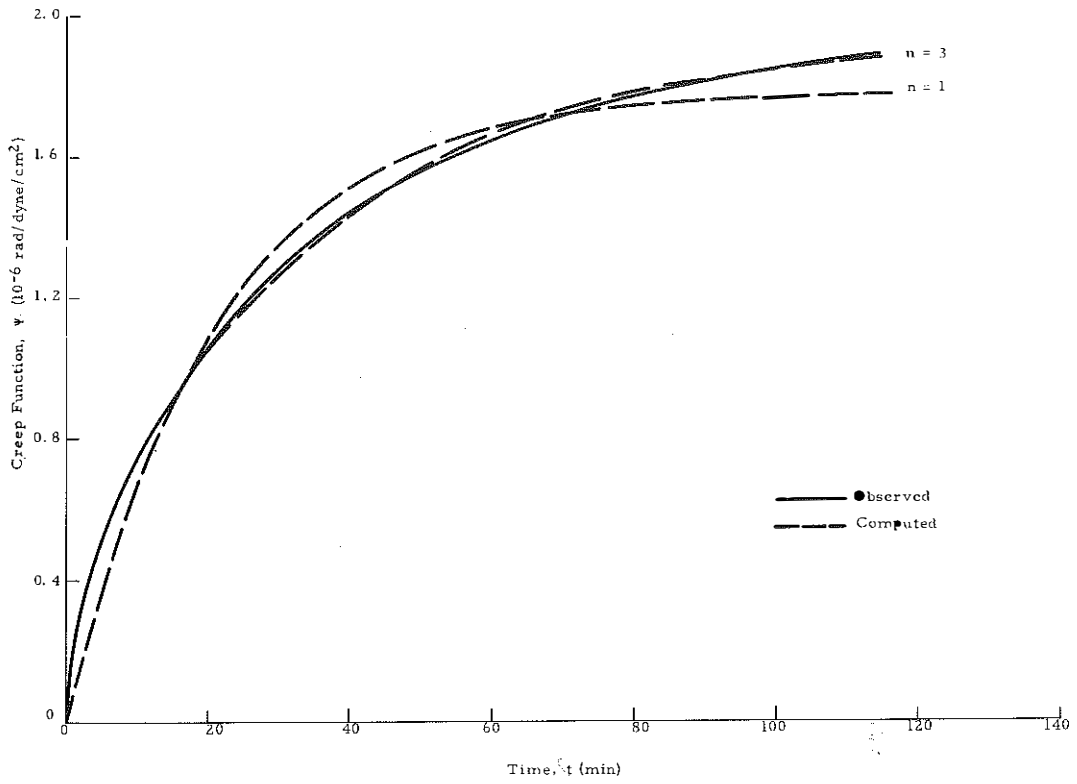


Figure 22. Comparison Between Observed and Computed Creep Functions for Asphalt 72.

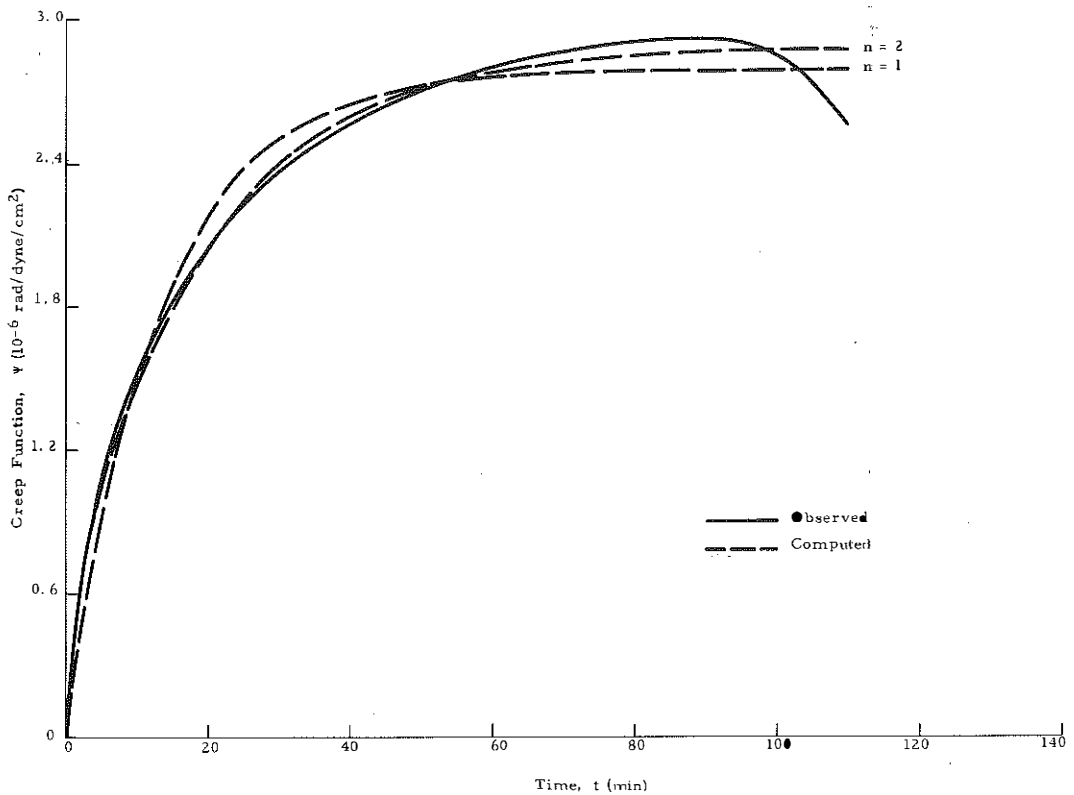


Figure 23. Comparison Between Observed and Computed Creep Functions for Asphalt 3.

TABLE II

VISCOELASTIC MATERIAL PARAMETERS EVALUATED AT 39.2°F

Asphalt Number	Optimal Number of Voigt Elements	Viscoelastic Parameters						Standard Deviation (10 ⁻⁸ rad/d/cm ²)
		First Element		Second Element		Third Element		
		G ₁ (10 ⁶ d/cm ²)	n ₁ (10 ⁹ poises)	G ₂ (10 ⁶ d/cm ²)	n ₂ (10 ⁹ poises)	G ₃ (10 ⁶ d/cm ²)	n ₃ (10 ⁹ poises)	
PR-103	1	3.17	1.38					2.60
3	2	0.41	1.1	2.27	0.15			4.35
13	2	0.48	1.02	2.34	0.26			2.34
53	2	0.68	1.09	4.18	0.46			1.50
71	2	0.64	1.26	5.82	0.62			0.94
91	2	1.09	5.67	9.54	0.27			3.30
116	2	0.86	1.47	7.76	0.63			3.41
45	3	0.70	1.54	2.92	1.05	7.92	0.21	0.64
67	3	0.49	0.95	2.38	0.46	7.64	0.10	1.49
72	3	0.67	1.52	3.06	1.09	7.69	0.21	0.61
127	3	0.81	1.68	3.82	0.92	12.10	0.21	0.90
200	3	3.71	0.11	0.53	1.07	0.87	0.33	2.92

¹ 1.70 x 10³⁸ poises

ascertaining the minimum number of elements for which the decrease in standard deviation due to an increase of one in the number of elements was less than 20 percent.

No particular physical significance should be attached to the optimal numbers of elements given in Table 11 since the analysis was based on empirical correlations and curve-fitting techniques. What is of importance, however, is the fact that the viscoelastic portion of the total flow behavior can be closely approximated by the generalized Voigt body consisting of a maximum of three elements.

ANALYSIS OF RESULTS

APPARENT VISCOSITY

The method for evaluating material parameters which has been used in preceding sections is based on an analysis of the complexity of flow exhibited by each asphalt under each set of test conditions. At the same time, the rotating coaxial cylinder viscometer can also be used to obtain a shear-dependent, apparent viscosity¹ which does not require an evaluation of the complexity of flow. The apparent viscosity is computed as follows:

$$\eta_a = \frac{CT}{\Omega} \quad (40)$$

where η_a = apparent viscosity

Ω = angular velocity of bob relative to cup.

The corresponding rate of shear and average rate of shear are given by Equations 15 and 16, respectively, which are repeated here for convenience.

$$\dot{\gamma}(r) = \left[\frac{2}{1/a_1^2 - 1/a_2^2} \right] \left[\frac{1}{r^2} \right] \Omega \quad (15)$$

¹The apparent viscosity (46) is the ratio of shearing stress to rate of shear and, for non-Newtonian liquids, is dependent upon rate of shear and, in some instances, upon shearing stress.

$$\dot{\gamma}(\text{av}) = \frac{2a_1a_2}{a_2^2 - a_1^2} \Omega \quad (16)$$

The angular velocity in these equations may be defined simply as the quotient of the angle of rotation and elapsed time. Figure 24 shows a hypothetical creep curve that may be used to

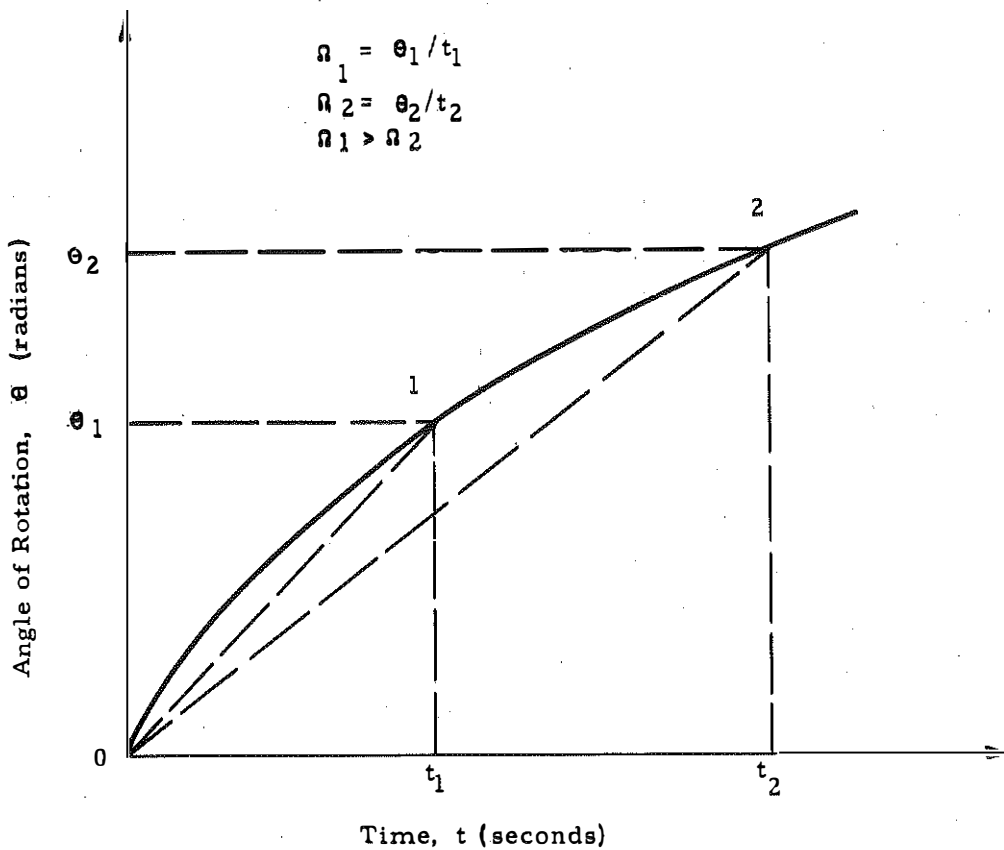


Figure 24. Evaluation of Angular Velocity by Secant Method.

illustrate this method of defining angular velocity by the secant method. For a creep curve having this characteristic shape, the angular velocity at point 1 exceeds that at point 2. According

to Equations 15, 16, and 40, the apparent viscosity is, therefore larger at point 2 while the shear rate is larger at point 1. Thus, for this type of creep testing and non-Newtonian materials, the apparent viscosity is obviously a function of shear rate.

When the shearing stress is changed, an entirely new relationship is obtained. This is illustrated in Figure 25 which shows viscosities obtained for asphalt 3 at 39.2°F. At this temperature, asphalt 3 has a creep curve similar in shape to

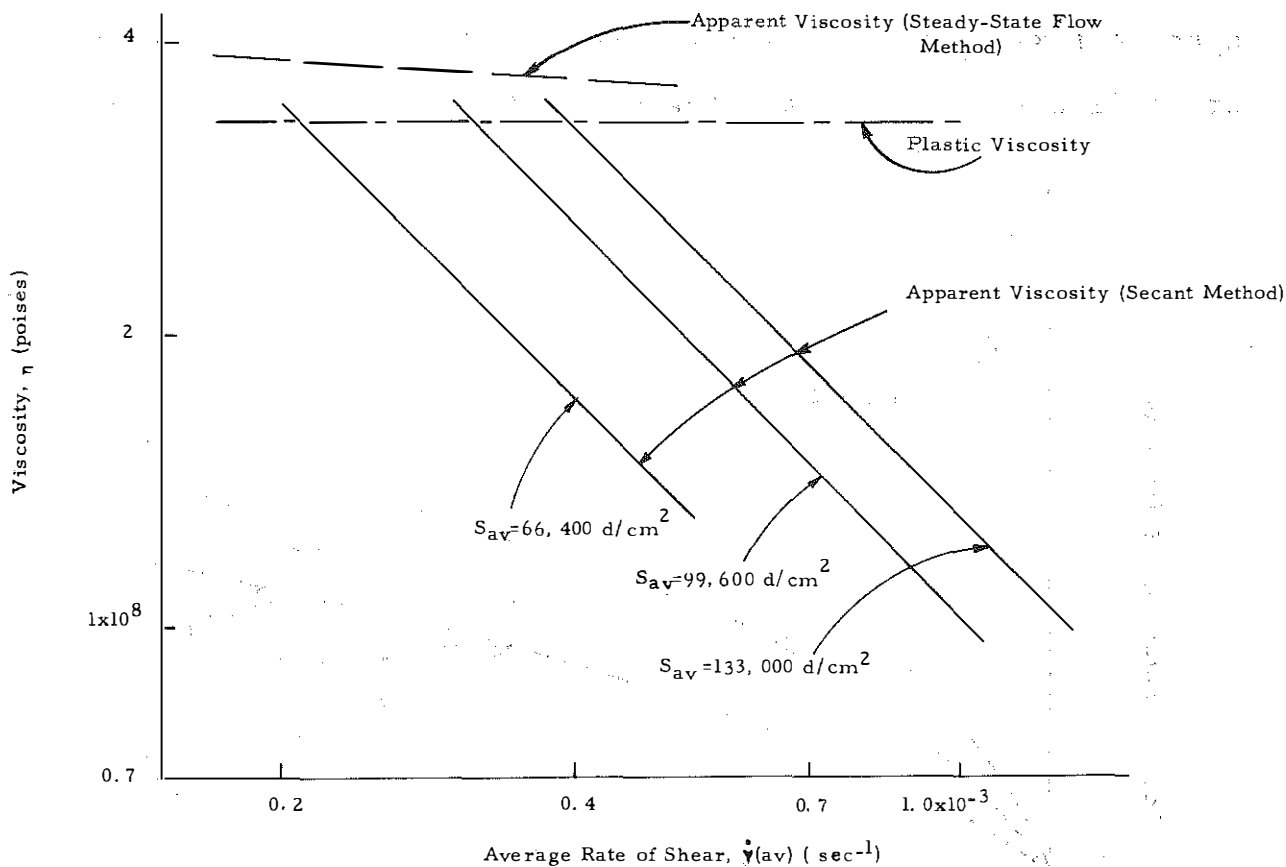


Figure 25. Comparison of Viscosities of Asphalt 3 at 39.2°F.

that shown in Figure 24. Examine now only those curves of Figure 25 for which the apparent viscosities have been computed using the previously explained secant method of defining angular velocity. The secant, apparent viscosity is obviously a function of both shearing stress and shearing rate.

Because of this dependence of the secant, apparent viscosity on both shearing stress and shearing rate, it is usual to redefine the angular velocity of Equation 40 as that velocity corresponding to steady-state flow (47). Figure 26 shows hypothetical creep curves which extend into the region of steady-state flow -- that is, the region in which there is a linear

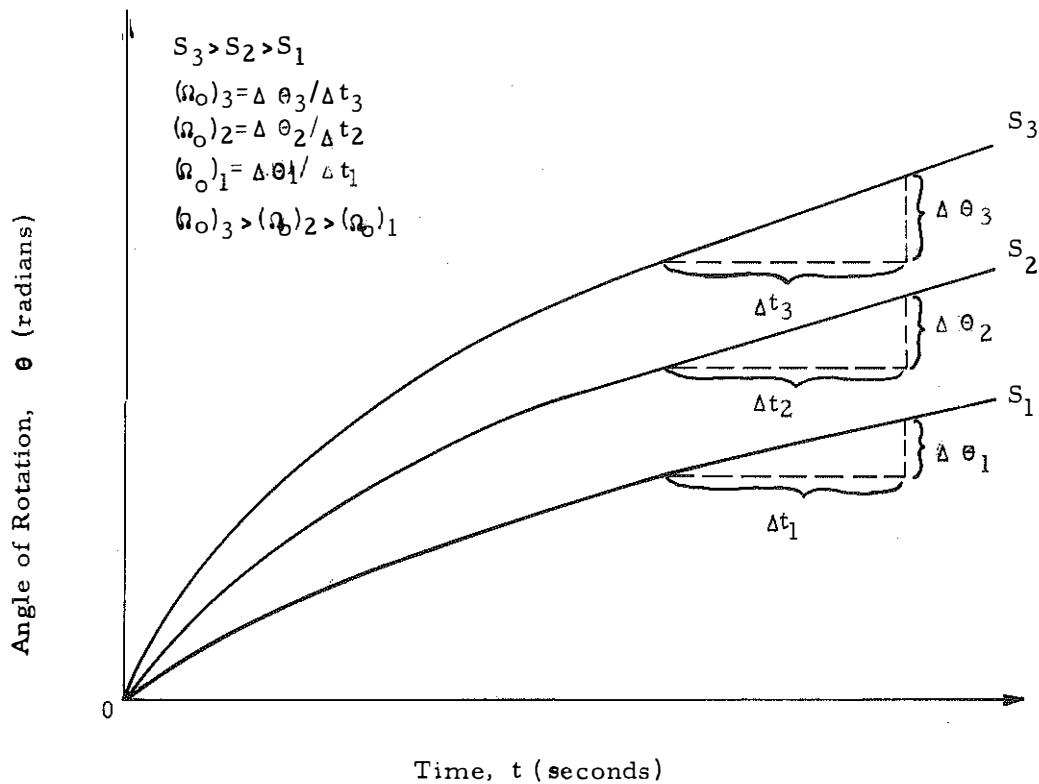


Figure 26. Evaluation of Angular Velocity in Region of Steady-State Flow.

relationship between angle of rotation and time. The steady-state, angular velocity then equals the slope of the creep curve in this region. Both the angular velocity and the shear rate in the steady-state region increase as the stress level is increased. Since the secant, angular velocities for a given shearing stress exceed the steady-state, angular velocities, the steady-state, apparent viscosities generally exceed the secant viscosities (Equation 40). This is also depicted in the actual data of Figure 25. From this figure, the apparent viscosities evaluated by the steady-state flow method are seen to be dependent only upon shearing rate. By specifying a standard shear rate, a viscosity measurement can be obtained which is useful in classifying or grading asphalts on the basis of consistency (46,47).

There are two other viscosity measurements of interest because of their independence of both shearing rate and shearing stress. The first of these is the limiting or initial viscosity which occurs at low rates of shear and low shearing stresses -- that is, when the material is behaving in a Newtonian fashion -- and which is generally considered to exceed the apparent viscosities evaluated in the shear-dependent region (48).

The second of these shear-independent viscosity measurements is that of plastic viscosity. Before evaluating the plastic viscosity, it is necessary to first establish that the behavior of asphalt cements in the steady-state flow regime may be represented by that of a Bingham plastic. Figures 16,17, and 18 indicate that the 13 asphalt cements of this study generally behave as Bingham plastics in the steady-state region (at least

for temperatures between 39.2°F and 104°F and for moderate shearing stresses). Figure 27 shows the theoretical relationship

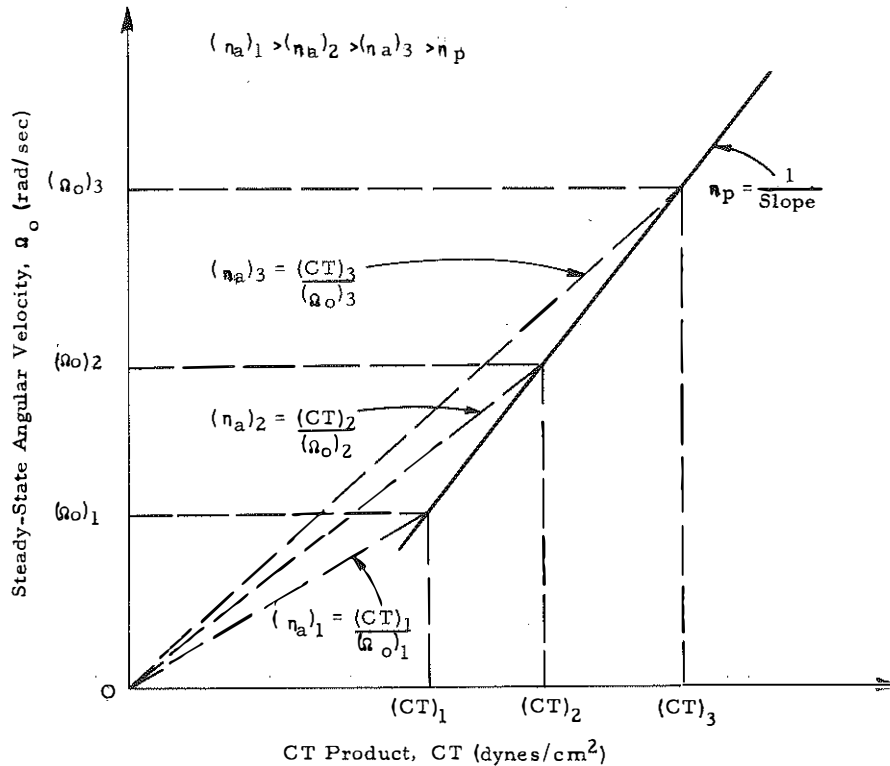


Figure 27. Theoretical Comparison of Steady-State, Apparent Viscosity, η_a , and Plastic Viscosity, η_p .

between the steady-state, apparent viscosities and the plastic viscosity, η_p . It is obvious from this figure that the steady-state, apparent viscosities should generally exceed the plastic viscosity and should approach its value only at high shearing stresses or high rates of shear¹. This is supported by the actual data of Figure 25.

¹A word of caution is warranted at this point. This observation is based on the premise that the steady-state flow behavior may be represented as a Bingham plastic. While this premise is supported by the data of this study, it may be in error if a wider range in shearing rates or temperatures is considered.

It is of interest to compare the apparent viscosity measurements obtained with the rotating coaxial cylinder viscometer with those obtained on identical asphalts but with a different type of viscometer. To enable such a comparison, the Bureau of Public Roads furnished three samples of their viscosity-graded asphalts. These samples were all of the AC-10 grade and were designated C-10, E-10, and O-10. A complete description of these asphalts and a summary of the viscosity measurements obtained by the Bureau may be found in Reference 48.

The Bureau used a sliding plate viscometer which was operated at controlled rates of shear. Computations of apparent viscosity were based on the maximum load attained at each rate of shear. The test equipment and procedures are fully described in Reference 46.

Figure 28 shows a comparison between the viscosities obtained with the coaxial cylinder viscometer and those obtained with the sliding plate viscometer for asphalt C-10 at 45°F. These results are generally indicative of those obtained for each of the three asphalts at all test temperatures. It was impossible to obtain a limiting viscosity for the tests with the coaxial cylinder viscometer since a rather limited range in shearing rates was employed. The apparent viscosities obtained with the coaxial cylinder viscometer were larger than those obtained with the sliding plate viscometer. Ideally, of course,

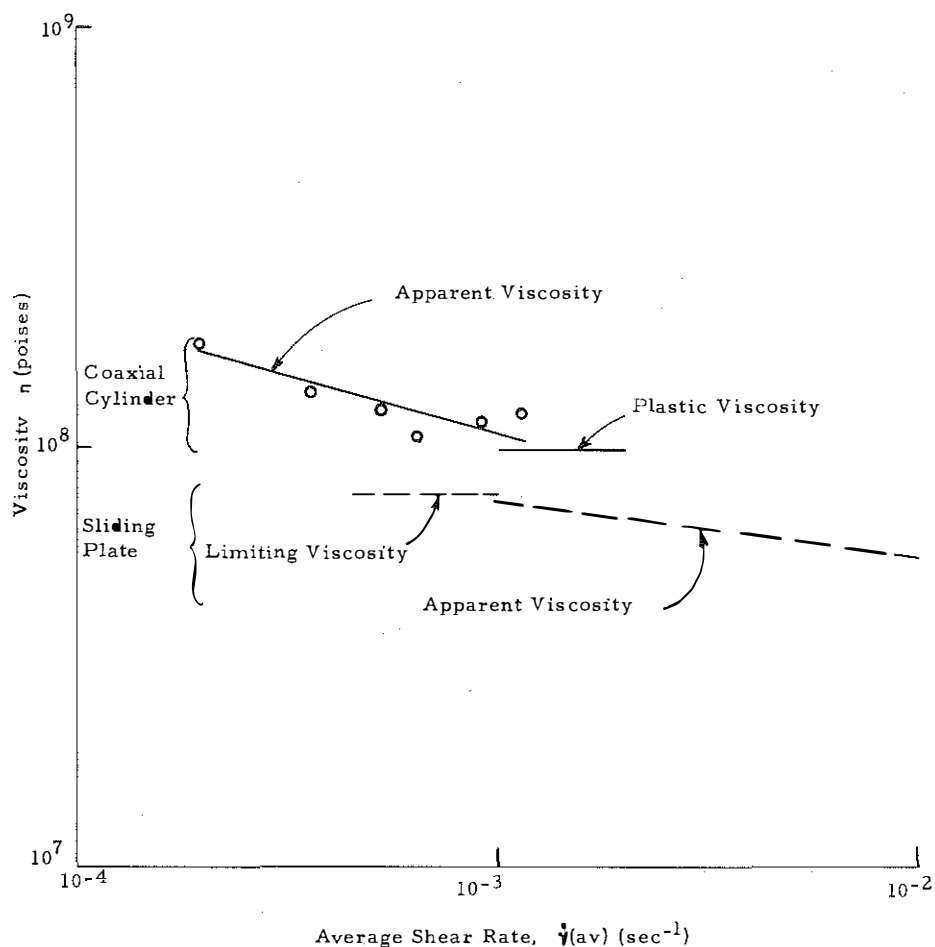


Figure 28. Comparison Between Viscosities Obtained with Rotating Coaxial Cylinder Viscometer and Sliding Plate Viscometer (Asphalt C-10 at 45°F).

they should have been equal. The plastic viscosity was also larger than the limiting viscosity. The preceding rationale would indicate that ideally the limiting viscosity should exceed the plastic viscosity.

The data of Table 12 may also be used to compare the two viscometers. The apparent viscosities at a specified shear rate of 0.001 sec^{-1} are tabulated for each of the three asphalts. Again the coaxial cylinder viscometer generally yielded viscosities in excess of those obtained with the sliding plate

TABLE 12

COMPARISON BETWEEN VISCOSITIES OBTAINED
WITH ROTATING COAXIAL CYLINDER VISCOMETER AND
SLIDING PLATE VISCOMETER

Asphalt Number	Temperature (°F)	Apparent Viscosity (Shear Rate of 0.001 sec ⁻¹)		Percentage Difference (%)	Limiting Viscosity ¹ (megapoises)	Plastic Viscosity (megapoises)
		Sliding Plate ¹ (megapoises)	Coaxial Cylinder (megapoises)			
C-10	45	73	107	+47	77	97.7
C-10	60	11.0	11.0	0	11.3	7.1
E-10	39.2	5770	2	-	36,000	45,400
E-10	45	3850	2	-	12,000	22,900
E-10	60	625	625	0	860	1,030
O-10	39.2	950	1200	+26	950	1,150
O-10	45	314	400	+27	315	396
O-10	60	21.5	26.5	+23	22.0	23.0

¹Obtained from Reference 48.

²Extrapolation impossible.

viscometer. The differences between the two types of viscosity measurements, expressed as a percentage of the viscosities obtained with the sliding plate viscometer, are also shown on Table 12. The average percentage difference between the apparent viscosities is 21 percent. Figure 29 compares the plastic viscosities (coaxial cylinder data) with the limiting viscosities (sliding plate data). Again the plastic viscosities are generally in excess of the limiting viscosities.

The data that have been presented definitely indicate a difference in viscosity measurements obtained using the two viscometers. The magnitude of the difference is not excessive, however, and may have been anticipated due to certain fundamental differences between the two viscometers and their operation by different laboratories. Several of these differences are listed in Table 13. The possible effects of these differences are generally unknown at this time.

It is concluded that the rotating coaxial cylinder viscometer can be effectively employed to evaluate apparent viscosities of asphalt cements at relatively low temperatures. Data obtained with this viscometer compare favorably with similar data obtained with the sliding plate viscometer.

TEMPERATURE SUSCEPTIBILITY

Data reported herein are sufficient to compare the susceptibilities of the consistency of the various asphalts to changes in temperature. Three of the techniques for defining the temperature susceptibility of asphalt cements are used in this comparison including the penetration ratio, the penetration index,

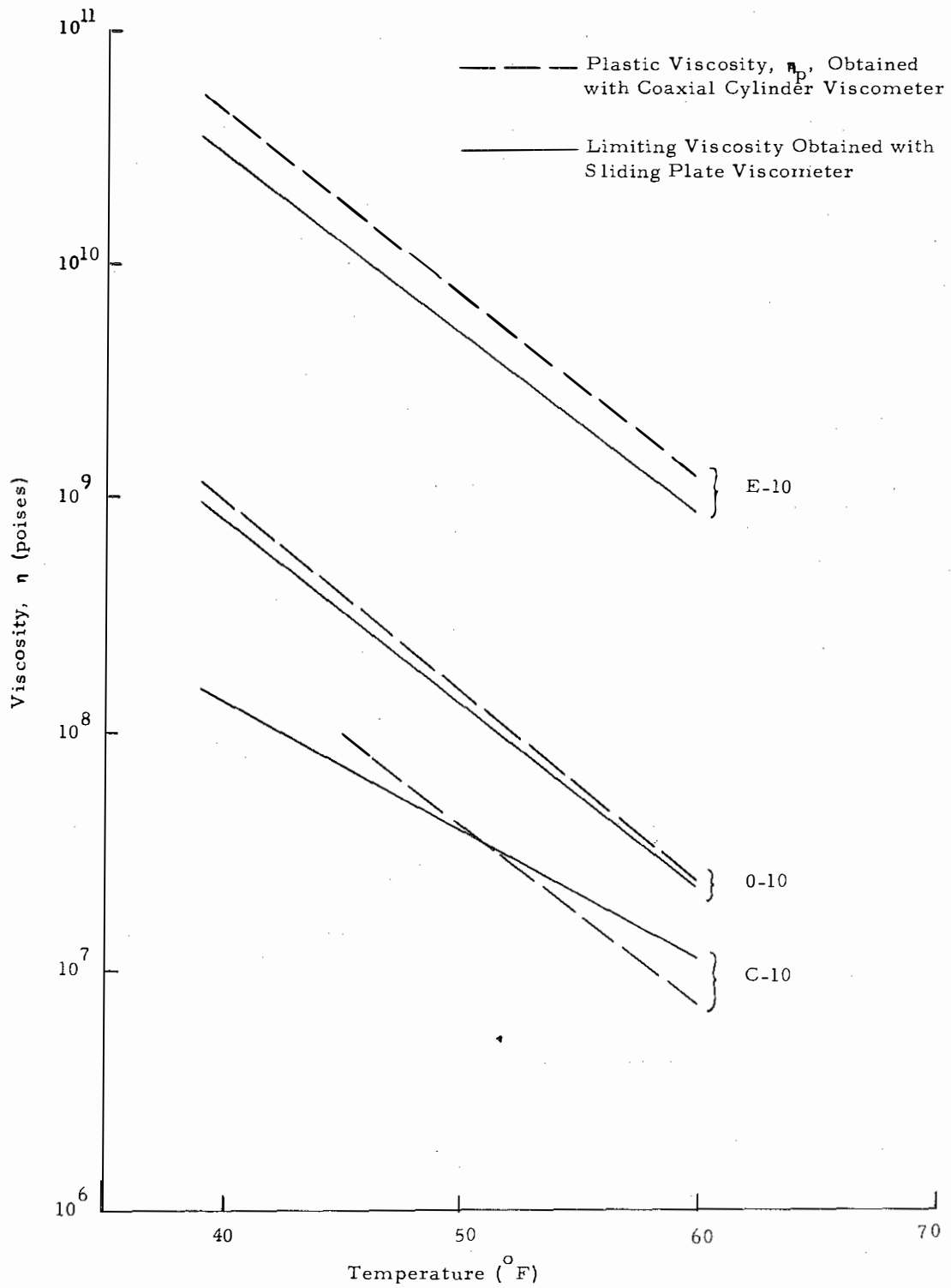


Figure 29. Comparison Between Limiting Viscosity and Plastic Viscosity.

TABLE 13

FUNDAMENTAL DIFFERENCES BETWEEN
VISCOMETERS AND TEST PROCEDURES

Variable	Sliding Plate Viscometer	Coaxial Cylinder Viscometer
Film Thickness(in.)	0.01-0.02	0.385
Stress or Strain History	Controlled rate of shear	Creep
Approximate Range in Shear Rates (sec ⁻¹)	10 ⁻³ - 10 ⁻¹	10 ⁻⁶ - 10 ⁻²
Specimen Preparation		
Approximate Melting Temperature (°F)	260-280	290
Time of Conditioning at Room Temperature (min)	60-90	30
Time to Reach Temperature Equilibrium (min)	25-30	60
Specimen Reuse	Permitted for several shear rates	Not permitted
Basis for Computations	Maximum load	Steady-state flow

and the slope of the viscosity-temperature relationship.

The penetration-ratio technique is based on determining the consistency of an asphalt cement at 39.2°F and 77°F by means of the standard penetration test. The penetration ratio is computed as follows:

$$\text{Pen. Ratio} = \frac{\text{Pen. @ } 39.2^{\circ}\text{F}}{\text{Pen. @ } 77^{\circ}\text{F}} \times 100. \quad (41)$$

A large temperature susceptibility connotes a low penetration ratio.

The penetration-index technique is based on two different consistency tests: the penetration test is used at the lower temperature (77°F) and the ring-and-ball softening point test is used at the higher temperature. The penetration index is computed

as follows:

$$PI = \frac{20 - 500A}{50A + 1} \quad (42)$$

where PI = penetration index

$$A = \frac{1.8 \log(800/Pen)}{\Delta T}$$

log = common logarithm

Pen = penetration at 77°F

ΔT = temperature difference (°F) between the ring-and-ball temperature and 77°F.

The penetration index normally varies between -2.5 and +8 (49).

A large temperature susceptibility yields a low penetration index.

The slope of the viscosity-temperature relationship may also be used as a measure of temperature susceptibility. This slope is normally determined from a plot of log log viscosity versus log absolute temperature. The following equation has been used in this determination:

$$VTS = \frac{\log \log \eta_{p(1)} - \log \log \eta_{p(2)}}{\log T_2 - \log T_1} \quad (43)$$

where VTS = viscosity-temperature slope

$\eta_{p(1)}$ = plastic viscosity in poises at T_1

$\eta_{p(2)}$ = plastic viscosity in poises at T_2

T_1 = largest temperature in °R(104°F)

T_2 = smallest temperature in °R(39.2°F).

Naturally a larger slope is associated with an asphalt of higher temperature susceptibility. This technique for evaluating temperature susceptibility is normally employed for a higher

temperature range, for example, 140°F to 275°F. However, it may still furnish a useful measure of temperature susceptibility within a lower temperature range such as that employed here (39.2°F to 104°F). This is particularly valid since the plastic viscosities are independent of shear rate at all temperatures.

The results of this analysis are shown in Table 14. With the possible exception of asphalt PR-132¹, there is not a great

TABLE 14
TEMPERATURE SUSCEPTIBILITY

Asphalt Number	Penetration Ratio	Penetration Index	Viscosity-Temperature Slope
3	49	+0.1	4.5
13	35	+0.8	5.0
45	32	-0.8	5.4
53	38	-0.1	5.5
67	46	0.0	4.8
71	25	-1.2	5.5
72	39	-0.7	5.4
91	26	-1.3	5.5
116	32	-1.1	6.1
127	49	-1.2	4.8
200	33	-0.1	5.2
PR-103	35	-1.0	6.0
PR-132	8	-1.2	-

deal of difference among the temperature susceptibilities of the various asphalts. All of the asphalts would be classified by Pfeiffer as normal types on the basis of their penetration indices ($-2.0 < PI < 2.0$) (49). Asphalts 71 and 91 exhibited

¹Asphalt PR-132 was not tested at 39.2°F and, hence, the viscosity-temperature slope could not be evaluated. However, it does have a low penetration ratio which would indicate a high temperature susceptibility.

perhaps the largest temperature susceptibilities and asphalt 3, the smallest. The viscosity-temperature relationships for asphalts 3 and 91 are compared on the Walther plot of Figure 30.

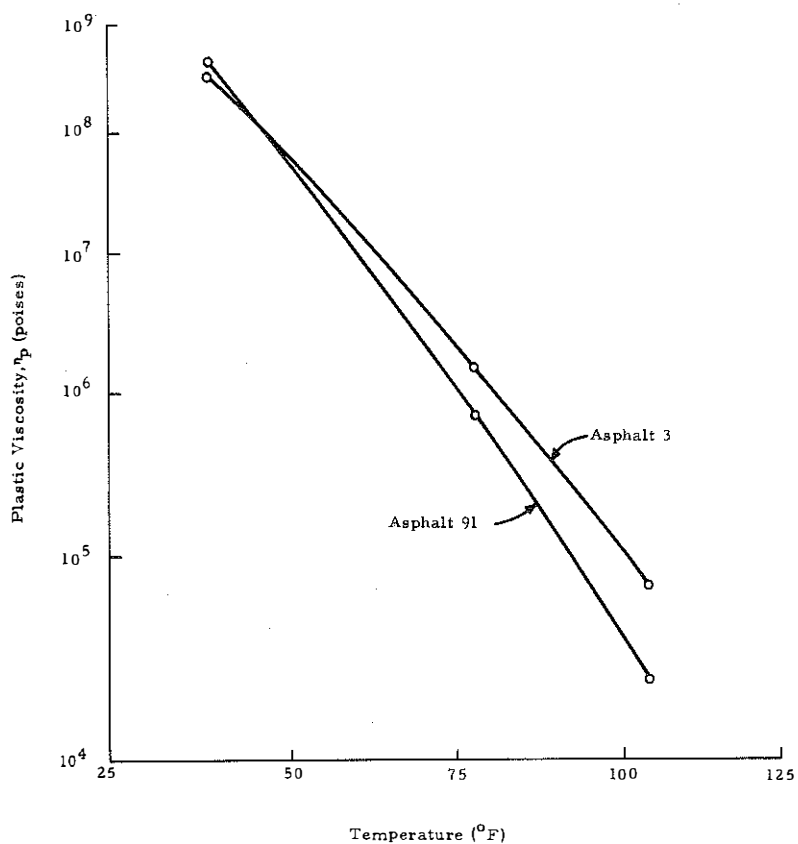


Figure 30. Largest and Smallest Temperature Susceptibilities.

The data of Table 14 are not sufficiently extensive to enable a thorough evaluation of the possible effects of crude source and manufacturing process on temperature susceptibility. The Venezuelan asphalts (asphalts 13, 127, and 200), which differ only in penetration grade, exhibited essentially identical

temperature susceptibilities. Asphalts in which air blowing was used (asphalts 53, 72, and 91) were not particularly resistant to changes in temperature. The Californian crude (asphalt 91) and a Midcontinent crude (asphalt 71) exhibited the highest temperature susceptibilities and the Mexican crude (asphalt 3), the lowest. However, since the differences were not large and since only a single asphalt from each crude source was evaluated, a definitive conclusion relative to crude source cannot be drawn on the basis of these data.

VISCOSITY-PENETRATION RELATIONSHIP

Figures 31 and 32 show the relationship between plastic viscosity and penetration at temperatures of 77°F and 39.2°F, respectively. Both figures indicate a clearly defined trend with increasing penetrations corresponding to decreasing viscosities. As expected, the variability is greater with the 39.2°F measurements than with the 77°F measurements. At 39.2°F, the penetrations are relatively small and within the length of the truncated cone portion of the penetration needle.

The viscosity measurements are considerably more sensitive than the penetration measurements both in evaluating the differences among asphalts at a single temperature and in evaluating the effect of temperature for a single asphalt. The variability¹ among asphalts at a given temperature averaged about 84 percent for the penetration measurements and about 250 percent for the viscosity measurements. In going from 77°F to 39.2°F, the mean penetration decreased about 64 percent while the mean viscosity increased about 63,000 percent.

¹In this case, the variability is expressed as the range of the measurements divided by their average values.

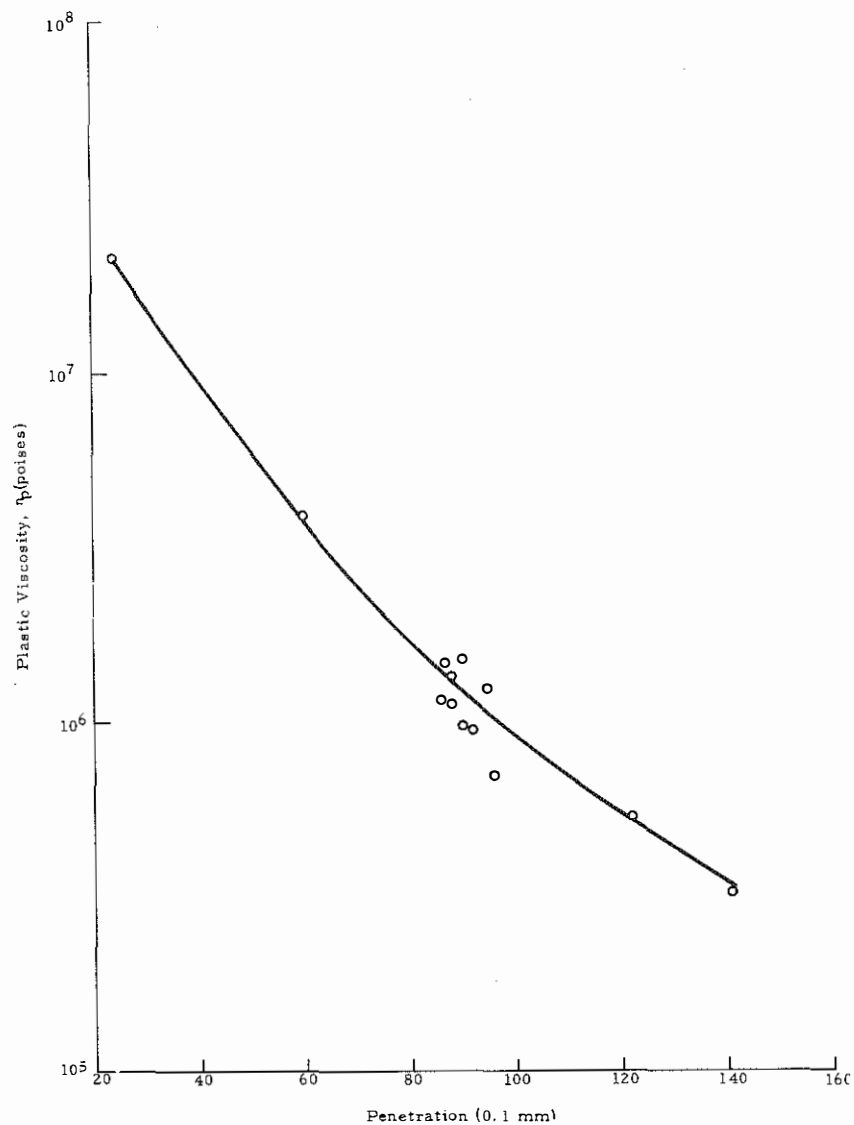


Figure 31. Relationship Between Plastic Viscosity and Penetration (100 g., 5 sec.) at 77°F.

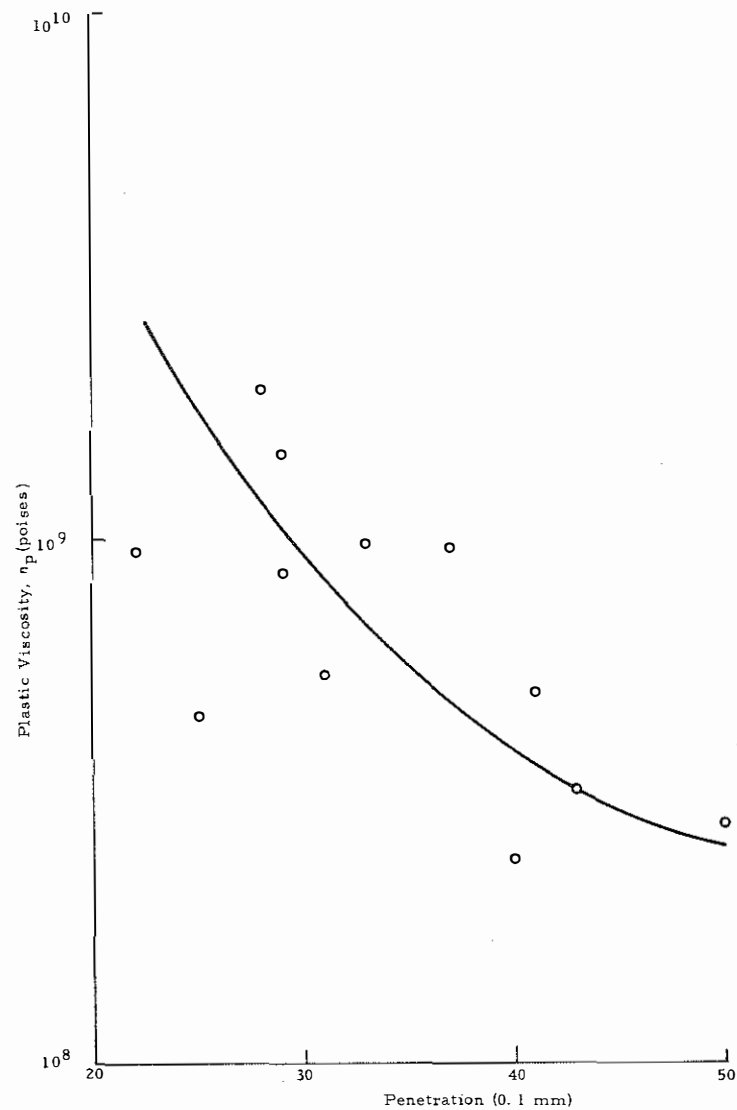


Figure 32. Relationship Between Plastic Viscosity and Penetration (200 g., 60 sec.) at 39.2°F.

TIME-TEMPERATURE SUPERPOSITION

Asphalt 53 was tested at 0°F in addition to the three temperatures which were employed for all of the asphalts. Three levels of shearing stress were applied at this temperature. The duration of each of the three tests was approximately two weeks. The characteristic relationship between angle of rotation and time was observed; that is, elastic, steady-state flow, and viscoelastic processes were all in evidence. The steady-state flow condition was reached after a period of approximately three to nine days depending upon the stress level. The material parameters evaluated at this temperature are summarized on Table 15. The two-element viscoelastic model was found to satisfactorily describe the viscoelastic portion of flow.

TABLE 15
MATERIAL PARAMETERS EVALUATED AT
0°F (ASPHALT 53)

Parameter	Value
Elastic Modulus, G_0	3.46×10^7 dynes/cm ²
Yield Stress, S_y	
Coefficient of Plastic Viscosity, η_p	1.65×10^{13} poises
Viscoelastic Parameters	
G_1	1.71×10^7 dynes/cm ²
η_1	5.05×10^{12} poises
G_2	3.39×10^7 dynes/cm ²
η_2	0.58×10^{12} poises

The tests using asphalt 53 covered a sufficiently wide range of temperatures and durations of loading to enable investigation of the possible applicability of the time-temperature superposition principle in the low-temperature region. As a basis for this investigation, the average creep function at each of the four

temperatures was plotted as shown on Figure 33. The total-angle creep functions, averaged for the three stress levels, are shown on this figure. The averaging process is thought to be valid since no evidence was found that the material is non-linear under the particular test conditions evaluated herein. The average creep function was reduced after the manner discussed by Ferry (50) by multiplying it by the ratio of the absolute value of the test temperature to the absolute value of a suitable reference temperature (in this case 50°F).

The reduced average creep functions of Figure 33 were then shifted horizontally until their overlapping portions were made to coincide. The magnitude of translation is defined as $\log \alpha_T$ where α_T is the shift factor. The shift factor was then adjusted to the reference temperature of 50°F; that is, $\log \alpha_T$ was adjusted to zero at a temperature of 50°F. The relationship between the shift factor, thus obtained, and the test temperature is shown on Figure 34.

The shift factor may also be computed from the following relationship (50):

$$\alpha_T = (\eta_{T_0} \rho_0) / (\eta_T \rho) \quad (44)$$

where α_T = shift factor

η = steady-flow viscosity at temperature, T

η_0 = steady-flow viscosity at temperature, T_0

T = any temperature in absolute units

T_0 = reference temperature in absolute units

ρ = density at temperature, T

ρ_0 = density at temperature, T_0 .

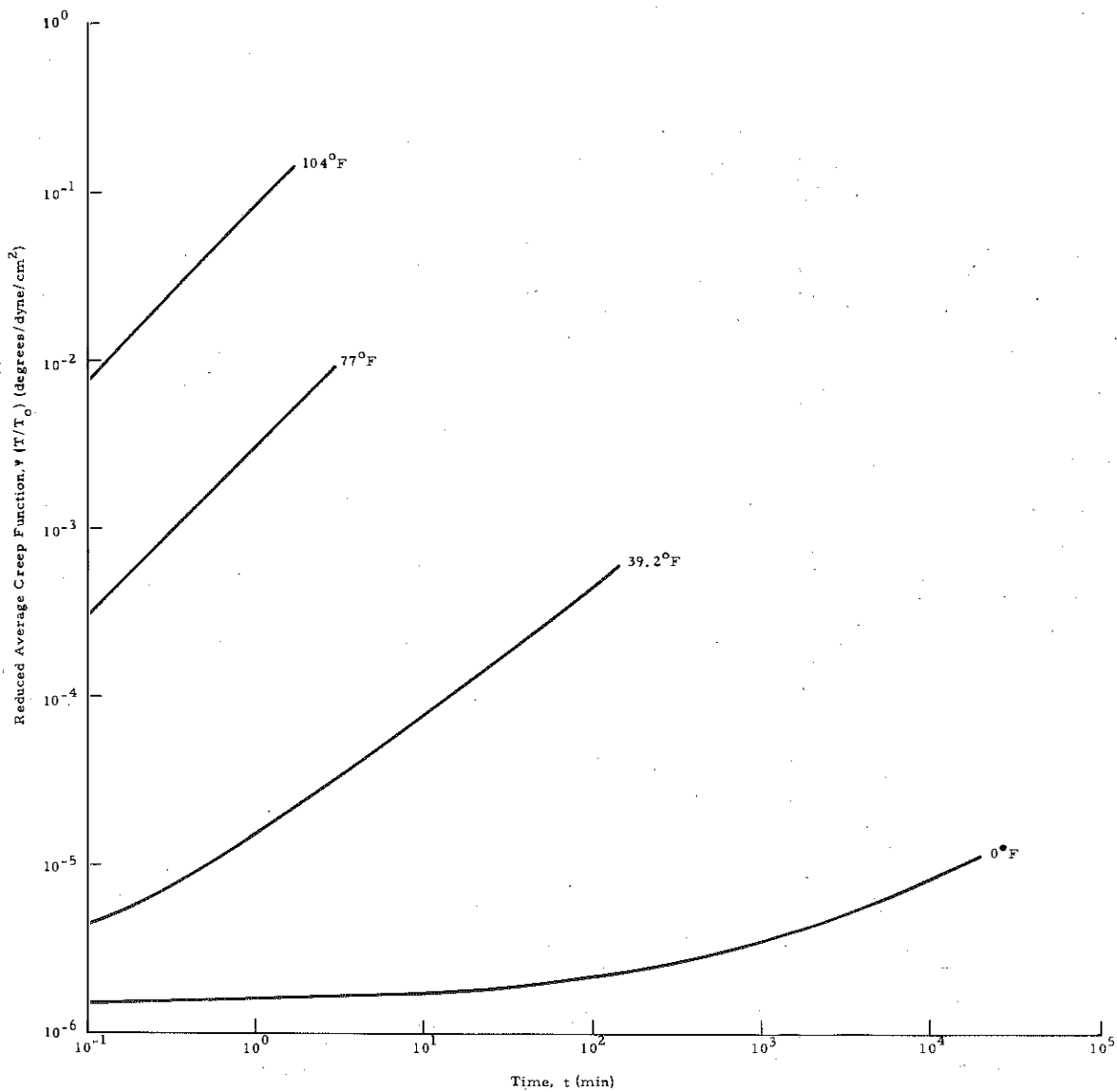


Figure 33. Average Creep Functions for Asphalt 53.

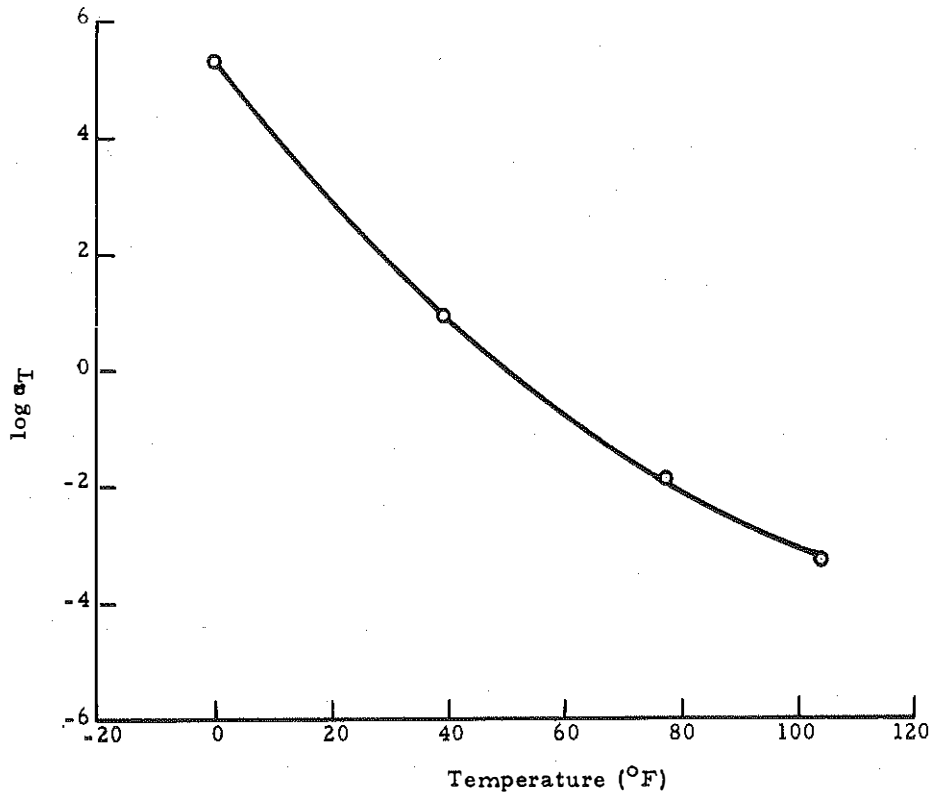


Figure 34. Relationship Between Shift Factor and Temperature.

This expression is theoretically valid for uncross-linked polymers of low molecular weight and, in certain instances, for those of high molecular weight (50). The shift factor was evaluated using Equation 44 which was slightly modified by omitting the density terms because of their minor importance. The coefficients of plastic viscosity were used to represent the viscosity measurements. A comparison between the computed and measured shift factors is given in Table 16. The agreement is relatively surprising even though the range in test temperatures is somewhat limited. The comparison demonstrates that the measured shift

TABLE 16
SHIFT FACTORS

Temperature (°F)	Computed Shift Factor, a_T (Equation 44)	Measured Shift Factor, a_T
0	1.63×10^5	2.14×10^5
39.2	8.99	8.70
77	0.98×10^{-2}	1.26×10^{-2}
104	2.88×10^{-4}	5.00×10^{-4}

factors are of the proper order of magnitude and are properly related to temperature within the low-temperature range of these tests.

Figure 35 shows the master creep function for asphalt 53 at a reference temperature of 50°F when the experimentally determined shift factors are applied to the data of Figure 33. The master creep function satisfactorily fits the data points obtained at the four different test temperatures.

Ferry (50) lists the following three criteria for determining the applicability of the time-temperature superposition principle (method of reduced variables) to a given set of test data: (1) exact matching of the shapes of adjacent curves obtained at different test temperatures, (2) superposition of the values of the shift factor for different viscoelastic functions, and (3) a reasonable form of the temperature dependence of the shift factor consistent with experience. A study of Figure 35 leads to the conclusion that the first criterion is satisfied for these data. The second criterion cannot be evaluated since only one viscoelastic function is available for comparison, that is, the creep function. The third criterion seems to have been

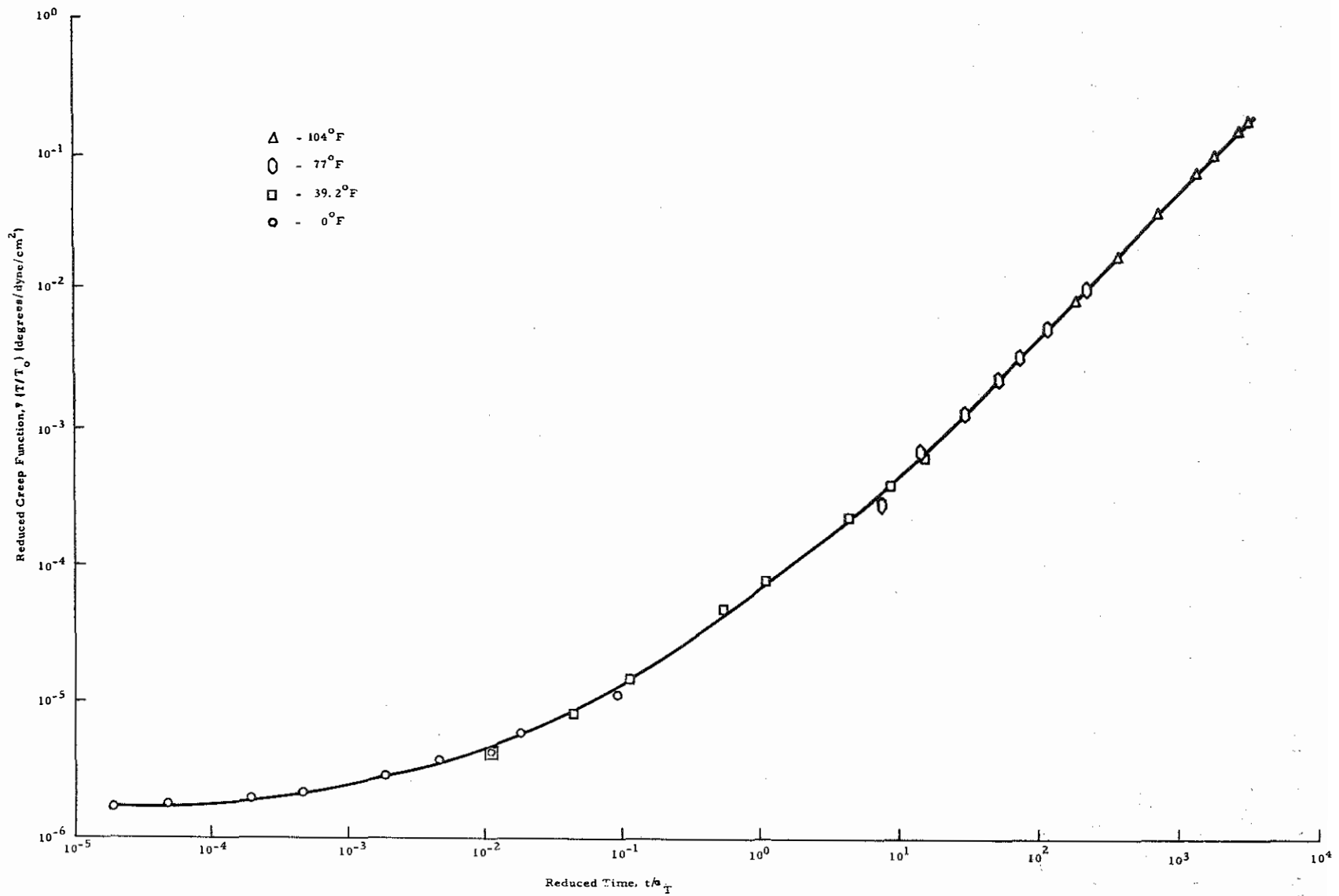


Figure 35. Master Creep Function for Asphalt 53 (Reference Temperature of 50°F).

satisfied by the comparison of Table 16. It is concluded, therefore, that the time-temperature superposition principle is valid for asphalt 53 when tested in the low-temperature range. A cursory evaluation of other of the asphalt cements tends to support the extension of this conclusion to all of the materials of this study.

CONCLUSIONS

The following conclusions are substantiated by the data obtained in this phase of the study:

1. The rotating coaxial cylinder viscometer is a useful research tool for examining the flow behavior of asphalt cements at relatively low temperatures. It may also be effectively employed to evaluate apparent viscosities of these materials.

2. The curve-fitting technique for evaluating the parameters of viscoelastic behavior has proven to be extremely useful and reliable. The principles underlying this technique may be readily extended to other types of equations in which a best fit by the least squares criterion is required.

3. All of the asphalt cements exhibited steady-state flow behavior at 77°F and 104°F. At these temperatures, their flow behavior under creep loading could satisfactorily be characterized by that of a Bingham plastic. At 39.2°F, however, all asphalts exhibited instantaneous and retarded elasticity, steady-state flow, and elastic recovery following load removal. This behavior could satisfactorily be characterized by a generalized model consisting of a series combination of an elastic element (spring), a Bingham element (steady-state liquid), and a viscoelastic body (generalized Voigt body). It follows, then, that the complexity of flow behavior increases as the temperature is reduced.

4. The steady-state flow behavior of each of the asphalt cements in the low-temperature range was found to be similar to

that of a Bingham plastic. The coefficient of plastic viscosity is an appropriate means for defining a shear-independent measure of consistency for classification purposes.

5. Coefficients of plastic viscosity in the range of 10^4 to 10^{13} poises were measured with the rotating coaxial cylinder viscometer. In no case was a discernable relationship observed between the yield stress and the coefficient of plastic viscosity.

6. For the one set of tests conducted at 0°F , steady-state flow was reached after a period of approximately three to nine days. For tests at 39.2°F , approximately one to five hours were necessary to achieve the steady-state condition. This emphasizes the necessity for a long-duration test when evaluating the steady-state flow behavior of asphalt cements at relatively low temperatures.

7. All of the asphalts appeared to behave linearly under the conditions of test employed herein. The tentative nature of this conclusion is emphasized, however, pending the outcome of a more exhaustive set of tests directed specifically to this determination.

8. The time-temperature superposition principle (method of reduced variables) appears to be applicable to the behavior of normal asphalt cements at least in the low-temperature range (0°F to 104°F).

9. A relationship exists between plastic viscosity evaluated with the rotating coaxial cylinder viscometer and the results of standard penetration tests when both types of tests are conducted at identical temperatures. The correlation at 77°F is superior to that at 39.2°F because of the varying nature of the shear strains and shear rates when the penetrations are small as they

were at 39.2°F. The viscosity measurements are considerably more sensitive both to changes in temperature and to changes in material properties than are the penetration measurements.

10. The effect of penetration grade was evaluated using the three asphalts obtained by vacuum and steam distillation from the Venezuelan crude. As anticipated, the viscosities of these asphalts were properly arranged in the order indicated by the penetration grade at all temperatures. The temperature susceptibilities of these asphalts were approximately the same: this indicates that asphalts produced from the same crude source by similar refining processes will have similar temperature susceptibilities.

11. The effect of manufacturing process on the viscosities of materials of the same penetration grade was somewhat indeterminate. Those asphalts in which air blowing was used, namely, asphalts 53, 72, and 91, did not have particularly low temperature susceptibilities. Asphalt 91 had a consistently low viscosity at all temperatures but asphalts 53 and 72 were not significantly different from the other 85-100 penetration materials in this respect.

12. The effect of crude source for materials of the same penetration grade is also difficult to evaluate. The Californian asphalt exhibited a lower viscosity than most of the other asphalts at all temperatures and the highest temperature susceptibility of the group. The Mexican asphalt exhibited relatively high viscosities at the two higher temperatures and the lowest temperature susceptibility of the group. However, since the differences

among asphalts was not large and since only a single asphalt from each of these two crude sources was evaluated, definitive conclusions as to the potential importance of crude source must be withheld.

13. Two of the 85-100 penetration asphalts, namely, asphalts 91 and 116, had significantly lower Saybolt Furol viscosities than the others. This lower consistency at the higher temperatures is reflected in the fact that the plastic viscosities of these asphalts at 104°F were the lowest of the 85-100 penetration grade asphalts. Due to the different temperature susceptibilities of the various asphalts, however, they did not maintain this relatively low ranking at the lower temperatures. Asphalts 91 and 116 were also less viscous at 104°F than the one 120-150 penetration asphalt that was tested. This emphasizes the necessity for specifying the consistency of asphalt cements at more than one temperature level.

REFERENCES

1. Mossbarger, W.A., Jr., "A Rheological Investigation of Asphaltic Materials," Research Report, Division of Research, Kentucky Department of Highways, January, 1964.
2. Peattie, K.R., "A Fundamental Approach to the Design of Flexible Pavements," Proceedings, International Conference on the Structural Design of Asphalt Pavements, 1963.
3. Skok, E.L., Jr. and Finn, F.N., "Theoretical Concepts Applied to Asphalt Concrete Pavement Design," Proceedings, International Conference on the Structural Design of Asphalt Pavements, 1963.
4. Jones, A., "Tables of Stresses in Three-Layer Elastic Systems," Bulletin 342, Highway Research Board, 1962.
5. Peattie, K.R., "Stress and Strain Factors for Three-Layer Elastic Systems," Bulletin 342, Highway Research Board, 1962.
6. Burmister, D.M., "The General Theory of Stresses and Displacements in Layered Systems," Journal of Applied Physics, Vol. 16, Nos. 2, 3, and 5, 1945.
7. Coffman, Bonner S., "The Structural Evaluation of Flexible Pavements," Report No. 235-2, Engineering Experiment Station, The Ohio State University, 1966.
8. Whiffin, A.C. and Lister, N.W., "The Application of Elastic Theory to Flexible Pavements," Proceedings, International Conference on the Structural Design of Asphalt Pavements, 1963.
9. Pister, K.S. and Westmann, R.A., "Analysis of Viscoelastic Pavements Subjected to Moving Loads," Proceedings, International Conference on the Structural Design of Asphalt Pavements, 1963.
10. Lee, E.H., "Stress Analysis in Viscoelastic Materials," Journal of Applied Physics, Vol. 27, 1956.
11. Lee, E.H., "Viscoelastic Stress Analysis," Structural Mechanics, Proceedings, First Symposium on Naval Structural Mechanics, edited by Goodier, J.N. and Nicholas, Jr., Pergamon Press, New York, 1960.

REFERENCES (Cont'd.)

12. Hoskins, B.C. and Lee, E.H., "Flexible Surfaces on Viscoelastic Subgrades," Proceedings, American Society of Civil Engineers, Vol. 85, No. EM 4, October, 1959.
13. Mase, G.E., "Behavior of Viscoelastic Plates in Bending," Proceedings, American Society of Civil Engineers, Vol. 86, No. EM 3, June, 1960.
14. Pister, K.S. and Williams, M.L., "Bending of Plates on a Viscoelastic Foundation," Proceedings, American Society of Civil Engineers, Vol. 86, No. EM 5, October, 1960.
15. Alfrey, T., Jr. and Doty, P., "The Methods of Specifying the Properties of Viscoelastic Materials," Journal of Applied Physics, Vol. 16, 1945.
16. Alfrey, T., Jr., Mechanical Behavior of High Polymers, Interscience Publishers Inc., New York, 1948.
17. Leaderman, H., "Viscoelastic Phenomena in Amorphous High Polymeric Systems," Rheology, Theory and Applications, Vol. 2, edited by Eirich, F.R., Academic Press Inc., New York, 1958.
18. Alfrey, T., Jr. and Gurnee, E.F., "Dynamics of Viscoelastic Behavior," Rheology, Theory and Applications, Vol. 1, edited by Eirich, F.R., Academic Press Inc., New York, 1956.
19. Ferry, J.D., "Experimental Techniques for Rheological Measurements on Viscoelastic Bodies," Rheology, Theory and Applications, Vol. 2, edited by Eirich, F.R., Academic Press Inc., New York, 1958.
20. Traxler, R.N., Schwyer, H.E., and Romberg, J.W., "Rheological Properties of Asphalt," Industrial and Engineering Chemistry, September, 1944.
21. Van Der Poel, C., "A General System Describing the Viscoelastic Properties of Bitumens and Its Relation to Routine Test Data," Journal of Applied Chemistry, Vol. 4, May, 1954.
22. Van Der Poel, C., "Road Asphalt," Building Materials, Their Elasticity and Inelasticity, edited by Reiner, M., Interscience Publishers Inc., New York, 1954.
23. Saal, R.N.J., "Physical Properties of Asphaltic Bitumen," Properties of Asphaltic Bitumen, edited by Pfeiffer, J.Ph., Elsevier Publishing Co., Inc., New York, 1950.
24. Brodnyan, J.G., "Use of Rheological and Other Data in Engineering Problems," Bulletin 192, Highway Research Board, 1958.

REFERENCES (Cont'd.)

25. Gaskins, F.H., Brodnyan, J.G., Philippoff, W., and Thelen, E., "The Rheology of Asphalt. II. Flow Characteristics of Asphalt," Transactions, Society of Rheology, Vol. IV, 1960.
26. Brodnyan, J.G., Gaskins, F.H., Philippoff, W., and Thelen, E., "The Rheology of Asphalt. III. Dynamic Mechanical Properties of Asphalt," Transactions, Society of Rheology, Vol. IV, 1960.
27. Brown, A.B., Sparks, J.W., and Smith, F.M., "Viscoelastic Properties of a High-Consistency Asphalt," Journal of Colloid Science, Vol. 12, No. 3, 1957.
28. Brown, A.B. and Sparks, J.W., "Viscoelastic Properties of a Penetration Grade Paving Asphalt at Winter Temperature," Proceedings, Association of Asphalt Paving Technologists, Vol. 27, 1958.
29. Wood, P.R., "Rheology of Asphalts and Its Relation to Behavior of Paving Mixtures," Bulletin 192, Highway Research Board, 1958.
30. Kuhn, S.H. and Rigden, P.J., "Measurement of Visco-Elastic Properties of Bitumen Under Dynamic Loading," Proceedings, Highway Research Board, Vol. 38, 1959.
31. Wood, L.E. and Goetz, W.H., "The Rheological Characteristics of a Sand-Asphalt Mixture," Proceedings, Association of Asphalt Paving Technologists, Vol. 28, 1959.
32. Pister, K.S. and Monismith, C.L., "Analysis of Viscoelastic Flexible Pavements," Bulletin 269, Highway Research Board, 1960.
33. Secor, K.E. and Monismith, C.L., "Analysis of Triaxial Test Data on Asphalt Concrete Using Viscoelastic Principles," Proceedings, Highway Research Board, Vol. 40, 1961.
34. Baker, R.F. and Papazian, H.A., "The Effect of Stiffness Ratio on Pavement Stress Analysis," Proceedings, Highway Research Board, Vol. 39, 1960.
35. Papazian, H.S., "The Response of Linear Viscoelastic Materials in the Frequency Domain," Report No. 172-2, Transportation Engineering Center, Engineering Experiment Station, Ohio State University, 1961.
36. Schiffman, R.L., "The Use of Viscoelastic Stress-Strain Laws in Soil Testing," STP No. 254, American Society for Testing Materials, 1959.

REFERENCES (Cont'd.)

37. Folque, J., "Rheological Properties of Compacted Unsaturated Soils," Proceedings, Fifth International Conference on Soil Mechanics and Foundation Engineering, Vol. I, Paris, 1961.
38. Murayama, S. and Shibata, T., "Rheological Properties of Clays," Proceedings, Fifth International Conference on Soil Mechanics and Foundation Engineering, Vol. I, Paris, 1961.
39. Vialov, S.S. and Skibitsky, A.M., "Problems of the Rheology of Soils," Proceedings, Fifth International Conference on Soil Mechanics and Foundation Engineering, Vol. I, Paris, 1961.
40. Goldstein, M.N., Misumsky, V.A., and Lapidus, L.S., "The Theory of Probability and Statistics in Relation to the Rheology of Soils," Proceedings, Fifth International Conference on Soil Mechanics and Foundation Engineering, Vol. I, 1961.
41. Tjong-Kie, Tan, "Consolidation and Secondary Time Effect of Homogenous, Anisotropic Saturated Clay Strata," Proceedings, Fifth International Conference on Soil Mechanics and Foundation Engineering, Vol. I, Paris, 1961.
42. Oka, S., "The Principles of Rheometry," Rheology - Theory and Applications, Vol. 3, edited by Eirich, F.R., Academic Press Inc., New York, 1960.
43. Wilkinson, W.L., Non-Newtonian Fluids - Fluid Mechanics, Mixing and Heat Transfer, Pergamon Press Ltd., New York, 1960.
44. Welborn, J. York and Halstead, Woodrow J., "Properties of Highway Asphalts - Part I, 85-100 Penetration Grade," Public Roads - A Journal of Highway Research, Vol. 30, No. 9, August, 1959.
45. Welborn, J. York, Halstead, Woodrow J., and Boone, J. Gayloid, "Properties of Highway Asphalts - Part II, Various Penetration Grades," Public Roads - A Journal of Highway Research, Vol. 31, No. 4, October, 1960.
46. "Proposed Method of Test for Viscosity of Asphalt with a Sliding Plate Viscometer at Controlled Rates of Shear," ASTM Standards, Part 11, March, 1966.
47. "Proposed Method of Test for Viscosity of Asphalt Cements with Falling Plunger Viscometer," ASTM Standards, Part 11, March, 1966.

REFERENCES (Cont'd.)

48. Welborn, J. York, Oglio, Edward R., and Zenewitz, Joseph A., "A Study of Viscosity-Graded Asphalt Cements," Public Roads - A Journal of Highway Research, Vol. 34, No. 2, June, 1966.
49. Pfeiffer, J. Ph. (ed), The Properties of Asphaltic Bitumen, Elsevier Publishing Co., Inc., New York, 1950.
50. Ferry, John D., Viscoelastic Properties of Polymers, John Wiley and Sons, Inc., New York, 1961.

APPENDIX A
TEST PROCEDURE

The following specification describes the procedures for testing with the rotating coaxial cylinder viscometer.

1. Water Bath

Temperature control shall be provided by immersing the specimen and portions of the viscometer in a suitable water bath. The bath shall be sufficiently large to contain the viscometer and to permit the specimen to be submerged to a depth of at least 1 inch below the water surface. The temperature of the bath shall be allowed to vary not more than 0.5°F from the specified test temperature.

2. Preparation of Viscometer

The appropriate cup-and-bob assembly and drive pulley shall be selected. The pulley, scale, and rotary differential transformer shall then be attached to the axle. The upper surfaces of the grooved brass base plate (used with the small cup-and-bob assembly) or the brass ring (used with the large assembly) shall be thoroughly amalgamated with mercury and properly positioned in the viscometer. A sufficient quantity of mercury shall be poured into the annulus of the base plate so that, when the bob and cup are assembled, the level of mercury will be slightly above the lower edge of the bob. The cup shall be rigidly affixed to the base of the viscometer. In a like manner, the bob shall be affixed to the axle of the load system and properly positioned

in its bearing receptacle.

3. Special Precautions for Handling Mercury

Due to the possible danger to health if mercury is handled carelessly, the following precautions shall be observed at all times:

- a. Mercury shall be stored in a closed jug or other suitable, unbreakable container in a cool place.
- b. Extreme care shall be exercised to avoid spilling any mercury.
- c. Mercury vapors shall be removed by working under a suitable hood with adequate ventilation.
- d. The amalgamated brass plates and other components of the viscometer shall be maintained at normal room temperature except when testing.

4. Weight Attachment

After the cup and bob have been properly assembled on the viscometer, the drive pulley shall be firmly anchored by placing the trip release in the locked position. The idle pulleys shall be aligned with the drive pulley. The weights necessary to produce the desired torque shall then be attached to the drive pulley and suspended over the idle pulleys. The weights shall be attached symmetrically so as to produce a couple and thus eliminate the possibility of introducing bending in the axle. Caution should be exercised at all times to prevent shearing the test material prior to the beginning of a test.

5. Preparation of Test Specimen

A suitable container holding the bituminous material to be tested shall be placed in an oil bath maintained at a temperature

of 290°F¹ (plus or minus 5°F). During heating, the sample shall be stirred intermittently to maintain, as well as possible, a uniform temperature distribution within the sample. When the sample has been completely melted, it shall be thoroughly stirred to insure that it is homogenous and free from air bubbles. The assembled viscometer, with weights attached, shall be placed on a perfectly level surface. In filling the annulus formed by the cup and bob, the material shall be poured in a thin stream from two separate containers at points approximately 180° apart. During filling, each container shall be moved back and forth over a 180° segment of the annulus until the annulus is slightly more than level full. The viscometer and test material shall be cooled at room temperature for a period of 30 minutes. They shall then be placed in the water bath maintained at the specified temperature of test for an additional period of 30 minutes. The excess bitumen shall then be struck off with a heated, straight-edged spatula or knife.

6. Establishment of Temperature Equilibrium

After trimming the specimen and prior to testing, the viscometer shall be returned to the water bath and maintained at the specified test temperature for a period of 30 minutes.

7. Testing

The recording equipment shall be started and the test shall

¹In no case shall the sample be heated to a temperature greater than 200°F above its softening point, determined in accordance with the Method of Test for Softening Point of Bituminous Materials (Ring-and-Ball Method, ASTM Designation: D36).

begin by actuating the trip release. At subsequent intervals of time, the angle of rotation shall be read directly from the recording equipment. Checks shall be made by noting the angle of rotation from the scale attached to the viscometer. The test shall be allowed to continue until a steady-state or near steady-state condition is reached, that is, until a linear relationship between the angle of rotation and time is observed. After the steady-state condition has been reached, the load shall be instantaneously removed and the rebound, if present, shall be recorded as a function of time. After rebound has been completed, the load shall be quickly applied and removed a number of times to assist in determining the instantaneous angle of rotation.

8. Procedures after Testing

The viscometer shall be disassembled and the height of the specimen determined. The apparatus shall then be cleaned in preparation for subsequent testing.

APPENDIX B

CURVE-FITTING TECHNIQUE

The following discussion describes a method for determining values of the constants, a_k and b_k , in an equation of the form

$$\psi = \sum_{k=1}^n a_k [1 - \exp(-b_k t)] \quad (B-1)$$

to yield the equation of a curve which gives the best fit by least squares criterion for a set of experimental data known to conform to a general equation of this type.

Initial values for the constants, a_k and b_k , say a_k^1 and b_k^1 , are assumed. It is preferable that a_k^1 and b_k^1 be close to the best values of a_k and b_k . Equation B-1 is expanded in a Taylor's series about the values a_k^1 and b_k^1 to yield:

$$\psi_a = f(\psi_1) + \sum_{k=1}^n \frac{\partial \psi}{\partial a_k} \bigg|_{a_k^1, b_k^1} \Delta a_k + \sum_{k=1}^n \frac{\partial \psi}{\partial b_k} \bigg|_{a_k^1, b_k^1} \Delta b_k \quad (B-2)$$

$$\text{where } f(\psi_1) = \sum_{k=1}^n a_k^1 [1 - \exp(-b_k^1 t)] \quad (B-3)$$

$$\Delta a_k = a_k - a_k^1 \quad (B-4)$$

$$\Delta b_k = b_k - b_k^1 \quad (B-5)$$

Equation B-2 actually represents an approximation to the Taylor's series expansion because terms containing second and higher order quantities have been neglected.

Performing the operations indicated in Equation B-2 on Equation B-1 yields:

$$\left. \frac{\partial \psi}{\partial a_k} \right|_{a_k^1, b_k^1} = [1 - \exp(-b_k^1 t)] \quad k=1,2,3\dots n \quad (B-6)$$

and

$$\left. \frac{\partial \psi}{\partial b_k} \right|_{a_k^1, b_k^1} = a_k^1 t [\exp(-b_k^1 t)]. \quad k=1,2,3\dots n \quad (B-7)$$

Substituting the results of Equations B-3, B-6, and B-7 back into Equation B-2 it is seen that

$$\begin{aligned} \psi_a = & \sum_{k=1}^n a_k^1 [1 - \exp(-b_k^1 t)] + \sum_{k=1}^n [1 - \exp(-b_k^1 t)] \Delta a_k \\ & + \sum_{k=1}^n a_k^1 t [\exp(-b_k^1 t)] \Delta b_k. \end{aligned} \quad (B-8)$$

Here the subscript "a" is placed on ψ to denote an approximation to the true value.

If the set of data points contains r observations, then Equation B-8 may be written:

$$\begin{aligned} \psi_{a(i)} = & \sum_{k=1}^n \left[a_k^1 [1 - \exp(-b_k^1 t_i)] + [1 - \exp(-b_k^1 t_i)] \Delta a_k \right. \\ & \left. + a_k^1 t_i [\exp(-b_k^1 t_i)] \Delta b_k \right] \end{aligned} \quad (B-9)$$

where $i = 1,2,3\dots r$.

Thus from Equation B-9, one has r linear equations in Δa_k and Δb_k .

The deviation, δ_i , which represents the difference between the Ψ 's calculated by Equation B-9 and the actual or observed Ψ 's may be determined from the relationship:

$$\delta_i = \Psi_{a(i)} - \Psi_i = \sum_{k=1}^n \left[a_k^1 [1 - \exp(-b_k^1 t_i)] + [1 - \exp(-b_k^1 t_i)] \Delta a_k + a_k^1 t_i [\exp(-b_k^1 t_i)] \Delta b_k \right] - \Psi_i. \quad (B-10)$$

The sum of the squares of the deviations, defined by the relationship

$$S = \sum_{i=1}^r \delta_i^2, \quad (B-11)$$

becomes

$$S = \sum_{i=1}^r \left[\sum_{k=1}^n \left[a_k^1 [1 - \exp(-b_k^1 t_i)] + [1 - \exp(-b_k^1 t_i)] \Delta a_k + a_k^1 t_i [\exp(-b_k^1 t_i)] \Delta b_k \right] - \Psi_i \right]^2. \quad (B-12)$$

Using the least-squares criterion, in order for Equation B-8 to yield a curve which fits the data, it is necessary that the parameters Δa_k and Δb_k be chosen so as to make the sum of the squares of the deviations a minimum. Thus it is necessary that the relationships

$$\frac{\partial S}{\partial (\Delta a_k)} = 0 \quad \text{and} \quad \frac{\partial S}{\partial (\Delta b_k)} = 0 \quad (B-13)$$

be satisfied.

From Equation B-11, it is seen that

$$\frac{\partial S}{\partial(\Delta a_j)} = 2 \sum_{i=1}^r \delta_i \frac{\partial \delta_i}{\partial(\Delta a_j)} \quad (B-14)$$

Returning to Equation B-10,

$$\frac{\partial \delta_i}{\partial(\Delta a_j)} = [1 - \exp(-b_j^1 t_i)] \quad (B-15)$$

Substitution of this result along with the result from Equation B-10 into Equation B-14 after simplification yields:

$$\begin{aligned} & \sum_{i=1}^r \sum_{k=1}^n [1 - \exp(-b_k^1 t_i)] [1 - \exp(-b_j^1 t_i)] \Delta a_k \\ & + \sum_{i=1}^r \sum_{k=1}^n a_k^1 t_i [\exp(-b_k^1 t_i)] [1 - \exp(-b_j^1 t_i)] \Delta b_k \\ & = \sum_{i=1}^r \psi_i [1 - \exp(-b_j^1 t_i)] \\ & - \sum_{i=1}^r \sum_{k=1}^n a_k^1 [1 - \exp(-b_k^1 t_i)] [1 - \exp(-b_j^1 t_i)]. \end{aligned} \quad (B-16)$$

j=1,2,3...n

Similarly, by taking the partial derivative of S with respect to Δb_j , it is found that

$$\begin{aligned} & \sum_{i=1}^r \sum_{k=1}^n [1 - \exp(-b_k^1 t_i)] [a_j^1 t_i \exp(-b_j^1 t_i)] \Delta a_k \\ & + \sum_{i=1}^r \sum_{k=1}^n a_k^1 t_i \exp(-b_k^1 t_i) [a_j^1 t_i \exp(-b_j^1 t_i)] \Delta b_k \\ & = \sum_{i=1}^r \psi_i [a_j^1 t_i \exp(-b_j^1 t_i)] \\ & - \sum_{i=1}^r \sum_{k=1}^n a_k^1 [1 - \exp(-b_k^1 t_i)] [a_j^1 t_i \exp(-b_j^1 t_i)]. \end{aligned} \quad (B-17)$$

j= 1,2,3...n

Simultaneous solution of Equations B-16 and B-17 will yield the Δa_k 's and Δb_k 's from which the a_k 's and b_k 's may be calculated using the relationships given by Equations B-4 and B-5. Once a_k and b_k are determined, they are substituted back into Equation B-1 and the sum of the squares of the deviations are calculated using the relationship:

$$S_1 = \sum_{i=1}^r \left[\sum_{k=1}^n a_k [1 - \exp(-b_k t_i)] - \psi_i \right]^2 \quad (B-18)$$

If S_1 is too large, the values of a_k and b_k as calculated above are used as new approximations, say a_k^2 and b_k^2 , and new values of Δa_k and Δb_k are determined using Equations B-16 and B-17. A new value for the sum of the squares of the deviations, S_2 , is calculated which will be less than S_1 . Again, if S_2 is too large, the newly determined values of a_k and b_k are used as new approximations, a_k^3 and b_k^3 , and new values of Δa_k and Δb_k are determined. This process is repeated until the difference between the sum of the squares of the deviations calculated for two successive approximations is less than or equal to an allowable difference. In equation form, this may be written:

$$S_{b-1} - S_b \leq \Delta S_a \quad (B-19)$$

where S_{b-1} and S_b = sum of the squares of the deviations for two successive approximations

ΔS_a = allowable difference.

The accuracy with which Equation B-1 fits a set of experimental data also depends on the value of n , that is, the number of terms used in the summation. Of course, the smaller the number of terms,

the simpler the equation; therefore, the first logical value for n would be one. If, after determining the final value for a_k and b_k (for $n=1$), it is found that the sum of the squares of the deviations (S_b) is greater than some predetermined allowable value, say S_a , then it will be necessary to assume a new value for n in Equation B-1 and determine the corresponding values for the a_k 's and b_k 's. Since it is desirable that n be as small as possible and still satisfy the condition that

$$S_b \leq S_a \tag{B-20}$$

it is logical that successive determinations be made for $n = 2$, $n = 3$, and so forth until Equation B-20 is satisfied.

As stated earlier, in order for this technique to work it is necessary that the assumed values for the a_k 's and b_k 's be reasonably close to their true values. If this condition is not met, the procedure yields diverging instead of converging values for the parameters. This a paradox which could limit the utility of the technique, particularly if there is no prior knowledge of reasonable values to assume. In order to eliminate this problem, a ratio test is performed which consists of examining the two ratios $\Delta a_k/a_k$ and $\Delta b_k/b_k$ after each iteration. It has been found from experience that the assumed values are close enough to the true values to yield convergence if these ratios are between the limits:

$$-1.0 < \Delta a_k/a_k < 5.0 \tag{B-21}$$

$$-1.0 < \Delta b_k/b_k < 5.0 \tag{B-22}$$

If a ratio falls outside these limits, the new or adjusted value of the parameter for the next iteration is evaluated from one of the following relationships:

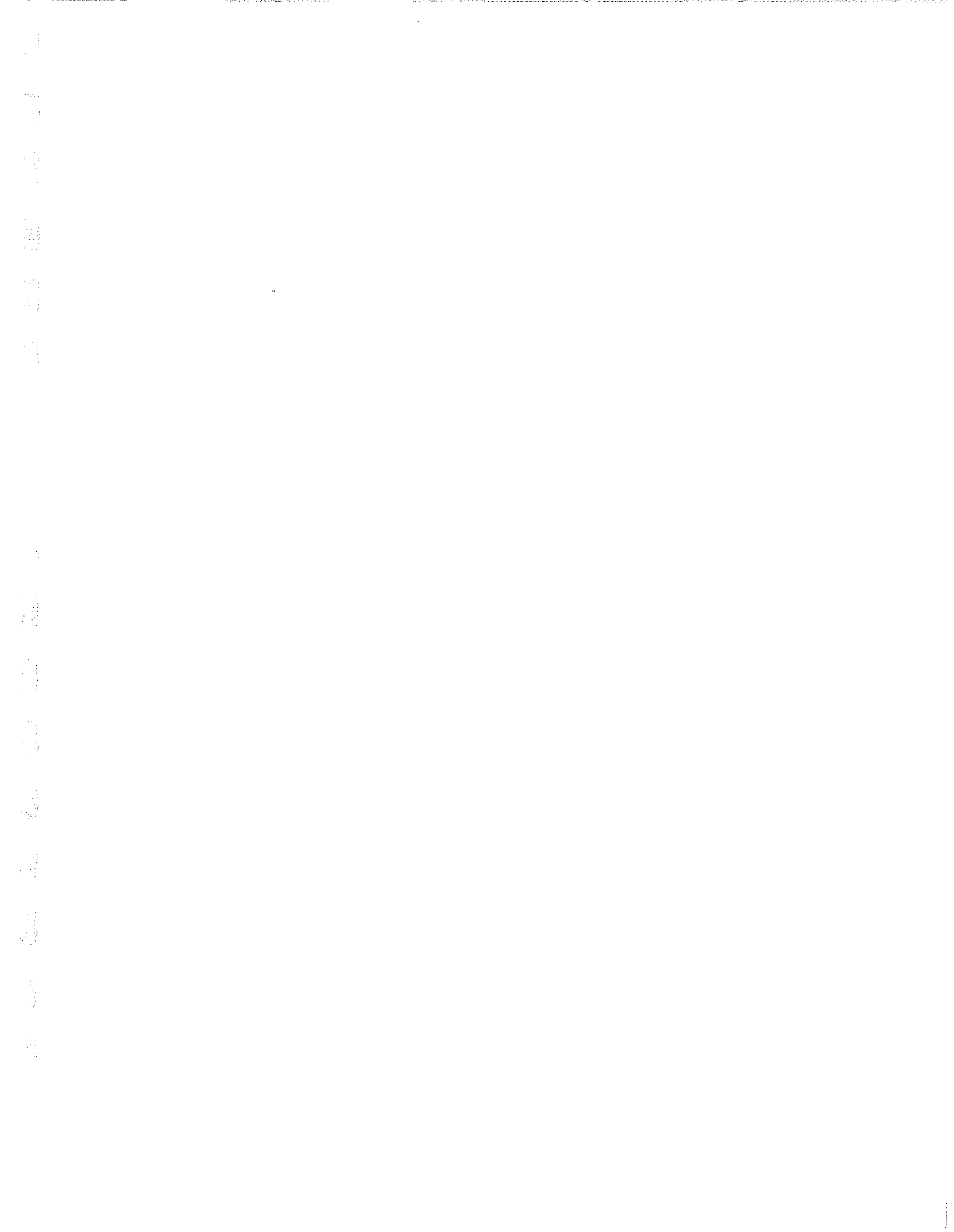
$$a_k = a_k^{\circ} \pm .40 a_k^{\circ} \quad (B-23)$$

$$b_k = b_k^{\circ} \pm .40 b_k^{\circ} \quad (B-24)$$

where a_k° and b_k° = previously assumed values of a_k and b_k .

If the ratio is positive the plus sign is used; if it is negative the minus sign is used. The factor of .40 was found by trial-and-error to be the most satisfactory adjusting factor to use. Of course, if the ratios fall within the limits given by Equations B-21 and B-22, the new or adjusted values for the next iteration are evaluated from Equations B-4 and B-5.

Using this ratio-test technique, results have been obtained using initially assumed parameter values which differed from the true values by as much as one million times. This permits an extremely wide range of "guesses" for the initial values thus increasing the usefulness of the method.



APPENDIX C

COMPUTER PROGRAM FOR VISCOELASTIC ANALYSIS

I. Purpose

The viscoelastic material parameters for asphalts tested in the rotating coaxial viscometer may be evaluated using a computer program. This program was written in FORTRAN IV for processing with the IBM 7040 computer system. The purpose of this program is essentially threefold. First, it computes that portion of the total angle of rotation which may be properly attributed to viscoelastic flow. Equation 37 is used for this computation. Second, it evaluates the constants in Equation B-1 which yield an equation which best fits the viscoelastic portion of flow by the least squares criterion. The techniques which are used in this evaluation are described in Appendix B. The viscoelastic parameters are computed from these constants by means of the following relationships:

$$G_k = 1/a_k \quad (C-1)$$

$$\tau_k = 60/b_k \quad (C-2)$$

and

$$\eta_k = G_k(\tau_k) \quad (C-3)$$

Third, it assesses the degree to which the equation of best fit approximates the experimental data. This is accomplished by calculating the square root of the average squared deviations between the experimental data and the equation of best fit. Such

standard deviations are computed with respect to the viscoelastic creep function and the total angles of rotation for each of three stress levels.

II. Limitations

It is necessary to provide, as input, data from the results of three tests, each of which is normally conducted at a different stress level. The number of data points (that is, pairs of observations between time and total angle of rotation) may be any integer not exceeding 120. The same number of points, however, must be provided for each of the three tests. The number of Voigt elements in the viscoelastic model is limited to a maximum of 10. Any number less than 10 may be evaluated.

III. Job Submission

To submit a job to the University of Kentucky IBM 7040 computer system, the following items must be submitted in the order indicated.

- A. \$JOB Card
- B. \$IBJOB NOSOURCE Card
- C. Viscoelastic Object Deck
- D. Matinv Object Deck
- E. \$ENTRY Card
- F. Data Cards for First Asphalt
 - 1. Asphalt Header Card
 - 2. Steady-State Angular Velocities Card
 - 3. Load Header Card (First Load)
 - 4. Data Cards (First Load)
 - 5. Load Header Card (Second Load)

6. Data Cards (Second Load)

7. Load Header Card (Third Load)

8. Data Cards (Third Load)

9. N-Card

10. Voigt Model Cards

G. Data Cards for Other Asphalts as Desired

IV. Input Data Cards

A. Asphalt Header Card

1. Format

<u>Columns</u>	<u>Symbol</u>	<u>Subject</u>	<u>Units</u>	<u>Format</u>
1-3	NØ	Asphalt number	--	I 3
4-7	L1	Smallest load	gms	I 4
8-13	L2	Intermediate load	gms	I 6
14-19	L3	Largest load	gms	I 6
20-24	TEMP	Test temperature	°F	F 5.1
25-32	CT1	Smallest CT product	d/cm ²	F 8.0
33-40	CT2	Intermediate CT product	d/cm ²	F 8.0
41-48	CT3	Largest CT product	d/cm ²	F 8.0
49-62	GØ	Instantaneous elastic shear modulus	d/cm ²	E14.7

2. Use

This card serves to identify the test results under consideration and to transmit the instantaneous elastic shear modulus for internal computations.

3. Remarks

The loads which are indicated are the total loads suspended on both sides of the pulley. The instantaneous elastic shear modulus is the load-independent modulus which has been

independently evaluated (see "Presentation of Results").

B. Steady-State Angular Velocities Card

1. Format

<u>Columns</u>	<u>Symbol</u>	<u>Subject</u>	<u>Units</u>	<u>Format</u>
1-14	WØ1	Steady-state angular velocity under smallest load	rad/sec	E 14.7
15-28	WØ2	Steady-state angular velocity under intermediate load	rad/sec	E 14.7
29-42	WØ3	Steady-state angular velocity under largest load	rad/sec	E 14.7

2. Remarks

The steady-state angular velocities under the three test conditions must be evaluated independently prior to the computer run. The techniques for this evaluation are presented in the section entitled "Presentation of Results".

C. Load Header Card

1. Format

<u>Columns</u>	<u>Symbol</u>	<u>Subject</u>	<u>Units</u>	<u>Format</u>
1-15	WØ	Steady-state angular velocity for given load	rad/sec	F 15.0
16-30	CT	CT product for given load	d/cm ²	F 15.0
31-40	T1	Corresponding time to achieve steady-state flow	min	F 10.0
41-50	THETF	Corresponding angle of rotation at T1	degrees	F 10.0
51-54	M	Number of data points	--	I 4

2. Use

This card furnishes the necessary information to enable the computation of the viscoelastic creep function for the given

load level. It also specifies the number of data points which follow on the data cards.

3. Remarks

One load header card is necessary for each of the three test conditions.

D. Data Card

1. Format

<u>Columns</u>	<u>Symbol</u>	<u>Subject</u>	<u>Units</u>	<u>Format</u>
1-6	T(I)	Time corresponding to Ith data point	min	F 6.2
7-12	THETA(I,J)	Angle of rotation corresponding to Ith data point and Jth load level	degrees	F 6.2

Times and angles of rotation are alternately punched to and including column 72. Six data points will thus be included on each card except perhaps the last.

2. Use

The basic data for the analysis are transmitted by means of these data cards.

3. Remarks

The data are punched in the order of increasing times. The number of cards necessary will be precisely $M/6$ if this quotient is an integer or $M/6$ (expressed as the nearest larger integer) if the quotient is not an integer. The cards must be ordered by increasing times.

E. N-Card

1. Format

<u>Columns</u>	<u>Symbol</u>	<u>Subject</u>	<u>Units</u>	<u>Format</u>
1-3	N	Minimum number of Voigt elements to consider	--	I 3

2. Use

This card establishes the minimum number of Voigt elements in the viscoelastic model. After evaluating the constants for the N-element model, the program proceeds to evaluate an (N + 1)-element model, and so forth until one of the following conditions occurs: (1) the product of one of the assumed B parameters and the time value corresponding to the second data point exceeds 30, (2) 100 iterations are tried for a specific number of elements without convergence, (3) a specified maximum time is exceeded, or (4) the number of Voigt elements exceeds 10. The first condition is provided in order to eliminate the inclusion of numerical quantities greater than those permitted by the computer. The second condition is provided as a means for discontinuing execution if divergence is occurring.

F. Voigt Model Card

1. Format

<u>Columns</u>	<u>Symbol</u>	<u>Subject</u>	<u>Units</u>	<u>Format</u>
1-14	A(K)	Best prior estimate of $1/G_k$ (the reciprocal of the shear modulus of the kth element)	cm^2/d	E 14.7
15-28	B(K)	Best prior estimate of $1/\tau_k$ (the reciprocal of the retardation time of the kth element)	min^{-1}	E 14.7

2. Use

The N, Voigt model cards which are necessary are ordered by increasing element numbers. The estimates of A(K) and B(K) serve as the initial point for the iteration process.

3. Remarks

The estimates of A(K) and B(K) may differ from the true values by a factor as large as 10^6 . The program uses an iteration process which evaluates a power series at successive values of A(K) and B(K) until the series converges. However, if the estimates of A(K) and B(K) are greatly in error, the iteration process will not be executed and the program will terminate.

If a value of N = 1 is specified by the N-Card, only one value of A(K) and B(K) must be estimated, that is, A(1) and B(1). For the tests reported herein (asphalt cements at 39.2°F), good estimates of A(1) and B(1) are 0.2×10^{-5} and 0.5×10^{-1} , respectively. The program then computes values of A(1) and B(1) by the iteration process which yield the best fit by the least squares criterion. From these values, G_1 and τ_1 are computed. The program then evaluates a two-element model. It first estimates A(1), B(1), A(2), and B(2) and then, by the iteration process, finds the best values for these four variables. G_1 , G_2 , τ_1 , and τ_2 are then computed. This process is repeated automatically until one of the four conditions of Section IV, E,2 is encountered.

V. Output

All output from this program is in the form of tabular printouts. The section entitled "Presentation of Results" describes

the content and format of these printouts. Output data for all of the asphalts tested at 39.2°F are included as Appendix D.

VI. . Source Program

A listing of the source program for the viscoelastic analysis is included as Figure C-1. A listing of the source program for the Matinv subprogram is included as Figure C-2. This subprogram, which was obtained from the University of Kentucky Computing Center, is used in the solution of the simultaneous equations (Equations B-16 and B-17).

```

        DIMENSION T(120),THET(120,3),CF(120,3),ADIFF(120)
30 READ(5,1) NO,L1,L2,L3,TEMP,CT1,CT2,CT3,GO
1  FORMAT(I3,I4,2I6,F5.1,3F8.0,E14.7)
   READ(5,9)W01,W02,W03,
9  FORMAT(3E14.7)
   IF(NO) 10,20,10
10 WRITE(6,8) NO,L1,L2,L3,TEMP,CT1,CT2,CT3
8  FORMAT (11H1,19X,40H SUMMARY SHEET FOR VISCOELASTIC ANALYSIS,/,9X,
112H ASPHALT NO-,I3,15X,7H LOADS-,I4,2I6,3H GM,/,9X,11H TEST TEMP-,
2F5.1,2H F,12X,6H CTS-,3F8.0,8H DY/SQCM,/, 88H TIME THETA 1
3  CF 1 THETA 2 CF 2 THETA 3 CF 3 AVG
4 CF,/, 89H MIN RAD RA/D/SQCM RAD RA/D/SQCM
5  RAD RA/D/SQCM RA/D/SQCM,/)
40 DO 50 J=1,3
   READ(5,2)W0,CT,T1,THETF,M
2  FORMAT (2F15.0,2F10.0,I4)
   W0 = W0 * 60.0
   DO 6 I=1,M,6
6  READ(5,3) T(I),THET(I,J),T(I+1),THET(I+1,J),T(I+2),THET(I+2,J),T(
1I+3),THET(I+3,J),T(I+4),THET(I+4,J),T(I+5),THET(I+5,J)
3  FORMAT (12F6.2)
   DO 50 J= 1,M
   THET (I,J) = THET (I,J) * .0174533
   CF(I,J)=(THET(I,J)-W0*T(I))/CT)-THET(I,J)/CT
50 CONTINUE
   DO 60 I = 1,M
   ADIFF(I)=(CF(I,1)+CF(I,2)+CF(I,3))/3.
60 WRITE(6,4) T(I),THET(I,1),CF(I,1),THET(I,2),CF(I,2),THET(I,3),CF(I
1,3),ADIFF(I)
4  FORMAT(F8.1,6E12.5,E14.7)
   DIMENSION DIFF(120,10),AA1(10,11,120), BA1(10,120), AA(100,21),
1A(10), B(10), DELTA(20),RATIO(20),G(10), TAU(10), VISC(10), C(10),
2D(10),EDIFF(120),S(120),THET1(120),THET2(120),THET3(120),S1(120),
3S2(120),S3(120)
   READ (5,12) N
12 FORMAT (I3)
   DO 70 K=1,N
70 READ(5,13) A(K),B(K)
13 FORMAT(E14.7,E14.7)
109 I = 0
26 N1 = N+1
   I1 = I1+1
   M2=M+1
   L1=2*N
   L2=2*N+1
   TEST=0.0
   TEST2 = 0.0
   DO 16 J=1,L1
   DO 16 I=1,L2
16 AA(I,I) =0.0
   DO 200 J=1,N
   DO 200 K=1,N1
   DO 200 I=1,M2
200 AA1(J,K,I)=0.0
   DO 202 J=1,N
   DO 202 K=1,N
   DO 203 I=1,M
   IF (B(K)*T(2).GE.30.0) GO TO 30
   IF (ABS(B(K)*T(I)).GE.30.0) GO TO 204
   X=1./EXP(B(K)*T(I))

```

Figure C-1. Source Program for Viscoelastic Analysis.

```
GO TO 205
204 X=0.0
205 IF (B(J)*T(2),GE,30.0) GO TO 30
IF (ABS(B(J)*T(I)),GE,30.0) GO TO 208
Y=1./EXP(B(J)*T(I))
GO TO 202
208 Y=0.0
209 AAL(J,K,I)=(1.-X)*(1.-Y)
203 AAL(J,K,M+1)=AAL(J,K,I) + AAL(J,K,M+1)
202 AAL(J,K)=AAL(J,K,M+1)
DO 300 J=1,N
DO 300 K=1,M1
DO 300 I=1,M2
300 AAL(J,K,I)=0.0
DO 302 J=1,N
DO 302 K=1,M1
DO 303 I=1,M
IF (ABS(B(K)*T(I)),GE,30.0) GO TO 304
X=1./EXP(B(K)*T(I))
GO TO 305
304 X=0.0
305 IF (ABS(B(J)*T(I)),GE,30.0) GO TO 308
Y=1./EXP(B(J)*T(I))
GO TO 300
308 Y=0.0
309 AAL(J,K,I)=A(K)*T(I)*(X)*(1.-Y)
303 AAL(J,K,M+1)=AAL(J,K,I) + AAL(J,K,M+1)
L=N+K
302 AAL(J,L)=AAL(J,K,M+1)
DO 400 J=1,N
DO 400 K=1,M1
DO 400 I=1,M2
400 AAL(J,K,I)=0.0
DO 401 J=1,N
DO 401 I=1,M2
401 BAL(J,I)=0.0
DO 408 J=1,N
DO 407 K=1,N
DO 406 I=1,M
IF (B(K)*T(I),GE,30.0) GO TO 402
X=1./EXP(B(K)*T(I))
GO TO 403
402 X=0.0
403 IF (B(J)*T(I),GE,30.0) GO TO 404
Y=1./EXP(B(J)*T(I))
GO TO 405
404 Y=0.0
405 BAL(J,I)=ADIFF(I)*(1.-Y)
AAL(J,K,I)=A(K)*(1.-X)*(1.-Y)
BAL(J,M+1)=BAL(J,I)+BAL(J,M+1)
406 AAL(J,K,M+1)=AAL(J,K,I)+AAL(J,K,M+1)
407 AAL(J,N+1,M+1)=AAL(J,K,M+1)+AAL(J,N+1,M+1)
R=N
408 AAL(J,I.2)=(BAL(J,M+1)/R)-AAL(J,N+1,M+1)
DO 500 J=1,N
DO 500 K=1,M1
DO 500 I=1,M2
500 AAL(J,K,I)=0.0
DO 502 J=1,N
DO 502 K=1,N
```

Figure C-1. Source Program for Viscoelastic Analysis (Cont'd.).

```
      DO 503 I=1,M
      IF (ABS(B(K)*T(I)).GE.30.0) GO TO 504
      X=1./EXP(B(K)*T(I))
      GO TO 505
504 X=0.0
505 IF (ABS(B(J)*T(I)).GE.30.0) GO TO 508
      Y=1./EXP(B(J)*T(I))
      GO TO 509
508 Y=0.0
509 AA1(J,K,I) =(1.- X)*A(J)*T(I)*Y
503 AA1(J,K,M+1)=AA1(J,K,I) + AA1(J,K,M+1)
      J2=N+J
502 AA(J2,K)=AA1(J,K,M+1)
      DO 600 J=1,N
      DO 600 K=1,N1
      DO 600 I=1,M2
600 AA1(J,K,I)=0.0
      DO 602 J=1,N
      DO 602 K=1,N
      DO 603 I=1,M
      IF (ABS(B(K)*T(I)).GE.30.0) GO TO 604
      X=1./EXP(B(K)*T(I))
      GO TO 605
604 X=0.0
605 IF (ABS(B(J)*T(I)).GE.30.0) GO TO 608
      Y=1./EXP(B(J)*T(I))
      GO TO 609
608 Y=0.0
609 AA1(J,K,I) =A(K)*T(I)*( X)*A(J)*T(I)*Y
603 AA1(J,K,M+1)=AA1(J,K,I) + AA1(J,K,M+1)
      L=N+K
      J2=N+J
602 AA(J2,L)=AA1(J,K,M+1)
      DO 700 J=1,N
      DO 700 K=1,N1
      DO 700 I=1,M2
700 AA1(J,K,I)=0.0
      DO 701 J=1,N
      DO 701 I=1,M2
701 BA1(J,I)=0.0
      DO 708 J=1,N
      DO 707 K=1,N
      DO 706 I=1,M
      IF (ABS(B(K)*T(I)).GE.30.0) GO TO 702
      X=1./EXP(B(K)*T(I))
      GO TO 703
702 X=0.0
703 IF (ABS(B(J)*T(I)).GE.30.0) GO TO 704
      Y=1./EXP(B(J)*T(I))
      GO TO 705
704 Y=0.0
705 BA1(J,I)=ADIFF(I)*A(J)*T(I)*Y
      AA1(J,K,I)=A(K)*(1.-X)*A(J)*T(I)*Y
      BA1(J,M+1)=BA1(J,I)+BA1(J,M+1)
706 AA1(J,K,M+1)=AA1(J,K,I)+AA1(J,K,M+1)
707 AA1(J,N+1,M+1)=AA1(J,K,M+1)+AA1(J,N+1,M+1)
      J2=N+J
      R=N
708 AA(J2,L2)=(BA1(J,M+1)/R)-AA1(J,N+1,M+1)
      DO 43 J=1,L1
```

Figure C-1. Source Program for Viscoelastic Analysis (Cont'd.).

```

43 DELTA(I)=AA(J,L2)
CALL MATINV (AA,I,DELTA,I,DET)
DO 100 I=1,N
L=N+I
RATIO (I) = DELTA(I)/A(I)
100 RATIO(L) = DELTA(L)/B(I)
GO 106 I=1,N
L=N+I
IF (RATIO (I).GT.5.0) GO TO 101
IF (RATIO (I).LT.(-1.0)) GO TO 102
GO TO 103
101 A(I)=A(I)+.40*A(I)
TEST2 = 2.0
GO TO 103
102 A(I)=A(I)-.40*A(I)
TEST2 = 2.0
103 IF (RATIO (L).GT.5.0) GO TO 104
IF (RATIO(L).LT.(-1.0)) GO TO 105
GOTO 106
104 B(I)=B(I)+.40*B(I)
TEST2 = 2.0
GO TO 106
105 B(I)=B(I)-.40*B(I)
TEST2 = 2.0
106 CONTINUE
IF (TEST2.EQ.2.0.AND.II.GT.1) GO TO 5
IF (TEST2.EQ.2.) GO TO 5
DO 29 K=1,N
L=N+K
IF (ABS(DELTA(K)).GE..001*A(K)) GO TO 27
IF (ABS(DELTA(L)).GE..001*B(K)) GO TO 27
GO TO 28
27 TEST=1.
28 A(K)=DELTA(K)+A(K)
29 B(K)=DELTA(L)+B(K)
IF (TEST.GT.0.0.OR.TEST2.GT.0.0) GO TO 5
GO TO 7
5 IF (II.LE.100) GO TO 26
WRITE (6,31)
31 FORMAT (1H1)
DO 900 K=1,N
900 WRITE (6,32) K,DELTA(K),K,A(K),K,RATIO(K)
32 FORMAT (4X,6H DELTA,11,2H =,E14.7,4X,2H A,11,2H =,E14.7,4X,6H R
ATIO,11,2H =,E14.7)
DO 901 K=1,N
L=N+K
901 WRITE (6,42) L,DELTA(L),K,B(K),L,RATIO(L)
42 FORMAT(4X,6H DELTA,11,2H =,E14.7,4X,2H B,11,2H =,E14.7,4X,6H RATIO
1,11,2H =,E14.7)
GO TO 30
7 DO 107 I=1,N
G(I) = 1./A(I)
TAU(I) = 60./B(I)
107 VISC(I)=G(I)*TAU(I)
WRITE(6,910)
910 FORMAT (1H1)
WRITE(6,108) (K,(TAU(K)),K,(G(K)),K,(VISC(K)),K=1,N)
108 FORMAT (1H0,10X,4H TAU,11,2H =,1X,E14.7,4H SEC,6X,2H G,11,2H =,1X,
1E14.7,12H DYNES/SQ CM,6X,5H VISC,11,2H =,1X,E14.7,7H POISES)
DO 807 I=1,N

```

Figure C-1. Source Program for Viscoelastic Analysis (Cont'd.).

```

DO 807 J=1,10
807 DIFF(I,J)=0.0
DO 808 I=1,M
DO 809 J=1,N
IF((T(I)*B(J)).GE.30.0) GO TO 812
Z=1./EXP(T(I)*B(J))
GOTO 813
812 Z=0.0
813 DIFF(I,J)=( 1. /G(J))*(1.-Z)
809 DIFF(I,N+1)=DIFF(I,N+1)+DIFF(I,J)
EDIFF(I)=DIFF(I,N+1)
THET1(I)=(CT1/G0)+(W01*T(I)*60.)+(CT1*EDIFF(I))
THET2(I)=(CT2/G0)+(W02*T(I)*60.)+(CT2*EDIFF(I))
808 THET3(I)=(CT3/G0)+(W03*T(I)*60.)+(CT3*EDIFF(I))
WRITE(6,810)
810 FORMAT(1H-,10H TIME OBSERVED CALCULATED OBSERVED CALCU
LATED OBSERVED CALCULATED ,/,110H
2(MIN) THETA 1 THETA 1 THETA 2 THETA 2 THETA
3 3 THETA 3 CP FUNCTION CP FUNCTION,/,110H (RAD)
4 (RAD) (RAD) (RAD) (RAD) (RAD)
5 (RA/D/SQCM) (RA/D/SQCM),/)
DO 850 I=1,M
850 WRITE(6,811)T(I),THET(I,1),THET1(I),THET(I,2),THET2(I),THET(I,3),T
HET3(I),ADIFF(I),EDIFF(I)
811 FORMAT(F8.1,8E13.5)
DO 822 I=1,120
S1(I)=0.0
S2(I)=0.0
S3(I)=0.0
822 S(I)=0.0
DO 820 I=1,M
S1(I)=(THET(I,1)-THET1(I))**2
S2(I)=(THET(I,2)-THET2(I))**2
S3(I)=(THET(I,3)-THET3(I))**2
S(I)=(ADIFF(I)-EDIFF(I))**2
S1(M+1)=S1(M+1)+S1(I)
S2(M+1)=S2(M+1)+S2(I)
S3(M+1)=S3(M+1)+S3(I)
820 S(M+1)=S(M+1)+S(I)
H=M
SD1=(S1(M+1)/H)**.5
SD2=(S2(M+1)/H)**.5
SD3=(S3(M+1)/H)**.5
SD=(S(M+1)/H)**.5
WRITE(6,821)SD1,SD2,SD3,SD
821 FORMAT(1H-,10H STD DEV =,3X,E12.5,14X,E12.5,14X,E12.5,14X,E12.5)
A(N+1) = A(N)*.1
B(N+1) = B(N)*10.
N=N+1
GO TO 109
20 CALL EXIT
END

```

Figure C-1. Source Program for Viscoelastic Analysis (Cont'd.).

```
C PROGRAM NO. 13-7040-F4
C TITLE - MATINV SUBROUTINE
C SPECIAL MACH REQ - NONE
C SUBROUTINES REQUIRED - NONE
C KEY WORKS - SIMULTANEOUS EQUATIONS, DETERMINANT, INVERSE, MATRIX
C
C $(BFTC CMV) FULLIST, REF CMV10010
C SUBROUTINE MATINV(A,N,B,M,DETERM)
C SUBROUTINE MATINV
C THIS SUBROUTINE COMPUTES THE INVERSE AND DETERMINANT OF MATRIX A,
C OF ORDER N, BY THE GAUSS-JORDAN METHOD. A-INVERSE REPLACES A, AND
C THE DETERMINANT OF A IS PLACED IN DETERM. IF M=1 THE VECTOR B
C CONTAINS THE CONSTANT VECTOR WHEN MATINV IS CALLED, AND THIS IS
C REPLACED WITH THE SOLUTION VECTOR IF M=0, NO SIMULTANEOUS
C EQUATION SOLUTION IS CALLED FOR, AND B IS NOT PERTINENT. N IS NOT
C TO EXCEED 100.
C A,N,B,M, AND DETERM THE ARGUMENT LIST ARE DUMMY VARIABLES.
C DIMENSION PIVOT(100), A(100,100), B(100,100), INDEX(100,2), PIVOT(100)
C INITIALIZATION
10 DETERM=1.0
15 DO 20 J=1,N
20 IPIVOT(J)=0
30 DO 50 I=1,N
C SEARCH FOR PIVOT ELEMENT
40 AMAX=0.0
45 DO 105 J=1,N
50 IF(IPIVOT(J).EQ.1) GO TO 105
60 DO 100 K=1,N
70 IF(IPIVOT(K).GT.1) GO TO 740
IF(IPIVOT(K).EQ.1) GO TO 100
80 IF(ABS(AMAX).GE.ABS(A(I,K))) GO TO 100
85 IROW=J
90 ICOLUM=K
95 AMAX=A(I,K)
100 CONTINUE
105 CONTINUE
110 IPIVOT(ICOLUM)=IPIVOT(ICOLUM)+1
C INTERCHANGE ROWS TO PUT PIVOT ELEMENT ON DIAGONAL
130 IF(IROW.EQ.ICOLUM) GO TO 260
140 DETERM=-DETERM
150 DO 200 L=1,N
160 SWAP=A(IROW,L)
170 A(IROW,L)=A(ICOLUM,L)
200 A(ICOLUM,L)=SWAP
205 IF(M.LE.0) GO TO 260
210 DO 250 L=1,M
220 SWAP=B(IROW,L)
230 B(IROW,L)=B(ICOLUM,L)
250 B(ICOLUM,L)=SWAP
260 INDEX(I,1)=IROW
270 INDEX(I,2)=ICOLUM
310 PIVOT(I)=A(ICOLUM,ICOLUM)
320 DETERM=DETERM*PIVOT(I)
C DIVIDE PIVOT ROW BY PIVOT ELEMENT
330 A(ICOLUM,ICOLUM)=1.0
340 DO 350 L=1,N
350 A(ICOLUM,L)=A(ICOLUM,L)/PIVOT(I)
355 IF(M.LE.0) GO TO 380
360 DO 370 L=1,M
```

Figure C-2. Source Program for Matinv Subprogram.


```
370 B(ICOLUM,L)=B(ICOLUM,L)/PIVOT(I)
C   REDUCE NON-PIVOT ROWS
380 DO550 L1=1,N
390 IF(L1.EQ.ICOLUM) GO TO 550
400 T=A(L1,ICOLUM)
420 A(L1,ICOLUM)=0.0
430 DO450 L=1,N
450 A(L1,L)=A(L1,L)-A(ICOLUM,L)*T
455 IF(M.LE.0) GO TO 550
460 DO500 L=L,M
500 B(L1,L)=B(L1,L)-B(ICOLUM,L)*T
550 CONTINUE
C   INTERCHANGE COLUMNS
600 DO710 I=1,N
610 L=N+1-I
620 IF(INDEX(L,1).EQ.INDEX(L,2)) GO TO 710
630 JROW=INDEX(L,1)
640 JCOLUM=INDEX(L,2)
650 DO 705 K=1,N
660 SWAP=A(K,JROW)
670 A(K,JROW)=A(K,JCOLUM)
700 A(K,JCOLUM)=SWAP
705 CONTINUE
710 CONTINUE
740 RETURN
     END
```

Figure C-2. Source Program for Matinv Subprogram (Cont'd.).

APPENDIX D
VISCOELASTIC ANALYSIS OF DATA

All of the test data taken at 39.2°F were analyzed using the computer program to evaluate the viscoelastic material parameters. All output from this analysis are summarized herein in tabular form. The format of these figures is described in the section entitled "Presentation of Results".

EQUATION OF BEST FIT n=3

EQUATION OF BEST FIT, n=4

TAU1 = 0.1637899E 04 SEC	GI = 0.6831088E 04 DYNES/CM	VISC1 = 0.111834E 10 POISES
TAU2 = 0.1373221E 04 SEC	G2 = 0.5887386E 07 DYNES/CM	VISC2 = 0.740881E 09 POISES
TAU3 = 0.243550E 04 SEC	G3 = 0.273182E 04 DYNES/CM	VISC3 = 0.714966E 09 POISES
TAU4 = 0.196597E 04 SEC	G4 = 0.104180E 04 DYNES/CM	VISC4 = 0.223123E 09 POISES

TIME	STRESS	STRAIN	STRESS	STRAIN	STRESS	STRAIN	STRESS	STRAIN	STRESS	STRAIN	STRESS	STRAIN	STRESS	STRAIN	STRESS	STRAIN	STRESS	STRAIN
TIME	STRESS	STRAIN	TIME	STRESS	STRAIN	TIME	STRESS	STRAIN	TIME	STRESS	STRAIN	TIME	STRESS	STRAIN	TIME	STRESS	STRAIN	
0.0	0.00000E+00	0.00000E+00	0.00000E+00	0.00000E+00	0.00000E+00	0.00000E+00	0.00000E+00	0.00000E+00	0.00000E+00	0.00000E+00	0.00000E+00	0.00000E+00	0.00000E+00	0.00000E+00	0.00000E+00	0.00000E+00	0.00000E+00	
0.1	0.34407E-02	0.13102E-01	0.19071E-01	0.23869E-01	0.41008E-02	0.39940E-01	1.30000E-02	0.44791E-02	0.24380E-02	0.19673E-02	0.23889E-02	0.23889E-02	0.24376E-02	0.24376E-02	0.24376E-02	0.24376E-02	0.24376E-02	
0.2	0.43673E-02	0.14213E-01	0.45379E-02	0.47533E-01	0.78940E-02	0.76350E-01	0.25825E-02	0.44820E-02	0.43833E-02	0.14041E-01	0.43379E-02	0.25731E-01	0.78940E-02	0.78940E-02	0.78940E-02	0.78940E-02	0.78940E-02	
0.3	0.47360E-02	0.14722E-01	0.49933E-02	0.50098E-01	0.86992E-02	0.84300E-01	0.27222E-02	0.47123E-02	0.46107E-02	0.14550E-01	0.45828E-02	0.26722E-01	0.86992E-02	0.86992E-02	0.86992E-02	0.86992E-02	0.86992E-02	
0.4	0.48887E-02	0.15048E-01	0.51304E+00	0.51877E-01	0.91770E-02	0.89240E-01	0.28104E-02	0.48353E-02	0.48353E-02	0.14777E-01	0.47123E-02	0.27222E-01	0.91770E-02	0.91770E-02	0.91770E-02	0.91770E-02	0.91770E-02	
0.5	0.49188E-02	0.15227E-01	0.52040E-01	0.52700E-01	0.95179E-02	0.92440E-01	0.28777E-02	0.49088E-02	0.49088E-02	0.14922E-01	0.47777E-02	0.27777E-01	0.95179E-02	0.95179E-02	0.95179E-02	0.95179E-02	0.95179E-02	
0.6	0.49348E-02	0.15364E-01	0.52677E-01	0.53333E-01	0.97500E-02	0.93700E-01	0.29222E-02	0.49777E-02	0.49777E-02	0.15077E-01	0.48123E-02	0.28222E-01	0.97500E-02	0.97500E-02	0.97500E-02	0.97500E-02	0.97500E-02	
0.7	0.49473E-02	0.15471E-01	0.53198E-01	0.53777E-01	0.98800E-02	0.94800E-01	0.29555E-02	0.50000E-02	0.50000E-02	0.15198E-01	0.48377E-02	0.28555E-01	0.98800E-02	0.98800E-02	0.98800E-02	0.98800E-02	0.98800E-02	
0.8	0.49573E-02	0.15557E-01	0.53613E-01	0.54133E-01	0.99200E-02	0.95200E-01	0.29800E-02	0.50222E-02	0.50222E-02	0.15298E-01	0.48523E-02	0.28800E-01	0.99200E-02	0.99200E-02	0.99200E-02	0.99200E-02	0.99200E-02	
0.9	0.49650E-02	0.15622E-01	0.53950E-01	0.54400E-01	0.99500E-02	0.95500E-01	0.29955E-02	0.50377E-02	0.50377E-02	0.15377E-01	0.48600E-02	0.29055E-01	0.99500E-02	0.99500E-02	0.99500E-02	0.99500E-02	0.99500E-02	
1.0	0.49700E-02	0.15677E-01	0.54213E-01	0.54588E-01	0.99700E-02	0.95650E-01	0.30000E-02	0.50422E-02	0.50422E-02	0.15422E-01	0.48623E-02	0.29122E-01	0.99700E-02	0.99700E-02	0.99700E-02	0.99700E-02	0.99700E-02	
1.1	0.49730E-02	0.15722E-01	0.54400E-01	0.54688E-01	0.99800E-02	0.95700E-01	0.30022E-02	0.50444E-02	0.50444E-02	0.15444E-01	0.48644E-02	0.29144E-01	0.99800E-02	0.99800E-02	0.99800E-02	0.99800E-02	0.99800E-02	
1.2	0.49750E-02	0.15757E-01	0.54500E-01	0.54777E-01	0.99850E-02	0.95750E-01	0.30044E-02	0.50466E-02	0.50466E-02	0.15466E-01	0.48666E-02	0.29166E-01	0.99850E-02	0.99850E-02	0.99850E-02	0.99850E-02	0.99850E-02	
1.3	0.49760E-02	0.15782E-01	0.54577E-01	0.54844E-01	0.99880E-02	0.95780E-01	0.30055E-02	0.50477E-02	0.50477E-02	0.15477E-01	0.48677E-02	0.29177E-01	0.99880E-02	0.99880E-02	0.99880E-02	0.99880E-02	0.99880E-02	
1.4	0.49760E-02	0.15797E-01	0.54613E-01	0.54888E-01	0.99890E-02	0.95790E-01	0.30060E-02	0.50480E-02	0.50480E-02	0.15480E-01	0.48680E-02	0.29180E-01	0.99890E-02	0.99890E-02	0.99890E-02	0.99890E-02	0.99890E-02	
1.5	0.49760E-02	0.15802E-01	0.54633E-01	0.54913E-01	0.99895E-02	0.95795E-01	0.30062E-02	0.50482E-02	0.50482E-02	0.15482E-01	0.48682E-02	0.29182E-01	0.99895E-02	0.99895E-02	0.99895E-02	0.99895E-02	0.99895E-02	
1.6	0.49760E-02	0.15807E-01	0.54648E-01	0.54933E-01	0.99898E-02	0.95798E-01	0.30064E-02	0.50484E-02	0.50484E-02	0.15484E-01	0.48684E-02	0.29184E-01	0.99898E-02	0.99898E-02	0.99898E-02	0.99898E-02	0.99898E-02	
1.7	0.49760E-02	0.15812E-01	0.54658E-01	0.54948E-01	0.99900E-02	0.95800E-01	0.30066E-02	0.50486E-02	0.50486E-02	0.15486E-01	0.48686E-02	0.29186E-01	0.99900E-02	0.99900E-02	0.99900E-02	0.99900E-02	0.99900E-02	
1.8	0.49760E-02	0.15817E-01	0.54668E-01	0.54958E-01	0.99902E-02	0.95802E-01	0.30068E-02	0.50488E-02	0.50488E-02	0.15488E-01	0.48688E-02	0.29188E-01	0.99902E-02	0.99902E-02	0.99902E-02	0.99902E-02	0.99902E-02	
1.9	0.49760E-02	0.15822E-01	0.54678E-01	0.54968E-01	0.99904E-02	0.95804E-01	0.30070E-02	0.50490E-02	0.50490E-02	0.15490E-01	0.48690E-02	0.29190E-01	0.99904E-02	0.99904E-02	0.99904E-02	0.99904E-02	0.99904E-02	
2.0	0.49760E-02	0.15827E-01	0.54688E-01	0.54978E-01	0.99906E-02	0.95806E-01	0.30072E-02	0.50492E-02	0.50492E-02	0.15492E-01	0.48692E-02	0.29192E-01	0.99906E-02	0.99906E-02	0.99906E-02	0.99906E-02	0.99906E-02	
2.1	0.49760E-02	0.15832E-01	0.54698E-01	0.54988E-01	0.99908E-02	0.95808E-01	0.30074E-02	0.50494E-02	0.50494E-02	0.15494E-01	0.48694E-02	0.29194E-01	0.99908E-02	0.99908E-02	0.99908E-02	0.99908E-02	0.99908E-02	
2.2	0.49760E-02	0.15837E-01	0.54708E-01	0.54998E-01	0.99910E-02	0.95810E-01	0.30076E-02	0.50496E-02	0.50496E-02	0.15496E-01	0.48696E-02	0.29196E-01	0.99910E-02	0.99910E-02	0.99910E-02	0.99910E-02	0.99910E-02	
2.3	0.49760E-02	0.15842E-01	0.54718E-01	0.55008E-01	0.99912E-02	0.95812E-01	0.30078E-02	0.50498E-02	0.50498E-02	0.15498E-01	0.48698E-02	0.29198E-01	0.99912E-02	0.99912E-02	0.99912E-02	0.99912E-02	0.99912E-02	
2.4	0.49760E-02	0.15847E-01	0.54728E-01	0.55018E-01	0.99914E-02	0.95814E-01	0.30080E-02	0.50500E-02	0.50500E-02	0.15500E-01	0.48700E-02	0.29200E-01	0.99914E-02	0.99914E-02	0.99914E-02	0.99914E-02	0.99914E-02	
2.5	0.49760E-02	0.15852E-01	0.54738E-01	0.55028E-01	0.99916E-02	0.95816E-01	0.30082E-02	0.50502E-02	0.50502E-02	0.15502E-01	0.48702E-02	0.29202E-01	0.99916E-02	0.99916E-02	0.99916E-02	0.99916E-02	0.99916E-02	
2.6	0.49760E-02	0.15857E-01	0.54748E-01	0.55038E-01	0.99918E-02	0.95818E-01	0.30084E-02	0.50504E-02	0.50504E-02	0.15504E-01	0.48704E-02	0.29204E-01	0.99918E-02	0.99918E-02	0.99918E-02	0.99918E-02	0.99918E-02	
2.7	0.49760E-02	0.15862E-01	0.54758E-01	0.55048E-01	0.99920E-02	0.95820E-01	0.30086E-02	0.50506E-02	0.50506E-02	0.15506E-01	0.48706E-02	0.29206E-01	0.99920E-02	0.99920E-02	0.99920E-02	0.99920E-02	0.99920E-02	
2.8	0.49760E-02	0.15867E-01	0.54768E-01	0.55058E-01	0.99922E-02	0.95822E-01	0.30088E-02	0.50508E-02	0.50508E-02	0.15508E-01	0.48708E-02	0.29208E-01	0.99922E-02	0.99922E-02	0.99922E-02	0.99922E-02	0.99922E-02	
2.9	0.49760E-02	0.15872E-01	0.54778E-01	0.55068E-01	0.99924E-02	0.95824E-01	0.30090E-02	0.50510E-02	0.50510E-02	0.15510E-01	0.48710E-02	0.29210E-01	0.99924E-02	0.99924E-02	0.99924E-02	0.99924E-02	0.99924E-02	
3.0	0.49760E-02	0.15877E-01	0.54788E-01	0.55078E-01	0.99926E-02	0.95826E-01	0.30092E-02	0.50512E-02	0.50512E-02	0.15512E-01	0.48712E-02	0.29212E-01	0.99926E-02	0.99926E-02	0.99926E-02	0.99926E-02	0.99926E-02	
3.1	0.49760E-02	0.15882E-01	0.54798E-01	0.55088E-01	0.99928E-02	0.95828E-01	0.30094E-02	0.50514E-02	0.50514E-02	0.15514E-01	0.48714E-02	0.29214E-01	0.99928E-02	0.99928E-02	0.99928E-02	0.99928E-02	0.99928E-02	
3.2	0.49760E-02	0.15887E-01	0.54808E-01	0.55098E-01	0.99930E-02	0.95830E-01	0.30096E-02	0.50516E-02	0.50516E-02	0.15516E-01	0.48716E-02	0.29216E-01	0.99930E-02	0.99930E-02	0.99930E-02	0.99930E-02	0.99930E-02	
3.3	0.49760E-02	0.15892E-01	0.54818E-01	0.55108E-01	0.99932E-02	0.95832E-01	0.30098E-02	0.50518E-02	0.50518E-02	0.15518E-01	0.48718E-02	0.29218E-01	0.99932E-02	0.99932E-02	0.99932E-02	0.99932E-02	0.99932E-02	
3.4	0.49760E-02	0.15897E-01	0.54828E-01	0.55118E-01	0.99934E-02	0.95834E-01	0.30100E-02	0.50520E-02	0.50520E-02	0.15520E-01	0.48720E-02	0.29220E-01	0.99934E-02	0.99934E-02	0.99934E-02	0.99934E-02	0.99934E-02	
3.5	0.49760E-02	0.15902E-01	0.54838E-01	0.55128E-01	0.99936E-02	0.95836E-01	0.30102E-02	0.50522E-02	0.50522E-02	0.15522E-01	0.48722E-02	0.29222E-01	0.99936E-02	0.99936E-02	0.99936E-02	0.99936E-02	0.99936E-02	
3.6	0.49760E-02	0.15907E-01	0.54848E-01	0.55138E-01	0.99938E-02	0.95838E-01	0.30104E-02	0.50524E-02	0.50524E-02	0.15524E-01	0.48724E-02	0.29224E-01	0.99938E-02	0.99938E-02	0.99938E-02	0.99938E-02	0.99938E-02	
3.7	0.49760E-02	0.15912E-01	0.54858E-01	0.55148E-01	0.99940E-02	0.95840E-01	0.30106E-02	0.50526E-02	0.50526E-02	0.15526E-01	0.48726E-02	0.29226E-01	0.99940E-02	0.99940E-02	0.99940E-02	0.99940E-02</		

DATA SHEET

EQUATION OF BEST FIT, n=1

EQUATION OF BEST FIT, n=2

SHELLY 31-ELT FOR VISCOELASTIC ANALYSIS										TALL = 0.15000000 IN SEC										G1 = 0.02500000 D' DYNES/CM										VISC2 = 0.12200000 IN PULSES									
ASPHALT %C/C		TEMP		LPTS		TIME		RHEO		CALC		OBS		CALC		OBS		CALC		OBS		CALC		OBS		CALC		OBS		CALC		OBS							
TIME	RAE	RAE	RAE	RAE	RAE	RAE	RAE	RAE	RAE	RAE	RAE	RAE	RAE	RAE	RAE	RAE	RAE	RAE	RAE	RAE	RAE	RAE	RAE	RAE	RAE	RAE	RAE	RAE	RAE	RAE	RAE	RAE							
0.0	0.000000	0.000000	0.000000	0.000000	0.000000	0.000000	0.000000	0.000000	0.000000	0.000000	0.000000	0.000000	0.000000	0.000000	0.000000	0.000000	0.000000	0.000000	0.000000	0.000000	0.000000	0.000000	0.000000	0.000000	0.000000	0.000000	0.000000	0.000000	0.000000	0.000000	0.000000	0.000000	0.000000	0.000000	0.000000				

Figure D-7. Viscoelastic Analysis for Asphalt 72 at 39.2°F.

DATA SHEET

EQUATION OF BEST FIT, n=1

EQUATION OF BEST FIT, n=2

SUMMARY SHEET FOR VISCOELASTIC ANALYSIS

TMAU = 0.15423528 CM SEC C1 = 0.32155816 CM DYNES/CM CM WISL1 = 0.14023070 CM POISES

ASPHALT NO. 200 LOGS-400 600 800 900 CM TREAT TEMP. 39.2 F C1C LOGS2_24222 LOGS3_24222 LOGS4_24222 LOGS5_24222

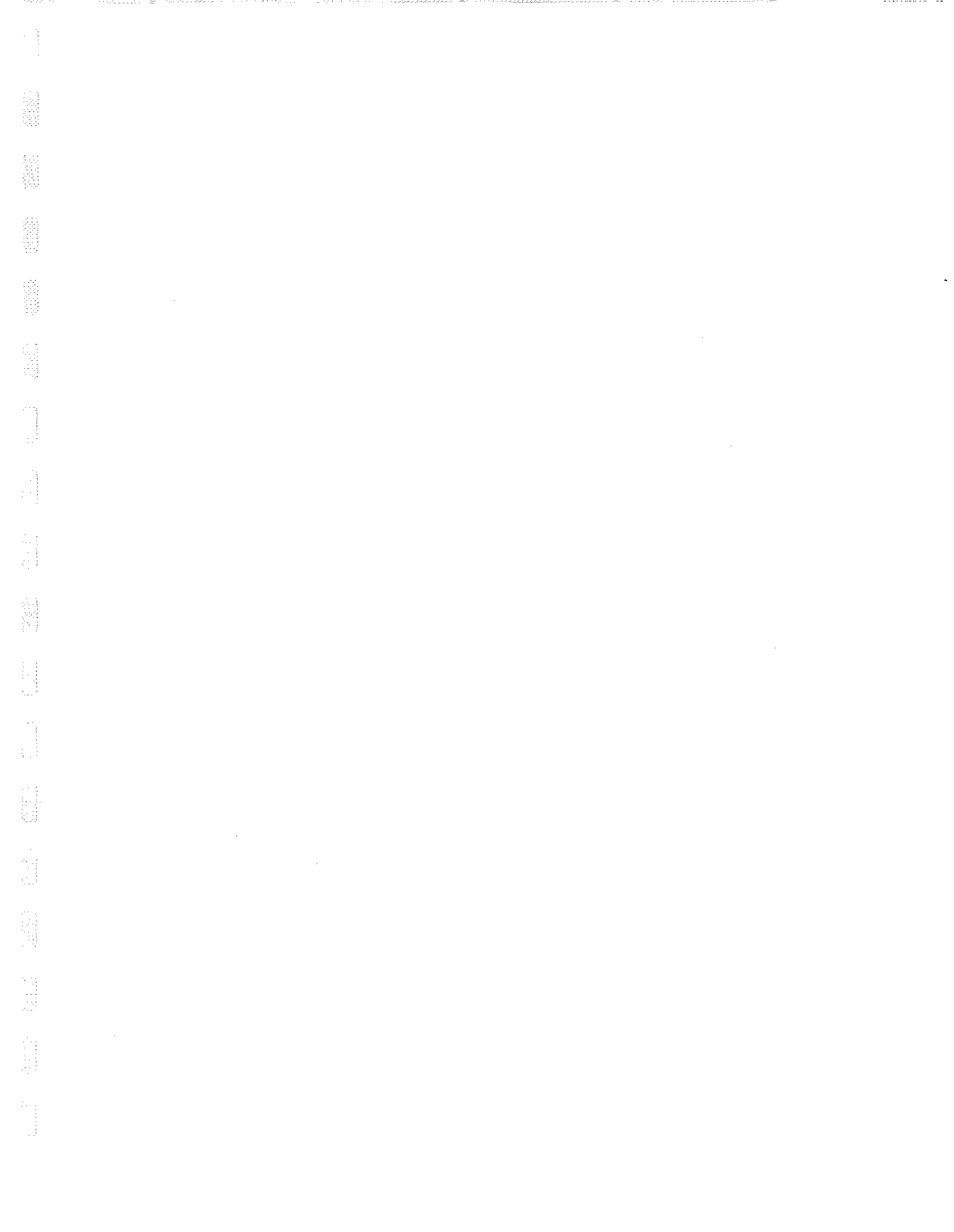
TMAU = 0.15423528 CM SEC C1 = 0.32155816 CM DYNES/CM CM WISL1 = 0.14023070 CM POISES

TMAU = 0.15974196 CM SEC C2 = 0.44856496 CM DYNES/CM CM WISL2 = 0.40657102 CM POISES

TIME	THETA 1	CF 1	THETA 2	CF 2	THETA 3	CF 3	AVG OF	OBSERVED		CALCULATED		OBSERVED		CALCULATED		OBSERVED		CALCULATED		OBSERVED		CALCULATED			
								LOAD	RAV/SQCM	LOAD	RAV/SQCM	LOAD	RAV/SQCM	LOAD	RAV/SQCM	LOAD	RAV/SQCM	LOAD	RAV/SQCM	LOAD	RAV/SQCM	LOAD	RAV/SQCM	LOAD	RAV/SQCM
0.1	0.174536	0.000000	0.174536	0.000000	0.174536	0.000000	0.000000	0.174536	0.000000	0.174536	0.000000	0.174536	0.000000	0.174536	0.000000	0.174536	0.000000	0.174536	0.000000	0.174536	0.000000	0.174536	0.000000	0.174536	0.000000

STD Dev = 0.84591E-02 0.86805E-02 0.23292E-01 0.13718E-02 STD Dev = 0.19234E-02 0.74451E-02 0.24749E-01 0.44838E-02

Figure D-11. Viscoelastic Analysis for Asphalt 200 at 39.2°F.



DATA SHEET

EQUATION OF BEST FIT, n=1

SUMMARY SHEET FOR VISCOELASTIC ANALYSIS

ASPHALT MIXTURE: LOADS=100 1400 2000 GA TEST TEMP: 39.2 F

LOADS=100 1400 2000 GA TEST TEMP: 39.2 F

FAUL = 0.4355422E-03 SEC CT = 0.1304904E-02 DYNES/CM VISCL = 0.138033E-02 POISES

TIME MIN	THETA 1 RAD	CF 1 RA7/D50CM	THETA 2 RAD	CF 2 RA7/D50CM	THETA 3 RAD	CF 3 RA7/D50CM	AVG CF	OBSERVED THETA 1 (RAD)	CALCULATED THETA 1 (RAD)	OBSERVED THETA 2 (RAD)	CALCULATED THETA 2 (RAD)	OBSERVED THETA 3 (RAD)	CALCULATED THETA 3 (RAD)	DOSAGE OBSERVED THETA 1 (RAD)	CALCULATED THETA 1 (RAD)	DOSAGE OBSERVED THETA 2 (RAD)	CALCULATED THETA 2 (RAD)	DOSAGE OBSERVED THETA 3 (RAD)	CALCULATED THETA 3 (RAD)
0.0	0.26185E-02	0.00000E-00	0.1418E-02	0.00000E-00	0.3407E-02	0.00000E-00	0.0000000E+00	0.4818E-02	0.2178E-02	0.2037E-02	0.1779E-02	0.2000E-02	0.1999E-02	0.1999E-02	0.2000E-02	0.1999E-02	0.2000E-02	0.1999E-02	0.2000E-02
0.2	0.24907E-02	0.46880E-02	0.2530E-02	0.2281E-02	0.4941E-02	0.2408E-02	0.161219E-02	0.24907E-02	0.24907E-02	0.24907E-02	0.24907E-02	0.24907E-02	0.24907E-02	0.24907E-02	0.24907E-02	0.24907E-02	0.24907E-02	0.24907E-02	0.24907E-02
0.4	0.23832E-02	0.71310E-02	0.4681E-02	0.3072E-02	0.6728E-02	0.2800E-02	0.289274E-02	0.43832E-02	0.23832E-02	0.23832E-02	0.23832E-02	0.23832E-02	0.23832E-02	0.23832E-02	0.23832E-02	0.23832E-02	0.23832E-02	0.23832E-02	0.23832E-02
0.6	0.22962E-02	0.91600E-02	0.6129E-02	0.3869E-02	0.5107E-02	0.3017E-02	0.346370E-02	0.52902E-02	0.22962E-02	0.22962E-02	0.22962E-02	0.22962E-02	0.22962E-02	0.22962E-02	0.22962E-02	0.22962E-02	0.22962E-02	0.22962E-02	0.22962E-02
0.8	0.22302E-02	0.10870E-01	0.7647E-02	0.4633E-02	0.3274E-02	0.2885E-02	0.292271E-02	0.61072E-02	0.22302E-02	0.22302E-02	0.22302E-02	0.22302E-02	0.22302E-02	0.22302E-02	0.22302E-02	0.22302E-02	0.22302E-02	0.22302E-02	0.22302E-02
1.0	0.21812E-02	0.13090E-01	0.9105E-02	0.5785E-02	0.3688E-02	0.2884E-02	0.272371E-02	0.69813E-02	0.21812E-02	0.21812E-02	0.21812E-02	0.21812E-02	0.21812E-02	0.21812E-02	0.21812E-02	0.21812E-02	0.21812E-02	0.21812E-02	0.21812E-02
1.2	0.21442E-02	0.14710E-01	0.10630E-01	0.6402E-02	0.4193E-02	0.3052E-02	0.265180E-02	0.78998E-02	0.21442E-02	0.21442E-02	0.21442E-02	0.21442E-02	0.21442E-02	0.21442E-02	0.21442E-02	0.21442E-02	0.21442E-02	0.21442E-02	0.21442E-02
1.4	0.21172E-02	0.16280E-01	0.12430E-01	0.7455E-02	0.4810E-02	0.3362E-02	0.248180E-02	0.89481E-02	0.21172E-02	0.21172E-02	0.21172E-02	0.21172E-02	0.21172E-02	0.21172E-02	0.21172E-02	0.21172E-02	0.21172E-02	0.21172E-02	0.21172E-02
1.6	0.20982E-02	0.17740E-01	0.14430E-01	0.8663E-02	0.5610E-02	0.3710E-02	0.232170E-02	0.10147E-01	0.20982E-02	0.20982E-02	0.20982E-02	0.20982E-02	0.20982E-02	0.20982E-02	0.20982E-02	0.20982E-02	0.20982E-02	0.20982E-02	0.20982E-02
1.8	0.20852E-02	0.19090E-01	0.16580E-01	0.1000E-01	0.9923E-02	0.6490E-02	0.217170E-02	0.12200E-01	0.20852E-02	0.20852E-02	0.20852E-02	0.20852E-02	0.20852E-02	0.20852E-02	0.20852E-02	0.20852E-02	0.20852E-02	0.20852E-02	0.20852E-02
2.0	0.20772E-02	0.20310E-01	0.18840E-01	0.11220E-01	0.11220E-01	0.64924E-02	0.188415E-02	0.13942E-01	0.20772E-02	0.20772E-02	0.20772E-02	0.20772E-02	0.20772E-02	0.20772E-02	0.20772E-02	0.20772E-02	0.20772E-02	0.20772E-02	0.20772E-02
2.2	0.20732E-02	0.21450E-01	0.21210E-01	0.1270E-01	0.1270E-01	0.64924E-02	0.157070E-02	0.15707E-01	0.20732E-02	0.20732E-02	0.20732E-02	0.20732E-02	0.20732E-02	0.20732E-02	0.20732E-02	0.20732E-02	0.20732E-02	0.20732E-02	0.20732E-02
2.4	0.20712E-02	0.22440E-01	0.2355E-01	0.1382E-01	0.1382E-01	0.64924E-02	0.131150E-02	0.17098E-01	0.20712E-02	0.20712E-02	0.20712E-02	0.20712E-02	0.20712E-02	0.20712E-02	0.20712E-02	0.20712E-02	0.20712E-02	0.20712E-02	0.20712E-02
2.6	0.20702E-02	0.23310E-01	0.2455E-01	0.1503E-01	0.1503E-01	0.64924E-02	0.11010E-02	0.17702E-01	0.20702E-02	0.20702E-02	0.20702E-02	0.20702E-02	0.20702E-02	0.20702E-02	0.20702E-02	0.20702E-02	0.20702E-02	0.20702E-02	0.20702E-02
2.8	0.20692E-02	0.24080E-01	0.2544E-01	0.1600E-01	0.1600E-01	0.64924E-02	0.94172E-03	0.18172E-01	0.20692E-02	0.20692E-02	0.20692E-02	0.20692E-02	0.20692E-02	0.20692E-02	0.20692E-02	0.20692E-02	0.20692E-02	0.20692E-02	0.20692E-02
3.0	0.20682E-02	0.24770E-01	0.2624E-01	0.1678E-01	0.1678E-01	0.64924E-02	0.80072E-03	0.18702E-01	0.20682E-02	0.20682E-02	0.20682E-02	0.20682E-02	0.20682E-02	0.20682E-02	0.20682E-02	0.20682E-02	0.20682E-02	0.20682E-02	0.20682E-02
3.2	0.20672E-02	0.25390E-01	0.2697E-01	0.1747E-01	0.1747E-01	0.64924E-02	0.68072E-03	0.19102E-01	0.20672E-02	0.20672E-02	0.20672E-02	0.20672E-02	0.20672E-02	0.20672E-02	0.20672E-02	0.20672E-02	0.20672E-02	0.20672E-02	0.20672E-02
3.4	0.20662E-02	0.25950E-01	0.2764E-01	0.1810E-01	0.1810E-01	0.64924E-02	0.58072E-03	0.19372E-01	0.20662E-02	0.20662E-02	0.20662E-02	0.20662E-02	0.20662E-02	0.20662E-02	0.20662E-02	0.20662E-02	0.20662E-02	0.20662E-02	0.20662E-02
3.6	0.20652E-02	0.26470E-01	0.2826E-01	0.1860E-01	0.1860E-01	0.64924E-02	0.49072E-03	0.19622E-01	0.20652E-02	0.20652E-02	0.20652E-02	0.20652E-02	0.20652E-02	0.20652E-02	0.20652E-02	0.20652E-02	0.20652E-02	0.20652E-02	0.20652E-02
3.8	0.20642E-02	0.26940E-01	0.2884E-01	0.1900E-01	0.1900E-01	0.64924E-02	0.41072E-03	0.19852E-01	0.20642E-02	0.20642E-02	0.20642E-02	0.20642E-02	0.20642E-02	0.20642E-02	0.20642E-02	0.20642E-02	0.20642E-02	0.20642E-02	0.20642E-02
4.0	0.20632E-02	0.27370E-01	0.2938E-01	0.1930E-01	0.1930E-01	0.64924E-02	0.34072E-03	0.19972E-01	0.20632E-02	0.20632E-02	0.20632E-02	0.20632E-02	0.20632E-02	0.20632E-02	0.20632E-02	0.20632E-02	0.20632E-02	0.20632E-02	0.20632E-02
4.2	0.20622E-02	0.27770E-01	0.2989E-01	0.1950E-01	0.1950E-01	0.64924E-02	0.28072E-03	0.20002E-01	0.20622E-02	0.20622E-02	0.20622E-02	0.20622E-02	0.20622E-02	0.20622E-02	0.20622E-02	0.20622E-02	0.20622E-02	0.20622E-02	0.20622E-02
4.4	0.20612E-02	0.28140E-01	0.3037E-01	0.1960E-01	0.1960E-01	0.64924E-02	0.23072E-03	0.20002E-01	0.20612E-02	0.20612E-02	0.20612E-02	0.20612E-02	0.20612E-02	0.20612E-02	0.20612E-02	0.20612E-02	0.20612E-02	0.20612E-02	0.20612E-02
4.6	0.20602E-02	0.28480E-01	0.3083E-01	0.1960E-01	0.1960E-01	0.64924E-02	0.19072E-03	0.20002E-01	0.20602E-02	0.20602E-02	0.20602E-02	0.20602E-02	0.20602E-02	0.20602E-02	0.20602E-02	0.20602E-02	0.20602E-02	0.20602E-02	0.20602E-02
4.8	0.20592E-02	0.28800E-01	0.3127E-01	0.1950E-01	0.1950E-01	0.64924E-02	0.16072E-03	0.20002E-01	0.20592E-02	0.20592E-02	0.20592E-02	0.20592E-02	0.20592E-02	0.20592E-02	0.20592E-02	0.20592E-02	0.20592E-02	0.20592E-02	0.20592E-02
5.0	0.20582E-02	0.29100E-01	0.3169E-01	0.1940E-01	0.1940E-01	0.64924E-02	0.13072E-03	0.20002E-01	0.20582E-02	0.20582E-02	0.20582E-02	0.20582E-02	0.20582E-02	0.20582E-02	0.20582E-02	0.20582E-02	0.20582E-02	0.20582E-02	0.20582E-02
5.2	0.20572E-02	0.29390E-01	0.3210E-01	0.1930E-01	0.1930E-01	0.64924E-02	0.11072E-03	0.20002E-01	0.20572E-02	0.20572E-02	0.20572E-02	0.20572E-02	0.20572E-02	0.20572E-02	0.20572E-02	0.20572E-02	0.20572E-02	0.20572E-02	0.20572E-02
5.4	0.20562E-02	0.29670E-01	0.3250E-01	0.1920E-01	0.1920E-01	0.64924E-02	0.09072E-03	0.20002E-01	0.20562E-02	0.20562E-02	0.20562E-02	0.20562E-02	0.20562E-02	0.20562E-02	0.20562E-02	0.20562E-02	0.20562E-02	0.20562E-02	0.20562E-02
5.6	0.20552E-02	0.29940E-01	0.3289E-01	0.1910E-01	0.1910E-01	0.64924E-02	0.08072E-03	0.20002E-01	0.20552E-02	0.20552E-02	0.20552E-02	0.20552E-02	0.20552E-02	0.20552E-02	0.20552E-02	0.20552E-02	0.20552E-02	0.20552E-02	0.20552E-02
5.8	0.20542E-02	0.30210E-01	0.3328E-01	0.1900E-01	0.1900E-01	0.64924E-02	0.07072E-03	0.20002E-01	0.20542E-02	0.20542E-02	0.20542E-02	0.20542E-02	0.20542E-02	0.20542E-02	0.20542E-02	0.20542E-02	0.20542E-02	0.20542E-02	0.20542E-02
6.0	0.20532E-02	0.30480E-01	0.3367E-01	0.1890E-01	0.1890E-01	0.64924E-02	0.06072E-03	0.20002E-01	0.20532E-02	0.20532E-02	0.20532E-02	0.20532E-02	0.20532E-02	0.20532E-02	0.20532E-02	0.20532E-02	0.20532E-02	0.20532E-02	0.20532E-02
6.2	0.20522E-02	0.30750E-01	0.3406E-01	0.1880E-01	0.1880E-01	0.64924E-02	0.05072E-03	0.20002E-01	0.20522E-02	0.20522E-02	0.20522E-02	0.20522E-02	0.20522E-02	0.20522E-02	0.20522E-02	0.20522E-02	0.20522E-02	0.20522E-02	0.20522E-02
6.4	0.20512E-02	0.31020E-01	0.3445E-01	0.1870E-01	0.1870E-01	0.64924E-02	0.04072E-03	0.20002E-01	0.20512E-02	0.20512E-02	0.20512E-02	0.20512E-02	0.20512E-02	0.20512E-02	0.20512E-02	0.20512E-02	0.20512E-02	0.20512E-02	0.20512E-02
6.6	0.20502E-02	0.31290E-01	0.3484E-01	0.1860E-01	0.1860E-01	0.64924E-02	0.03072E-03	0.20002E-01	0.20502E-02	0.20502E-02	0.20502E-02	0.20502E-02	0.20502E-02	0.20502E-02	0.20502E-02	0.20502E-02	0.20502E-02	0.20502E-02	0.20502E-02
6.8	0.20492E-02	0.31560E-01	0.3523E-01	0.1850E-01	0.1850E-01	0.64924E-02	0.02072E-03	0.20002E-01	0.20492E-02	0.20492E-02	0.20492E-02	0.20492E-02	0.20492E-02	0.20492E-02	0.20492E-02	0.20492E-02	0.20492E-02	0.20492E-02	0.20492E-02
7.0	0.20482E-02	0.31830E-01	0.3562E-01	0.1840E-01	0.1840E-01	0.64924E-02	0.01072E-03	0.20002E-01	0.20482E-02	0.20482E-02	0.20482E-02	0.20482E-02	0.20482E-02	0.20482E-02	0.20482E-02	0.20482E-02	0.20482E-02	0.20482E-02	0.20482E-02
7.2	0.20472E-02	0.32100E-01	0.3601E-01	0.1830E-01	0.1830E-01	0.64924E-02	0.00072E-03	0.20002E-01	0.20472E-02	0.20472E-02	0.20472E-02	0.20472E-02	0.20472E-02	0.20472E-02	0.20472E-02	0.20472E-02	0.20472E-02	0.20472E-02	0.20472E-02
7.4	0.20462E-02	0.32370E-01	0.3640E-01	0.1820E-01	0.1820E-01	0.64924E-02	0.00000E-03	0.20002E-01	0.20462E-02	0.20462E-02	0.20462E-02	0.20462E							

